UNIVERSITY OF KWAZULU-NATAL

THERMAL EVOLUTION OF RADIATING SPHERES UNDERGOING DISSIPATIVE GRAVITATIONAL COLLAPSE

KEVIN POOBALAN REDDY

2014

UNIVERSITY OF KWAZULU-NATAL

Thermal evolution of radiating spheres undergoing dissipative gravitational collapse

by

KEVIN POOBALAN REDDY

Submitted in fulfilment of the

academic requirements for the degree of

Doctor of Philosophy

in the

School of Mathematics, Statistics and Computer Science

University of KwaZulu-Natal

Durban

November 2014

As the candidate's supervisor I have approved this dissertation for submission.

Signed:	Name: Dr M Govender	Date: .....
Signed:	Name: Prof S D Maharaj	Date: .....

Abstract

In this study we investigate the physics of a relativistic radiating star undergoing dissipative collapse in the form of a radial heat flux. Our treatment clearly demonstrates how the presence of shear affects the collapse process; we are in a position to contrast the physical features of the collapsing sphere in the presence of shear with the shear-free case. We first consider a particular exact solution found by Thirukkanesh *et al* [1] which is expanding, accelerating and shearing. By employing a causal heat transport equation of the Maxwell-Cattaneo form we show that the shear leads to an enhancement of the core stellar temperature thus emphasizing that relaxational effects cannot be ignored when the star leaves hydrostatic equilibrium. We also employ a perturbative scheme to study the evolution of a spherically symmetric stellar body undergoing gravitational collapse. The Bowers and Liang [2] static model is perturbed, and its subsequent dynamical collapse is studied in the linear perturbative regime. We find that anisotropic effects brought about by the differences in the radial and tangential pressures enhance the perturbations to the temperature, and that causal and non–causal cases yield identical profiles.

This thesis is dedicated to

My Dad, Mr. Gengiah Reddy, who passed away on 23^{rd} *January 2014.*
Thank you Dad for giving me the gift of education and for
always believing in me. I have finished the journey you never got to begin.
I am convinced that had you received the love and support that I
got from you, you would have arrived at this very place.
Rest in peace Dad, I love you.

I want to give glory to the
Lord Jesus Christ for providing
strength, knowledge and understanding
in my time of need... Philippians 4:13,19

COLLEGE OF AGRICULTURE, ENGINEERING AND SCIENCE

DECLARATION 1 - PLAGIARISM

I, Kevin Poobalan Reddy, student number: 951060388, declare that

1. The research reported in this thesis, except where otherwise indicated, is my original research.

2. The following thesis has not been submitted for any degree or examination at any other university.

3. The following thesis does not contain other persons data, pictures, graphs or other information, unless specifically acknowledged as being sourced from other persons.

4. The following thesis does not contain other persons' writing, unless specifically acknowledged as being sourced from other researchers. Where other written sources have been quoted, then:

    a. Their words have been re-written but the general information attributed to them has been referenced.

    b. Where their exact words have been used, then their writing has been placed in italics and inside quotation marks, and referenced.

5. This thesis does not contain text, graphics or tables copied and pasted from the Internet, unless specifically acknowledged, and the source being detailed in the thesis and in the References sections.

Signed: ..... Kevin Poobalan Reddy Date: .....

COLLEGE OF AGRICULTURE, ENGINEERING AND SCIENCE

DECLARATION 2 - PUBLICATIONS

Details of contribution to publications that form part of the research presented in this thesis.

Publication 1

Govender M, Reddy K P and Maharaj S D, The role of shear in dissipative gravitational collapse, *Int. J. Mod. Phys. D* **23**, 1450013 (2014).

Publication 2

Reddy K P, Govender M and Maharaj S D, Impact of anisotropic stresses during dissipative gravitational collapse, *Gen. Relativ. Gravit.*, in press (2014).

Regular meetings transpired between myself and my supervisors to discuss the problems pertaining to this study, which eventually resulted in the above mentioned research outputs. The form and structure of the research publications as well as the analysis of the results were done collaboratively. The research outputs were written primarily by myself with guidance and input from my supervisors.

Acknowledgements

There are some important role players I would like to acknowledge for helping make this dissertation possible:

- My supervisor Dr Megandhren Govender, for his expert guidance, generosity of time, encouraging words and unending passion and energy. It was truly a honour and privilege to work with Dr Govender, and his enthusiasm and quest for excellence in Astrophysics is both inspirational and refreshing. Thank you for all you input and assistance.

- My co–supervisor Prof Sunil D Maharaj, who is a living legend in the area of Cosmology, General Relativity and Astrophysics. Thank you for welcoming me into your research group and for believing that I had the ability to take on and finish this mammoth task. Your humility, fatherly mannerisms and professionalism are priceless.

- The University of KwaZulu–Natal for financial assistance for the duration of this study.

- Prof. Sibu Moyo, Director of Research at the Durban University of Technology. I would like to thank your office for financial support for a portion of this study.

- My wife, Hannah Reddy, and our daughters, Levina Robyn Reddy and Kalista Raphaella Reddy. Thank you for your patience, prayer, support, encouraging

words and the countless hours you've sacrificed to allow me to progress academically. My sincere wish and prayer is that I will be able to make up for "all" that was lost in the process.

- My mum, Cecilia Prema Reddy, for always believing in me. Thank you for your prayer, support and for always spurring me on to success. You really made up for Dad's absence. Most importantly, I want to thank Daddy and you for giving me the gift of education.

- My parents inlaw (my other Mum and Dad, Leela and Siva Pillay) for their prayer, encouragement and support. Thank you for filling up the gaps my studies created and for picking up the slack and doing for me what very few would do.

Contents

Chapter 1

Introduction

Since time immemorial stars have been a source of fascination and intrigue to people of all ages. What is a star? A star begins it's life as a collection of molecules and dust pulled together by gravity into a giant molecular cloud. When light elements in this molecular cloud are close enough, nuclear fusion occurs with the release of huge amounts of energy which is carried away from the core via convection and/or free-streaming radiation (photons). This bulk movement of the stellar fluid carrying energy away from the core results in an outward pressure which is able to overcome the pull of gravity and stabilize the star, for a period of time, against continual gravitational collapse. Once a star's nuclear fuel is depleted it can no longer counter the gravitational forces and subsequently gravity dominates and the star begins to collapse once again. A star could end its journey as a white dwarf if it possesses a mass which is below the Chandrasekhar limit [3] of $\approx 1.3M_{\odot}$, and in this scenario electron degeneracy pressure provides the restraining force which counteracts the gravitational force. A star could also achieve stability as a neutron star, if it's mass does not exceed $\approx 3M_{\odot}$ [4]. For such a star, neutron degeneracy pressure is responsible for balancing the gravitational pull and maintaining stability within the fluid distribution. However, stars which are too massive to achieve stable configurations such as white dwarfs or neutron stars continue to collapse under gravity's ever increasing dominance. See [5] for details.

The final outcome of a massive star experiencing continued collapse under it's own gravity is a contentious issue. The general theory of relativity postulates that the end state of such a self–gravitating system will be a spacetime singularity, and this implies that all the physical properties of the star will diverge. Oppenheimer and Snyder [6], working with an idealized spherically symmetric fluid distribution, reported the formation of an event horizon prior to the formation of a black hole containing the singularity predicted by general relativity. The Cosmic Censorship Conjecture (CCC) proposed by Penrose [7] tells us that continued gravitational collapse of a physically reasonable matter distribution must ultimately result in a singularity which is contained within a black hole as opposed to a naked singularity. The CCC has come under much scrutiny by researchers [8]–[10], who point out that general relativity does not make any claim or prediction as to whether or not the singularity will be contained within a black hole, invisible to an external observer, or be a naked singularity which is visible to an outside observer. Singularity theorems predict the possibility of the formation of singularities which are not covered by an event horizon and are visible to an external observer.

Joshi [8] showed that singularities without trapped surfaces are not necessarily a characteristic feature of a naked singularity. A characteristic property of a naked singularity is the existence of future directed timelike curves whose past originated at the singularity. For naked singularities there is a causal relationship or connection between the region of the singularity and an outside, distant observer. Thus photons and information from ultra-high dense regions on the inside are allowed to travel to faraway external observers. This helps to distinguish between black holes and naked singularities. Joshi [8] lists various conditions under which the formation of naked singularities could be avoided altogether. These could add credence and support for the CCC. Joshi and Malafarina [9] state that "*The key physical feature that decides the visibility or otherwise of the singularity is the interplay between the structure and time–curve of the singularity and that of the trapped surface formation of the black*

hole".

The big question is whether or not a massive star, undergoing continued collapse will do so according to the model of Oppenheimer and Snyder and whether its singularity will necessarily be contained within an event horizon. We have to bear in mind that the Oppenheimer and Snyder model is based on an ideal stellar fluid, so in reality it may be possible that the CCC could be violated and the existence of naked singularities is indeed possible. To date there is no derivation of censorship from fundamental physical principles that informs and guides the study of black hole physics. The delay in such a derivation is probably due to the highly non–linear nature of Einstein's field equations. Some of the latest developments by Patil and Joshi [11] show that naked singularities would make better particle accelerators than their black hole counterparts as a result of the divergence of the centre of mass energy which occurs to a greater degree. This is due to the fact that infalling particles are able to be accelerated to regions extremely close to the singularity, thereby obtaining very high velocities. Joshi *et al* [12] have also conducted work on distinguishing black holes from naked singularities by studying properties of their respective accretion discs. They have found that the accretion disc around a naked singularity is more luminous and contains a series of high frequency power law segments compared to that of black holes.

In 1916 Karl Schwarzschild [13, 14] published an exact solution to the Einstein field equations for a spherically symmetric bounded matter distribution with uniform density and surrounded by a vacuum. The Schwarzschild solution allows us to calculate the Schwarzschild radius whose boundary represents the event horizon, within which is a black hole containing the spacetime singularity. Physically viable models of gravitational collapse became attainable when Vaidya [15] published an exact solution to the field equations describing the exterior gravitational field of a radiating, spherically symmetric mass distribution. Since the star is radiating energy to the exterior spacetime its atmosphere is no longer empty but contains null radiation. Having generated solutions for both the interior and the exterior spacetimes, the matching of

these solutions at the boundary becomes necessary. Santos [16] produced the first set of junction conditions which he obtained by matching the interior spacetime of the collapsing star to Vaidya's outgoing solution. This pioneering work paved the way for studying dissipative gravitational collapse. It became possible to study more realistic scenarios of gravitational collapse which incorporates dissipative fluxes such as heat flow [17, 18], shear viscosity [19], bulk viscosity [20] as well as the electromagnetic field [21]. The impact of dissipation on the stability of a gravitationally collapsing stellar fluid has been extensively studied. It is well established that relativistic corrections as a result of heat flow decreases the adiabatic index (which measures the "stiffness" of the collapsing fluid) and renders the fluid less unstable [18, 19]. We will study dynamical instabilities in more detail later.

In order to study the thermal behaviour of a star undergoing dissipative gravitational collapse we need to invoke the transport equations for the relevant dissipative fluxes. To this end, several thermodynamic theories involving irreversible processes have been proposed. The Eckart theory [22] forecasts propagation velocities, for the thermal signals, that lie outside the causal cone of propagation, and is additionally plagued with unstable equilibrium states. The "pathological problems" inherent in the Eckart model were addressed, in the context of extended irreversible thermodynamics, by several authors [23, 24, 25, 26] by taking into account relaxation time associated with the dissipative fluxes. These models yield hyperbolic transport equations that are of the Cattaneo form [27] which obey the causality principle as well as ensuring stable equilibrium states. Di Prisco *et al* [28] have estimated the relaxation times for neutron star matter, for early stages of gravitational collapse, to be as small as 0.1 ms for a core temperature of 10^9K and as large as 100 s at 10^6K. Work done by Anile *et al* [29] also indicate that relaxational effects are significant, and Herrera and Martinez [30] show explicitly that the thermal relaxation time has a direct impact on the luminosity profiles as well as the compactness of the star.

The effect of the relaxation time on the thermal evolution and luminosity profile of

shear-free gravitational collapse has been investigated with the aid of causal transport equations of the Maxwell-Catteneo form for the thermodynamical fluxes [28, 30, 31, 32, 33]. Other shear-free models with acceleration and constant (and non-constant) collision time have also been studied in detail [34, 35, 36] and these investigators have also found that the star exhibits higher central temperatures when relaxational effects are taken into account. One of the first exact models describing shearing, radiating collapse with pressure anisotropy was presented by Naidu *et al* [37]. Their work gives insight into the thermodynamic behaviour of the stellar fluid, and the impact of shear on the relaxation time during the collapse process. This model which is acceleration-free and results in infinite central pressure and density, was later generalised by Rajah and Maharaj [38]. Maharaj *et al* [39] have explicitly shown how perturbations (in the linear regime) to the temperature profile of a star undergoing shear-free, isotropic dissipative collapse is enhanced throughout the stellar range by relaxation effects. Up to that point none of the exact models had a shear-free limit, i.e. the shear could not be switched off, and it was therefore not possible to highlight the effect of shear directly onto the collapse process. A particular collapse model presented by Thirukkanesh *et al* [1] has a shear-free limit, ie., the shear can be switched off and the corresponding shear-free collapse ensues. Govender *et al* [40] were able to highlight the impact of shear on the temperature and luminosity profiles of this particular model.

The origin and role of anisotropy has been an area of major interest since the early 1970's. Superdense stars such as pulsars may be anisotropic for certain density ranges due to phase transitions [41]. Cold matter, above certain high density ranges, may consist of a solid core that is responsible for local anisotropy [42]. Other possible sources of anisotropy are strong electric fields within the star [43], strong magnetic fields [44], the presence of shear [45] and shear viscous pressures [46], amongst other factors. The pioneering work conducted by Bowers and Liang [2] made it possible to study the impact of anisotropy on the physical behaviour (radial pressure, critical mass and maximum surface redshift) of a static star. By varying the degree of anisotropy,

Dev and Gleiser [47] have reported an increase in the critical mass with anisotropy when compared with the mass at the isotropic limit. They also reported a rise in surface redshifts with anisotropy, in particular when the tangential pressure dominates the radial pressure. Investigations [48, 49] clearly indicate that anisotropy leads to more stable configurations. Herrera [50] found that local pressure anisotropy is one of the factors responsible for energy density inhomogeneities. A recent paper by Sharma and Das [51] gives insight into the impact of the variation of anisotropy on the collapse rate as well as the evolution of the surface temperature of a gravitationally collapsing star with radial heat flux.

Chapter 2

General relativity in astrophysics

2.1 Introduction

Einstein's general relativity is essentially a geometric theory of gravity. It utilises a complicated mathematical structure to yield a profound equation that tells us that the gravitational acceleration between two nearby particles is due to the curvature of spacetime. In this chapter we present a brief overview of general relativity leading to the Einstein field equations. The field equations govern the gravitational collapse of relativistic stars and predict that the end state of ongoing collapse will be a singularity (a violation of the physical properties of the star, including it's curvature) in the space-time continuum. In §2.2 we introduce the concepts of vectors, covectors (1-forms) and tensors which are going to be used extensively in this study. The geometry of curved spacetime, leading to the Einstein curvature tensor, is introduced in general in §2.3. In §2.4 we present a general overview of the energy momentum tensor. The intention is to provide the reader with a deeper understanding of the physical meaning of the components of this tensor which describes the matter distribution of the star. In §2.5 we derive the Einstein tensor components for a spherically symmetric spacetime, we present a general energy momentum tensor describing an imperfect fluid distribution, and we introduce the associated kinematical quantities. The Einstein field equations

for shearing spacetimes are given in §2.6 while the shear–free equations are presented in §2.7. The chapter then concludes with §2.8 where we discuss the Vaidya solution which represents the solution of the Einstein field equations for the exterior spacetime in which null radiation is present. In this chapter we follow a similar treatment to that of Govender [52], except that our energy momentum tensor is charge–free and has been extended to include shear viscosity and bulk viscosity.

2.2 Vectors, covectors and tensors

2.2.1 Vectors

A vector is set of elements that can be added together or undergo scalar multiplication and still be an element of that set. In other words the properties of a vector are preserved under addition or scalar multiplication. We can define a set of basis vectors, viz. $\vec{e}_\mu \quad (\mu = 1, 2, ...n)$, such that any vector $\vec{V}$ can be expressed as a linear combination of the basis vectors as

$$\vec{V} = \vec{e}_1 V^1 + \vec{e}_2 V^2 + \vec{e}_3 V^3 + ... + \vec{e}_n V^n,$$

or in a more compact form, by employing the Einstein summation convention, as

$$\vec{V} = \vec{e}_\mu V^\mu,$$

where the V^μ are the components of the vector $\vec{V}$ along the basis vectors $\vec{e}_\mu$.

2.2.2 Covectors

A covector is also referred to as a dual vector or a one-form. A covector $\tilde{P}$ accepts a vector as an input and "operates" on it to produce a real scalar output. Passing the basis vectors $\vec{e}_\mu$ to $\tilde{P}$ yields the components of $\tilde{P}$ which are given by

$$\tilde{P}(\vec{e}_\mu) = P_\mu.$$

A covector can be expressed as a linear combination of its basis covectors $\tilde{e}^{\mu}$ as

$$\tilde{P} = \tilde{e}^{\mu} P_{\mu}.$$

It can be easily shown that applying $\tilde{P}$ to a vector $\vec{V}$ will yield a scalar output given by

$$\tilde{P}(\vec{V}) = V^{\mu} P_{\mu}.$$

Finally if

$$\vec{V} = \vec{e}_{\mu} V^{\mu}$$

and

$$\tilde{P} = \tilde{e}^{\nu} P_{\nu},$$

then

$$\tilde{P}(\vec{V}) = V^{\mu} P_{\nu} \tilde{e}^{\nu}(\vec{e_{\mu}}) = P_{\nu} V^{\mu} \delta^{\nu}_{\mu} = P_{\nu} V^{\mu}.$$

2.2.3 Tensors

A tensor is a linear machine or operator that has h input slots for h covectors and k input slots for k vectors and outputs a real number i.e. $\mathbf{T}(\vec{A}, \vec{B}, ...\tilde{P}, \tilde{Q}, ...) = \mathcal{N}$, where $\mathcal{N}$ is a real number. The rank or order of a tensor is $r = h + k$. It then follows quite easily that a vector is a (1,0) tensor having an input slot for one covector in order to produce a scalar output; a covector is a (0,1) tensor which requires a single vector input to yield a scalar output. Consider a (1,2) tensor $\mathbf{S}(\vec{A}, \tilde{B}, \tilde{C})$. In order to produce a scalar output it must accept one covector and two vectors as inputs. The components of a tensor are obtained by applying the tensor to basis vectors and basis covectors. Thus the components of tensor $\mathbf{S}$ can be obtained by passing to $\mathbf{S}$ one basis covector $\tilde{e}^{\nu}$ and two basis vectors viz. $\vec{e}_{\mu}$ and $\vec{e}_{\lambda}$, to yield its components $S^{\nu}_{\mu\lambda}$. Similarly, $\mathbf{T}(\vec{e}_{\alpha}, \vec{e}_{\beta}) = T_{\alpha\beta}$ and $\mathbf{T}(\vec{e}_1, \vec{e}_3) = T_{13}$ is a component of $\mathbf{T}$. Consider $\mathbf{T}(\vec{A}, \vec{B}, \tilde{C})$. Passing $\vec{A} = \vec{e}_{\mu} A^{\mu}$, $\vec{B} = \vec{e}_{\nu} B^{\nu}$ and $\tilde{C} = \tilde{e}^{\lambda} C_{\lambda}$ to tensor $\mathbf{T}$ we obtain $\mathbf{T} = A^{\mu} B^{\nu} C_{\lambda} \mathbf{T}(\vec{e}_{\mu}, \vec{e}_{\nu}, \tilde{e}^{\lambda}) = A^{\mu} B^{\nu} C_{\lambda} T^{\lambda}_{\mu\nu}$. Since all the dummy indices (or repeated indices)

are balanced (up and down), the quantity $A^{\mu}B^{\nu}C_{\lambda}T^{\lambda}_{\mu\nu}$ is a real number. Whenever an upper index balances a lower index, that particular index is said to contract.

2.3 Geometry of curved spacetime

In the framework of the general theory of relativity we represent curved spacetime as a four–dimensional manifold that is differentiable everywhere on the spacetime fabric with a symmetric metric tensor **g** with signature $(-+++)$. Any event or point on the spacetime manifold is represented by $x^a = (x^0, x^1, x^2, x^3)$, where x^0 is the temporal component and x^1,x^2 and x^3 are the spatial components. The metric tensor, which is locally Lorentz in nature, acts as a bilinear machine which facilitates the computation of the invariant distance between two nearby (infinitesimally close) events and is given by

$$ds^2 = g_{ab}dx^a dx^b, \tag{2.3.1}$$

which is known as the *line element*. The metric connection coefficients, $\Gamma^a{}_{bc}$, also known as the Christoffel symbols of the second kind, are expressed in terms of the metric tensor and its derivatives to yield

$$\Gamma^a{}_{bc} = \tfrac{1}{2}g^{ad}(g_{cd,b} + g_{db,c} - g_{bc,d}), \tag{2.3.2}$$

where commas imply partial differentiation. In simple terms, $\Gamma^a{}_{bc}$ represents the "a" component of the change in the basis vectors $\vec{e}_b$ as a consequence of parallel transport of a vector along the basis vectors $\vec{e}_c$ [53]. The connection coefficients preserve inner products under parallel transport and take into account the variation in the basis vectors from one event to another in spacetime. This encapsulates the fundamental theorem of Riemann geometry.

The Riemann curvature tensor, which is really an instrument that is used to measure the spacetime curvature, is obtained from the connection coefficients (2.3.2) and is given

by

$$R^{a}{}_{bcd} = \Gamma^{a}{}_{bd,c} - \Gamma^{a}{}_{bc,d} + \Gamma^{a}{}_{ec}\Gamma^{e}{}_{bd} - \Gamma^{a}{}_{ed}\Gamma^{e}{}_{bc}. \tag{2.3.3}$$

When we contract the Riemann tensor (2.3.3), with the aid of the metric tensor g_{ab}, we obtain the Ricci tensor R_{ab} given by

$$R_{ab} = g_{ea}g^{cd}R^{e}{}_{bcd} = \Gamma^{d}{}_{ab,d} - \Gamma^{d}{}_{ad,b} + \Gamma^{e}{}_{ab}\Gamma^{d}{}_{ed} - \Gamma^{e}{}_{ad}\Gamma^{d}{}_{eb}. \tag{2.3.4}$$

The Ricci scalar, R, is simply obtained by contracting the Ricci tensor (2.3.4) and is expressed as

$$R = g^{ab}R_{ab} = R^{a}{}_{a}. \tag{2.3.5}$$

The Einstein curvature, a rank two symmetric tensor, obtained from the Ricci tensor and Ricci scalar, is given by

$$G_{ab} = R_{ab} - \tfrac{1}{2}Rg_{ab}. \tag{2.3.6}$$

The covariant derivative of (2.3.6) has the form

$$G^{ab}{}_{;b} = 0, \tag{2.3.7}$$

where semicolons imply covariant differentiation. It is worthwhile noting that the (2.3.7) is known as the contracted Bianchi identity. The Einstein tensor is divergence–free, implying the local conservation of energy and momentum.

2.4 General overview of the energy momentum tensor

Up to this point, the emphasis has been on the description of the geometry of spacetime. We now focus on the description of the matter distribution which is represented by the energy momentum tensor T_{ab}. Being a tensor of rank two, T_{ab} has sixteen components. The sixteen components of the energy momentum tensor T_{ab} are explained in detail by Hartle [54]. Here we present an adapted version (in terms of indices a,b) based on the explanation due to Hartle [54]:

- T_{00} represents the energy density.
- T_{a0} represents the momentum density in direction "a".
- T_{ab} represents the a^{th} component of the force per unit area (shear stress) across a surface having a normal in the b^{th} direction ($a \neq b$).
- T_{0a} represents the energy flux in the a^{th} direction - energy flux $\equiv$ momentum density.
- $T_{ab} = p\delta_{ab}$ represent the diagonal pressure components ($a, b \neq 0$).

T_{ab}, is illustrated in Fig. 2.1.

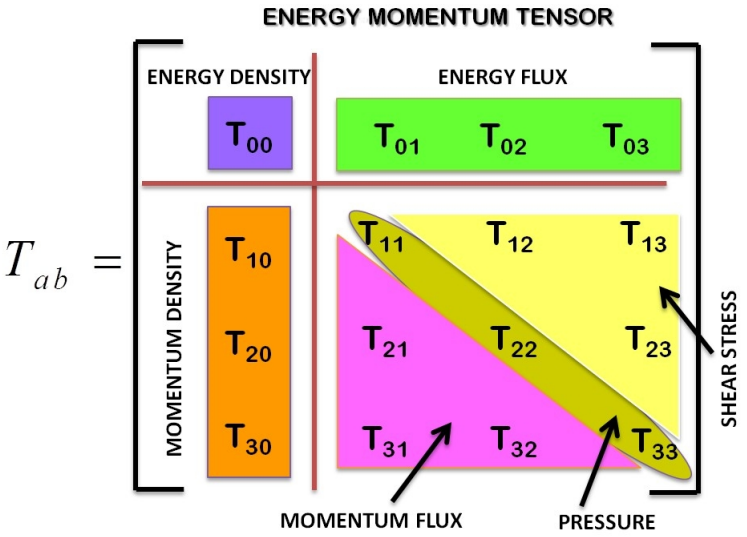

Figure 2.1: Overview of the energy momentum tensor.

Thus far, we have introduced the Einstein curvature tensor and we have discussed the energy momentum tensor which describes the matter distribution. Einstein, simply and elegantly, showed that spacetime curvature and matter energy are intimately and inextricably linked. In fact, according to Einstein, "*Space acts on matter, telling it how to move. In turn, matter reacts back on space, telling it how to curve*" [53]. This

relationship, expressed in geometrized units, is given by one of the most profound equations in physics

$$G_{ab} = T_{ab}. \tag{2.4.1}$$

Throughout this dissertation, we employ geometrized units wherein the speed of light c, and the coupling coefficient $8\pi G/c^4$ are taken to be unity. Equation (2.4.1) will be unpacked in great detail later to yield Einstein's field equations.

2.5 Spherically symmetric spacetimes

2.5.1 Line element

As explained earlier the line element measures the distance between two infinitesimally close points in spacetime. Here we obtain the line element for a particular choice of coordinate system. For a comoving reference frame the most general spherically symmetric line element, expressed in spherical coordinates $(x^a) = (t, r, \theta, \phi)$, is given by

$$ds^2 = -A^2dt^2 + B^2dr^2 + Y^2(d\theta^2 + \sin^2\theta d\phi^2), \tag{2.5.1}$$

where $A(t, r)$, $B(t, r)$ and $Y(t, r)$ represent gravitational potentials, and are also referred to as the metric coefficients. We note that the coordinates used in (2.5.1) are non–isotropic.

The metric tensor, g_{ab} associated with the line element (2.5.1) is a diagonal 4×4 matrix of the form

$$g_{ab} = \begin{pmatrix} -A^2 & 0 & 0 & 0 \\ 0 & B^2 & 0 & 0 \\ 0 & 0 & Y^2 & 0 \\ 0 & 0 & 0 & Y^2\sin^2\theta \end{pmatrix}. \tag{2.5.2}$$

The metric tensor g_{ab} is used extensively to raise or lower the indices of tensor quantities of different rank.

2.5.2 Christoffel symbols

The Christoffel symbols represent the magnitude of a vector's partial derivative of its basis vectors along the direction of the basis vectors themselves. For the line element (2.5.1), only sixteen non-zero connection coefficients (of the possible sixty four) remain and are of the form:

$$\Gamma^0{}_{00} = \frac{\dot{A}}{A} \qquad \Gamma^0{}_{01} = \frac{A'}{A} \qquad \Gamma^0{}_{33} = \frac{Y\dot{Y}\sin^2\theta}{A^2} \tag{2.5.3a}$$

$$\Gamma^0{}_{11} = \frac{B\dot{B}}{A^2} \qquad \Gamma^0{}_{22} = \frac{Y\dot{Y}}{A^2} \qquad \Gamma^1{}_{00} = \frac{AA'}{B^2} \tag{2.5.3b}$$

$$\Gamma^1{}_{01} = \frac{\dot{B}}{B} \qquad \Gamma^1{}_{11} = \frac{B'}{B} \qquad \Gamma^1{}_{22} = -\frac{YY'}{B^2} \tag{2.5.3c}$$

$$\Gamma^1{}_{33} = -\frac{YY'\sin^2\theta}{B^2} \qquad \Gamma^2{}_{02} = \frac{\dot{Y}}{Y} \qquad \Gamma^2{}_{12} = \frac{Y'}{Y} \tag{2.5.3d}$$

$$\Gamma^2{}_{33} = -\sin\theta\cos\theta \qquad \Gamma^3{}_{03} = \frac{\dot{Y}}{Y} \qquad \Gamma^3{}_{13} = \frac{Y'}{Y} \tag{2.5.3e}$$

$$\Gamma^3{}_{23} = \cot\theta, \tag{2.5.3f}$$

where dots and primes refer to differentiation with respect time and radial coordinates respectively.

2.5.3 Ricci tensor components and Ricci scalar

The non–zero Ricci tensor components (2.3.4) take the form

$$R_{00} = -\frac{\ddot{B}}{B} + \frac{\dot{A}}{A}\frac{\dot{B}}{B} + 2\frac{\dot{A}}{A}\frac{\dot{Y}}{Y} - 2\frac{\ddot{Y}}{Y}$$

$$+\frac{A^2}{B^2}\left(\frac{A''}{A} - \frac{A'}{A}\frac{B'}{B} + 2\frac{A'}{A}\frac{Y'}{Y}\right), \tag{2.5.4a}$$

$$R_{01} = 2\left(\frac{\dot{B}}{B}\frac{Y'}{Y} + \frac{A'}{A}\frac{\dot{Y}}{Y} - \frac{\dot{Y}'}{Y}\right), \tag{2.5.4b}$$

$$R_{11} = -\frac{A''}{A} + \frac{A'}{A}\frac{B'}{B} + 2\frac{B'}{B}\frac{Y'}{Y} - 2\frac{Y''}{Y}$$

$$+\frac{B^2}{A^2}\left(\frac{\ddot{B}}{B} - \frac{\dot{A}}{A}\frac{\dot{B}}{B} + 2\frac{\dot{B}}{B}\frac{\dot{Y}}{Y}\right), \tag{2.5.4c}$$

$$R_{22} = \frac{Y\dot{Y}}{A^2}\left(\frac{\dot{B}}{B} - \frac{\dot{A}}{A} + \frac{\dot{Y}}{Y} + \frac{\ddot{Y}}{\dot{Y}}\right)$$

$$+\frac{YY'}{B^2}\left(\frac{B'}{B} - \frac{A'}{A} - \frac{Y'}{Y} - \frac{Y''}{Y'}\right) + 1, \tag{2.5.4d}$$

$$R_{33} = \sin^2\theta R_{22}, \tag{2.5.4e}$$

for the line element given by (2.5.1). With the aid of (2.5.4a)–(2.5.4e), the Ricci scalar (2.3.5) becomes

$$R = \frac{2}{A^2}\left(\frac{\ddot{B}}{B} - \frac{\dot{A}}{A}\frac{\dot{B}}{B} + 2\frac{\dot{B}}{B}\frac{\dot{Y}}{Y} - 2\frac{\dot{A}}{A}\frac{\dot{Y}}{Y} + \frac{\dot{Y}^2}{Y^2} + 2\frac{\ddot{Y}}{Y}\right)$$

$$- \frac{2}{B^2}\left(\frac{A''}{A} - \frac{A'}{A}\frac{B'}{B} - 2\frac{B'}{B}\frac{Y'}{Y} + 2\frac{A'}{A}\frac{Y'}{Y} + \frac{Y'^2}{Y} + 2\frac{Y''}{Y}\right) + \frac{2}{Y^2}, \tag{2.5.5}$$

for the line element given by (2.5.1).

2.5.4 Einstein tensor components

By making use of (2.5.2), (2.5.4a)–(2.5.4e) and (2.5.5) in (2.3.6), we obtain the non–vanishing Einstein tensor components

$$G_{00} = 2\frac{\dot{B}}{B}\frac{\dot{Y}}{Y} + \frac{\dot{Y}^2}{Y^2} - \frac{A^2}{B^2}\left(-2\frac{B'}{B}\frac{Y'}{Y} + \frac{Y'^2}{Y^2} + 2\frac{Y''}{Y}\right) + \frac{A^2}{Y^2}, \tag{2.5.6a}$$

$$G_{11} = \frac{B^2}{A^2}\left(2\frac{\dot{A}}{A}\frac{\dot{Y}}{Y} - \frac{\dot{Y}^2}{Y^2} - 2\frac{\ddot{Y}}{Y}\right) + 2\frac{A'}{A}\frac{Y'}{Y} + \frac{Y'^2}{Y^2} - \frac{B^2}{Y^2}, \tag{2.5.6b}$$

$$G_{01} = 2\left(\frac{\dot{B}}{B}\frac{Y'}{Y} + \frac{A'}{A}\frac{\dot{Y}}{Y} - \frac{\dot{Y}'}{Y}\right), \tag{2.5.6c}$$

$$G_{22} = -\frac{Y^2}{A^2}\left(\frac{\ddot{B}}{B} - \frac{\dot{A}}{A}\frac{\dot{B}}{B} + \frac{\dot{B}}{B}\frac{\dot{Y}}{Y} - \frac{\dot{A}}{A}\frac{\dot{Y}}{Y} + \frac{\ddot{Y}}{Y}\right) + \frac{Y^2}{B^2}\left(\frac{A''}{A} - \frac{A'}{A}\frac{B'}{B} + \frac{A'}{A}\frac{Y'}{Y} - \frac{B'}{B}\frac{Y'}{Y} + \frac{Y''}{Y}\right), \tag{2.5.6d}$$

$$G_{33} = \sin^2\theta G_{22}, \tag{2.5.6e}$$

for spherically symmetric shearing spacetimes.

2.5.5 Energy momentum tensor: Imperfect fluid

The energy momentum tensor determines the amount of mass–energy which is contained in a unit volume. The mass–energy is the source of spacetime curvature which is measured by the Einstein tensor G_{ab}. A perfect fluid (modeled as an ideal gas) can be described as a collection of non-interacting particles traveling through spacetime with a four–velocity $\mathbf{V}$ and having energy density ρ and isotropic pressure p. It is worthwhile noting that the energy density ρ comprises the rest mass energy of the

particles, the kinetic energy of the particles, the energy associated with compression and nuclear binding energies to name but a few. See [53] for a more detailed treatment. If the fluid contains bulk viscosity, shear stresses, heat flow, anisotropic pressure and free–streaming radiation (photons) etc., then the fluid is not perfect. Following a similar treatment due to Herrera *et al* [55] we define the energy momentum tensor for an imperfect fluid to be given by

$$T_{ab} = (\rho + p_t + \Pi)V_a V_b + (p_t + \Pi)g_{ab} + (p_r - p_t)\chi_a\chi_b + q_a V_b + q_b V_a + \epsilon l_a l_b + \pi_{ab}, \quad (2.5.7)$$

where ρ is the energy density, p_r is the radial pressure, p_t is the tangential pressure, Π the bulk viscosity, V^a is the comoving unit timelike fluid four–velocity, χ_a is a radial unit four–vector, q^a is the heat flux, ϵ is the null radiation density, l_a is the null four-vector and π_{ab} is the shear viscosity tensor. These quantities satisfy

$$V^a V_a = -1, \qquad V^a q_a = 0, \qquad l^a V_a = -1, \qquad l^a l_a = 0, \quad (2.5.8a)$$

$$\chi^a\chi_a = 1, \qquad \chi^a V_a = 0, \qquad \pi_{ab}V^b = 0, \qquad \pi_{[ab]} = 0, \quad (2.5.8b)$$

$$\pi^a_a = 0, \quad (2.5.8c)$$

where $[ab]$ implies antisymmetrisation with respect to indices a, b. For the comoving metric (2.5.1) we have

$$V^a = (A^{-1}, 0, 0, 0), \qquad q^a = (0, q_1, 0, 0), \quad (2.5.9a)$$

$$l_a = (A^{-1}, B^{-1}, 0, 0), \qquad \chi^a = (0, B^{-1}, 0, 0), \quad (2.5.9b)$$

for the vectorial quantities.

2.5.6 Kinematical quantities

The kinematical quantities defined here are of paramount importance in the understanding of the physical behaviour of a dynamical system, such as a radiating star undergoing gravitational collapse.

Fluid four-acceleration

The four–acceleration vector **a** is given (in component form) by

$$\begin{aligned} a^a &= V^a{}_{;b} V^b \\ &= \Big(V^a{}_{,b} + \Gamma^a{}_{bc} V^c \Big) V^b. \end{aligned} \tag{2.5.10}$$

The only non-zero component of (2.5.10) for the line element (2.5.1) is along the radial direction

$$a^a = \left(0, \frac{A'}{A}, 0, 0 \right). \tag{2.5.11}$$

The magnitude of the acceleration is easily calculated to yield

$$|a| = (a^a a_a)^{1/2} = \frac{A'}{AB}. \tag{2.5.12}$$

Expansion scalar (rate of collapse)

The rate of collapse, Θ, which measures the "shrinkage" of the spherical stellar fluid as it collapses, has the from

$$\Theta = V^a{}_{;a} = \frac{1}{A} \Big(\frac{\dot{B}}{B} + 2 \frac{\dot{Y}}{Y} \Big). \tag{2.5.13}$$

Shear tensor

The shear tensor can be expressed in component form as

$$\sigma_{ab} = V_{(a;b)} + a_{(a} V_{b)} - \frac{1}{3} \Theta \big(g_{ab} + V_a V_b \big). \tag{2.5.14}$$

It can be easily shown that the non–zero components of the shear tensor are

$$\sigma_{11} = \frac{2}{3} B^2 \sigma, \quad \sigma_{22} = \frac{\sigma_{33}}{\sin^2 \theta} = -\frac{1}{3} Y^2 \sigma, \tag{2.5.15}$$

where the magnitude of the shear

$$\sigma = \frac{1}{A} \Big(\frac{\dot{B}}{B} - \frac{\dot{Y}}{Y} \Big), \tag{2.5.16}$$

is obtained from

$$\sigma_{ab} \sigma^{ab} = \frac{2}{3} \sigma^2. \tag{2.5.17}$$

Shear viscosity tensor

With the aid of (2.5.8) and (2.5.9) we can show that the non-zero components of π_{ab} are given by

$$\pi_{11} = -2\pi_{22} = -2\pi_{33}. \tag{2.5.18}$$

The shear viscosity tensor can be expressed as

$$\pi_{ab} = \Omega\Big(\chi_a\chi_b - \frac{1}{3}h_{ab}\Big), \tag{2.5.19}$$

where $h_{ab} = g_{ab}+V_aV_b$ is the projection tensor and $\Omega = \frac{3}{2}\pi_1^1$. In the context of standard irreversible thermodynamics [55, 56] the shear viscosity tensor, which is a measure of the internal friction between layers of the stellar fluid, can be given in terms of the shear tensor by

$$\pi_{ab} = -2\eta\sigma_{ab}, \tag{2.5.20}$$

where η is the coefficient of shear viscosity. With the aid of (2.5.19) and (2.5.20) it can be easily shown that $\Omega = -2\eta\sigma$.

Bulk viscosity

Once again, if we restrict ourselves to standard irreversible thermodynamics the bulk viscosity can be expressed [55] in terms of the expansion scalar as

$$\Pi = -\zeta\Theta, \tag{2.5.21}$$

where ζ is the coefficient of bulk viscosity. It has been pointed out [55, 56] that equations (2.5.20) and (2.5.21) will not be valid for the full causal treatment. See [57] (and references therein) for the details of the full causal expressions for equations (2.5.20) and (2.5.21).

2.6 Einstein's field equations: Shearing spacetimes

The Einstein field equations are obtained by equating the non-zero components of the Einstein curvature tensor G_{ab}, given by equations (2.5.6a)–(2.5.6e), to the corresponding non-zero components of the energy momentum tensor T_{ab} given by (2.5.7). This yields the Einstein field equations

$$\begin{aligned}\rho+\epsilon &= \frac{1}{A^2}\left(2\frac{\dot{B}}{B}+\frac{\dot{Y}}{Y}\right)\frac{\dot{Y}}{Y} \\ &\quad -\frac{1}{B^2}\left[2\frac{Y''}{Y}+\left(\frac{Y'}{Y}\right)^2-2\frac{B'}{B}\frac{Y'}{Y}-\left(\frac{B}{Y}\right)^2\right],\end{aligned} \tag{2.6.1a}$$

$$\begin{aligned}\Pi+p_r+\epsilon+\frac{2}{3}\Omega &= -\frac{1}{A^2}\left[2\frac{\ddot{Y}}{Y}-\left(2\frac{\dot{A}}{A}-\frac{\dot{Y}}{Y}\right)\frac{\dot{Y}}{Y}\right] \\ &\quad +\frac{1}{B^2}\left(2\frac{A'}{A}+\frac{Y'}{Y}\right)\frac{Y'}{Y}-\frac{1}{Y^2},\end{aligned} \tag{2.6.1b}$$

$$\begin{aligned}p_t+\Pi-\frac{1}{3}\Omega &= -\frac{1}{A^2}\left[\frac{\ddot{B}}{B}+\frac{\ddot{Y}}{Y}-\frac{\dot{A}}{A}\left(\frac{\dot{B}}{B}+\frac{\dot{Y}}{Y}\right)+\frac{\dot{B}}{B}\frac{\dot{Y}}{Y}\right] \\ &\quad +\frac{1}{B^2}\left[\frac{A''}{A}+\frac{Y''}{Y}-\frac{A'}{A}\frac{B'}{B}+\left(\frac{A'}{A}-\frac{B'}{B}\right)\frac{Y'}{Y}\right],\end{aligned} \tag{2.6.1c}$$

$$q_1 B+\epsilon = \frac{2}{AB}\left(\frac{\dot{Y}'}{Y}-\frac{\dot{B}}{B}\frac{Y'}{Y}-\frac{\dot{Y}}{Y}\frac{A'}{A}\right), \tag{2.6.1d}$$

where we note that $\Omega=-2\eta\sigma$. The field equations (2.6.1a)–(2.6.1d) comprise a system of four coupled partial differential equations with ten unknowns. The field equations hold knowledge about the equations of motion for matter whose energy momentum produces the curvature of spacetime. They govern and fully describe how a massive star experiencing ongoing gravitational collapse ends up as a black hole or a singularity in the spacetime fabric [53]. We employ the Einstein field equations to study the gravitational collapse of a massive star. We seek to describe the gravitational behaviour of such as star by assuming a spherically symmetric matter distribution comprising of heat flux, free–streaming radiation (photons), shear viscosity and bulk viscosity. By making suitable choices for the metric functions A, B and Y, it is possible (after some

tedious calculations or computations) to determine ρ, p_r, p_t, q_1, Ω and Π.

The magnitude of the radially directed heat flow is given by

$$Q = (q^a q_a)^{\frac{1}{2}} = q_1 B. \tag{2.6.2}$$

Equation (2.6.1d) can be re-written using (2.5.13) and (2.5.16) as follows

$$q_1 B + \epsilon = \frac{1}{B}\Big[\frac{2}{3}\big(\Theta - \sigma\big)' - \frac{2Y'\sigma}{Y}\Big]. \tag{2.6.3}$$

The mass function $m(t,r)$ is given by

$$m(t,r) = \frac{Y}{2}\left[\left(\frac{\dot{Y}}{Y}\right)^2 - \left(\frac{Y'}{B}\right)^2 + 1\right]. \tag{2.6.4}$$

The non–zero components of the Bianchi identities, $T^{ab}{}_{;b} = 0$ yield (in the absence of bulk viscosity and shear viscosity)

$$\begin{aligned} T^{ab}{}_{;b}V_a &= -\frac{1}{A}\left[\dot{\mu} + \dot{\epsilon} + 2\frac{A'}{B}\left(q_1 B + \epsilon\right) + q_1' A + \frac{\epsilon' A}{B} + \frac{\dot{B}}{B}\left(\mu + 2\epsilon + p_r\right)\right. \\ &\quad \left. + \frac{2\dot{Y}}{Y}\left(\mu + \epsilon + p_t\right) + 2\frac{AY'}{YB}\left(q_1 B + \epsilon\right) + \frac{q_1 B' A}{B}\right] = 0, \end{aligned} \tag{2.6.5}$$

which represents energy conservation, and

$$\begin{aligned} T^{ab}{}_{;b}\chi_a &= \frac{1}{B}\left[\frac{B}{A}\left(\dot{q}_1 B + \dot{\epsilon}\right) + \frac{\dot{B}}{A}\left(3Bq_1 + 2\epsilon\right) + \frac{A'}{A}\left(p_r + \mu + 2\epsilon\right) + {p_r}' + \epsilon'\right. \\ &\quad \left. + 2\frac{\dot{Y}B}{YA}\left(q_1 B + \epsilon\right) + 2\frac{Y'}{Y}\left(p_r + \epsilon - p_t\right)\right] = 0, \end{aligned} \tag{2.6.6}$$

which represents momentum conservation.

2.7 Field equations: Shear-free spacetimes

For the shear–free case we set $\sigma = 0$ in equation (2.5.16) to obtain the shear–free condition

$$\frac{\dot{B}}{B} = \frac{\dot{Y}}{Y},$$

where $Y = rB$. The shear–free line element is then

$$ds^2 = -A^2 dt^2 + B^2\left[dr^2 + r^2(d\theta^2 + \sin^2\theta d\phi^2)\right], \tag{2.7.1}$$

where A, B are both functions of t and r. We note that the line element given by (2.7.1) is isotropic and comoving. For this line element (2.7.1) the Einstein field equations (2.6.1a)–(2.6.1d), in the absence of shear ($\Omega = 0$), become

$$\rho + \epsilon = \frac{3}{A^2}\frac{\dot{B}^2}{B^2} - \frac{1}{B^2}\left(2\frac{B''}{B} - \frac{B'^2}{B^2} + \frac{4}{r}\frac{B'}{B}\right), \tag{2.7.2a}$$

$$\begin{aligned} p_r + \Pi + \epsilon &= \frac{1}{A^2}\left(-2\frac{\ddot{B}}{B} - \frac{\dot{B}^2}{B^2} + 2\frac{\dot{A}}{A}\frac{\dot{B}}{B}\right) \\ &\quad + \frac{1}{B^2}\left(\frac{B'^2}{B^2} + 2\frac{A'}{A}\frac{B'}{B} + \frac{2}{r}\frac{A'}{A} + \frac{2}{r}\frac{B'}{B}\right), \end{aligned} \tag{2.7.2b}$$

$$\begin{aligned} p_t + \Pi &= -2\frac{1}{A^2}\frac{\ddot{B}}{B} + 2\frac{\dot{A}}{A^3}\frac{\dot{B}}{B} - \frac{1}{A^2}\frac{\dot{B}^2}{B^2} + \frac{1}{r}\frac{A'}{A}\frac{1}{B^2} \\ &\quad + \frac{1}{r}\frac{B'}{B^3} + \frac{A''}{A}\frac{1}{B^2} - \frac{B'^2}{B^4} + \frac{B''}{B^3}, \end{aligned} \tag{2.7.2c}$$

$$q_1 B + \epsilon = \frac{2}{AB}\left(\frac{\dot{B}'}{B} - \frac{B'\dot{B}}{B^2} - \frac{A'}{A}\frac{\dot{B}}{B}\right). \tag{2.7.2d}$$

It is important to define the anisotropic parameter, Δ, which is the difference between the radial and the tangential pressure in the stellar fluid distribution.

$$\Delta = p_t - p_r. \tag{2.7.3}$$

For pressure isotropy we set $\Delta = 0$ in equation (2.7.3), effectively equating the radial and the tangential pressures. By employing the condition for pressure isotropy in the radiation–free limit ($\epsilon = 0$), the field equations (2.7.2b) and (2.7.2c) imply

$$\frac{A''}{A} + \frac{B''}{B} = \left(2\frac{B'}{B} + \frac{1}{r}\right)\left(\frac{A'}{A} + \frac{B'}{B}\right). \tag{2.7.4}$$

This condition has to be solved to describe the interior matter distribution and the physical behaviour of the system.

2.8 Exterior spacetime: Vaidya atmosphere

In 1939 Oppenheimer and Snyder [6] published their non-static solution to the Einstein field equations based on their study of continued gravitational collapse of a star (which had exhausted it's nuclear fuel) modeled as a spherically symmetric dust cloud surrounded by vacuum (the Schwarzschild exterior spacetime). This work paved the way for the study of gravitational collapse of massive stars and in particular led to the Vaidya [15] solution (for a non-static null fluid) based on the idea that any dissipating matter distribution ought to be radiating energy into its surrounding atmosphere. The Vaidya solution is the unique solution of the Einstein's field equations and describes the exterior spacetime of a spherically symmetric star radiating energy in the form of neutrinos, electromagnetic waves of high frequency or incoherent electromagnetic radiation. This metric is given by

$$ds^2 = -\left(1 - \frac{2m(v)}{\mathcal{R}}\right) dv^2 - 2dvd\mathcal{R} + \mathcal{R}^2\left(d\theta^2 + \sin^2\theta d\phi^2\right), \tag{2.8.1}$$

with coordinates given by $(x^a) = (v, \mathcal{R}, \theta, \phi)$. The quantity $m(v)$ is simply the Newtonian mass of the self–gravitating object that an observer an infinite distance away will measure. The energy momentum tensor for the exterior matter distribution, i.e. the null radiation, is given by

$$T_{ab} = \epsilon l_a l_b.$$

where $l_a = (1, 0, 0, 0)$ is a radial null four–vector defined for the Vaidya solution satisfying the condition $l^a l_a = 0$. The Ricci tensor has only one non-vanishing component, viz.

$$R_{00} = -\frac{2}{\mathcal{R}^2}\frac{dm}{dv}.$$

The Ricci scalar (2.3.5) for the line element given by (2.5.1) is $R = 0$. Thus the only non-zero component of the Einstein tensor (2.3.6) is

$$G_{00} = -\frac{2}{\mathcal{R}^2}\frac{dm}{dv}. \tag{2.8.2}$$

It can be shown that the only surviving component of T_{ab} is given by

$$T_{00} = \epsilon.$$

From the Einstein equation $G_{ab} = T_{ab}$ it follows that

$$\epsilon = -\frac{2}{\mathcal{R}^2}\frac{dm}{dv}. \tag{2.8.3}$$

The radiation energy density (ϵ) has to be positive. Therefore it follows that

$$\frac{dm}{dv} \leq 0.$$

A negative rate of change of mass implies that the mass function $m(v)$ decreases with proper time v which is reasonable since the star is losing energy in the form of radially directed radiation.

Chapter 3

Junction conditions

A star essentially separates spacetime into two very distinguishable regions, viz. the interior of a star (everything from the surface inward) containing matter and radiation and the exterior of a star (outside the star's surface) which generally contains radiation emanating from the interior of the star [58]. Solutions to Einstein's field equations for the interior of a star have been obtained by Oppenheimer and Snyder [6], for the non-adiabatic collapse of a spherically symmetric matter distribution in the form of a dust cloud having a Schwarzschild exterior, and by Misner and Sharp [59] for an interior matter distribution modeled as a perfect fluid with a static exterior. The solution to Einstein's field equations for a vacuum exterior is the Schwarzschild [13, 14] solution while the Vaidya [15] solution describes the exterior of a star containing null radiation. The solutions to Einstein's field equations for both the interior and the exterior spacetime can be "glued" together to produce a complete picture of the collapse process. We call this the matching of the interior and exterior spacetimes of the star, and this is achieved by employing a set of junction conditions. The criteria for the smooth matching or continuity of the interior and exterior solutions are due to Darmois [60], Lichnerowicz [61] and O' Brien and Synge [62]. The junction conditions given by Darmois and O' Brien and Synge are equivalent as shown by Bonnor and Vickers [63].

Early work [59], [64] on adiabatic collapse showed that the pressure vanishes at the

boundary of a static star, which was widely accepted for a notable period of time. Then, Santos [16], employing the approach of Israel [65], produced the first set of shear–free junction conditions for dissipative collapse (non–adiabatic with null radiation) which tells us that the pressure at the boundary of a star is proportional to the magnitude of the heat flow. Applying these junction conditions to the Einstein field equations yields the temporal evolution equation for the metric functions as shown in [16, 18, 19, 20]. Santos [16] points out that the pressure at the boundary is non–vanishing in general and will only disappear when the heat flow vanishes. Santos also shows that his boundary conditions are a consequence of the "*local conservation of momentum*" across the hypersurface (see references within [16]). This pioneering work by Santos opened the floodgate to the study of dissipative collapse and led to the derivation of an array of junction conditions for viz. shear (geodesic motion) [66], shearing viscous collapse [67, 68], nonadiabatic charged collapse [21, 69] as well as for a full causal treatment which includes bulk viscosity [55]. In this chapter we employ a similar approach to junction conditions to that of Govender [52], Naidu [70] and Fleming [71]. However, we provide more detail regarding the derivations of the junction conditions and we generalise their expressions (for the charge–free case) to include bulk viscosity, shear viscosity and free–streaming radiation.

3.1 Shearing spacetimes

For spherically symmetric spacetimes, moving along the world line of constant time (timelike) will yield concentric spherical surfaces called three–surfaces. These can be likened to looking at two–dimensional surfaces in three–dimensional space. We consider such three–surfaces, also referred to as the boundary or hypersurface, as a spherical timelike three–space (Σ) of a radiating star which separates spacetime into two well defined and distinguishable regions, viz. the interior spacetime ($\mathcal{Z}^-$) and the exterior spacetime ($\mathcal{Z}^+$). Each of these regions ($\mathcal{Z}^-$ and $\mathcal{Z}^+$) is described by a unique continuous

four–dimensional manifold containing a timelike three–space Σ as its boundary. We follow the treatments employed by Santos [16] and Oliveira and Santos [17] (effectively utilizing the Darmois [60] conditions) to generate the junction conditions for our model. This entails the smooth matching of the coordinates describing the interior spacetime with the coordinates on the hypersurface (timelike) which is then matched to the exterior spacetime. We know that the coordinates describing the respective spacetimes and the hypersurface will each have an associated curvature - related to the appropriate metric tensor. Matching of the curvature (interior to hypersurface and hypersurface to exterior) will be done and that will conclude the application of the junction conditions. We derive junction conditions for a dissipative system with heat flow, shear viscosity, bulk viscosity and null radiation, similar to work carried out by Herrera *et al* [55].

We assume that the boundary Σ is furnished with an intrinsic metric g_{ij} such that

$$ds^2_\Sigma = g_{ij}d\xi^i d\xi^j.$$

It follows that the intrinsic coordinates to Σ are given by ξ^i where $i, j = 1, 2, 3$ i.e. (η, θ, ϕ). We note that η is the proper time on the hypersurface Σ. The line elements in the regions $\mathcal{Z}^\pm$ take the form

$$ds^2{}_\pm = g_{ab}d\mathcal{X}^a_\pm d\mathcal{X}^b_\pm.$$

The coordinates in $\mathcal{Z}^\pm$ are $\mathcal{X}^a_\pm$ where $a = 0, 1, 2, 3$ i.e. $\mathcal{X}^a_- = (t, r, \theta, \phi)$ for the interior spacetime and $\mathcal{X}^a_+ = (v, \mathcal{R}, \theta, \phi)$ for the exterior spacetime, where v is the retarded time. When approaching Σ from the exterior $\mathcal{Z}^+$ or the interior spacetime $\mathcal{Z}^-$ we demand

$$(ds^2_-)_\Sigma = (ds^2_+)_\Sigma = ds^2_\Sigma, \tag{3.1.1}$$

where $(\ )_\Sigma$ represents the value of $(\ )$ on the hypersurface Σ. As a result, the coordinates of Σ in $\mathcal{Z}^\pm$ are a function of the intrinsic coordinates and are given by $\mathcal{X}^a_\pm = \mathcal{X}^a_\pm(\xi^i)$. Continuity of the intrinsic metrics across Σ generates the first junction condition. The second junction condition is obtained by requiring the continuity of the

extrinsic curvature components of Σ across the boundary. This yields

$$K_{ij}^{+} = K_{ij}^{-}, \tag{3.1.2}$$

where

$$K_{ij}^{\pm} \equiv -n_a^{\pm} \frac{\partial^2 \mathcal{X}_{\pm}^a}{\partial \xi^i \partial \xi^j} - n_a^{\pm} \Gamma^a{}_{cd} \frac{\partial \mathcal{X}_{\pm}^c}{\partial \xi^i} \frac{\partial \mathcal{X}_{\pm}^d}{\partial \xi^j}, \tag{3.1.3}$$

and $n_a^{\pm}(\mathcal{X}_{\pm}^b)$ represent the components of the vector normal to Σ. For a more detailed formulation of the junction conditions the reader is referred to the works by Bonnor and Vickers [63] and Lake [72]. The junction conditions given by (3.1.1) and (3.1.2) correspond to those obtained by Lichnerowicz [61] and O'Brien and Synge [62].

3.1.1 Matching: Interior spacetime $\mathcal{Z}^-$ to the hypersurface Σ

First junction condition: Matching of the metrics

The intrinsic metric to the hypersurface Σ is given by line the element

$$ds_{\Sigma}^2 = -d\eta^2 + \mathcal{Y}^2(d\theta^2 + \sin^2\theta d\phi^2), \tag{3.1.4}$$

with coordinates $\xi^i = (\eta, \theta, \phi)$ and $\mathcal{Y} = \mathcal{Y}(\eta)$. We note that the time coordinate η is defined only on the hypersurface surface Σ. It is an intermediate variable which will be eliminated later. The interior spacetime $\mathcal{Z}^-$, in comoving coordinates, is described by a spherically symmetric line element given by (2.5.1)

$$ds^2 = -A^2 dt^2 + B^2 dr^2 + Y^2(d\theta^2 + \sin^2\theta d\phi^2).$$

The boundary of the interior matter distribution $\mathcal{Z}^-$ is described by the relation

$$f(t, r) = r - r_{\Sigma} = 0,$$

where r_{Σ} is a constant. The vector having components $\dfrac{\partial f}{\partial \mathcal{X}_{-}^a}$ is orthogonal to the hypersurface Σ. We define a radially directed vector $n_a = (0, 1, 0, 0)$ on $f(t, r)$ orthogonal to the hypersurface Σ such that the unit normal to Σ is given by

$$n_a^{-} = \frac{n_a}{|n_a|}.$$

It is easy to show that

$$n^a = \Big(0, \frac{1}{B^2(t, r_\Sigma)}, 0, 0\Big),$$

and

$$|n_a| = \sqrt{n^a n_a} = \frac{1}{B(t, r_\Sigma)}.$$

Hence the unit vector normal to Σ takes the form

$$n_a^- = [0, B(t, r_\Sigma), 0, 0]. \tag{3.1.5}$$

The first junction condition (3.1.1), for the metrics (3.1.4) and (2.5.1), yields the restrictions

$$A(t, r_\Sigma)\dot{t} \;=\; 1, \tag{3.1.6a}$$

$$Y(t, r_\Sigma) \;=\; \mathcal{Y}(\eta), \tag{3.1.6b}$$

where

$$\dot{t} = \frac{dt}{d\eta}.$$

3.1.2 Matching: Exterior spacetime $\mathcal{Z}^+$ to the hypersurface Σ

First junction condition: Matching of the metrics

The exterior spacetime $\mathcal{Z}^+$ of the radiating star is described by the Vaidya line element (2.8.1) introduced earlier

$$ds^2 = -\left(1 - \frac{2m(v)}{\mathcal{R}}\right) dv^2 - 2dvd\mathcal{R} + \mathcal{R}^2\left(d\theta^2 + \sin^2\theta d\phi^2\right),$$

which can be re–cast as

$$ds^2 = -\left(1 - \frac{2m(v)}{\mathcal{R}} + 2\frac{d\mathcal{R}}{dv}\right) dv^2 + \mathcal{R}^2\left(d\theta^2 + \sin^2\theta d\phi^2\right). \tag{3.1.7}$$

The defining equation for the surface Σ in $\mathcal{Z}^+$ is given by

$$f(v, \mathcal{R}) = \mathcal{R} - \mathcal{R}_\Sigma(v) = 0,$$

We define the vector orthogonal to Σ as

$$n_a = \frac{\partial f}{\partial \mathcal{X}^a_+} = \left(-\frac{d\mathcal{R}_\Sigma}{dv}, 1, 0, 0\right),$$

such that the unit normal to Σ is given by

$$n^+_a = \frac{n_a}{|n_a|}.$$

After some calculations it can be shown that

$$n^a = \left(-1, 1 - \frac{m(v)}{\mathcal{R}_\Sigma} + 2\frac{d\mathcal{R}_\Sigma}{dv}, 0, 0\right),$$

and

$$|n_a| = \sqrt{n^a n_a} = \left(1 - 2\frac{m(v)}{\mathcal{R}_\Sigma} + 2\frac{d\mathcal{R}_\Sigma}{dv}\right)^{\frac{1}{2}}.$$

Hence the unit normal to Σ can be cast into the following form

$$n^+_a = \left(1 - \frac{2m(v)}{\mathcal{R}_\Sigma} + 2\frac{d\mathcal{R}_\Sigma}{dv}\right)^{-\frac{1}{2}} \left(-\frac{d\mathcal{R}_\Sigma}{dv}, 1, 0, 0\right). \tag{3.1.8}$$

For $\mathcal{Z}^+$ the first junction condition (3.1.1) is satisfied by matching the intrinsic line element (3.1.4) to the line element of the exterior Vaidya spacetime (2.8.1). Subsequently we arrive at the conditions.

$$\mathcal{R}_\Sigma(v) = \mathcal{Y}(\eta), \tag{3.1.9a}$$

$$\left(1 - \frac{2m(v)}{\mathcal{R}} + 2\frac{d\mathcal{R}}{dv}\right)_\Sigma = \left(\frac{1}{\dot{v}^2}\right)_\Sigma, \tag{3.1.9b}$$

where

$$\dot{v} = \frac{dv}{d\eta}. \tag{3.1.10}$$

3.1.3 Summary: The first junction condition

The results of the first junction condition (3.1.1) can be collectively written as

$$A(t, r_\Sigma)\dot{t} = 1, \tag{3.1.11a}$$

$$Y(t, r_\Sigma) = \mathcal{Y}(\eta), \tag{3.1.11b}$$

$$\mathcal{R}_\Sigma(v) = \mathcal{Y}(\eta), \tag{3.1.11c}$$

$$\left(1 - \frac{2m(v)}{\mathcal{R}} + 2\frac{d\mathcal{R}}{dv}\right)_\Sigma = \left(\frac{1}{\dot{v}^2}\right)_\Sigma. \tag{3.1.11d}$$

Upon eliminating η from the above equations we are able to obtain the necessary and sufficient conditions required by the spacetime geometry for the first junction condition (3.1.1) to be satisfied. These conditions are as follows

$$A(t, r_\Sigma)dt = \left(1 - \frac{2m(v)}{\mathcal{R}_\Sigma} + 2\frac{d\mathcal{R}_\Sigma}{dv}\right)^{\frac{1}{2}} dv, \tag{3.1.12a}$$

$$Y(t, r_\Sigma) = \mathcal{R}_\Sigma(v). \tag{3.1.12b}$$

3.1.4 The second junction condition: Matching curvature

Extrinsic curvature: Interior spacetime K^-_{ij}

The extrinsic curvature for the interior spacetime K^-_{ij} can be determined by employing (2.3.2), (2.5.1), (3.1.3) and (3.1.5). After tedious calculation we obtain the nonzero

components of K^{-}_{ij} to be given by

$$K^{-}_{\eta\eta} = \left(-\frac{1}{B}\frac{A'}{A}\right)_{\Sigma}, \tag{3.1.13a}$$

$$K^{-}_{\theta\theta} = \left(\frac{YY'}{B}\right)_{\Sigma}, \tag{3.1.13b}$$

$$K^{-}_{\phi\phi} = \sin^2\theta\, K^{-}_{\theta\theta}, \tag{3.1.13c}$$

which are valid on the hypersurface Σ.

Extrinsic curvature: Exterior spacetime K^{+}_{ij}

With the aid of (3.1.9b) we can rewrite the unit normal vector (3.1.8) as

$$n^{+}_{a} = (-\dot{\mathcal{R}}, \dot{v}, 0, 0), \tag{3.1.14}$$

where dots represent differentiation with respect to η. After lengthy calculations, the nonvanishing components of the extrinsic curvature tensor for the exterior spacetime emerge as

$$K^{+}_{\eta\eta} = \left[\frac{\ddot{v}}{\dot{v}} - \dot{v}\frac{m(v)}{\mathcal{R}^2}\right]_{\Sigma}, \tag{3.1.15a}$$

$$K^{+}_{\theta\theta} = \left[\dot{v}\left(1 - \frac{2m(v)}{\mathcal{R}}\right)\mathcal{R} + \mathcal{R}\dot{\mathcal{R}}\right]_{\Sigma}, \tag{3.1.15b}$$

$$K^{+}_{\phi\phi} = \sin^2\theta\, K^{+}_{\theta\theta}, \tag{3.1.15c}$$

which are valid on the hypersurface Σ.

Upon equating the corresponding extrinsic curvature components for the interior (3.1.13) and exterior (3.1.15), the second set of junctions stipulated by (3.1.2) are

obtained as follows

$$\left(-\frac{1}{B}\frac{A^{'}}{A}\right)_{\Sigma} = \left[\frac{\ddot{v}}{\dot{v}} - \dot{v}\frac{m(v)}{\mathcal{R}^2}\right]_{\Sigma}, \tag{3.1.16a}$$

$$\left(\frac{YY^{'}}{B}\right)_{\Sigma} = \left[\dot{v}\left(1-\frac{2m(v)}{\mathcal{R}}\right)\mathcal{R} + \mathcal{R}\dot{\mathcal{R}}\right]_{\Sigma}. \tag{3.1.16b}$$

From (3.1.12b) and (3.1.6a) we can write

$$\dot{\mathcal{R}}_{\Sigma} = \left(\frac{\dot{Y}}{A}\right)_{\Sigma}. \tag{3.1.17}$$

Upon substitution for $\mathcal{R}_{\Sigma}$ from (3.1.12b), $\dot{\mathcal{R}}_{\Sigma}$ from (3.1.17) and

$$\dot{v} = \left[-\frac{2\dot{Y}}{A} \pm \sqrt{\left(\frac{2\dot{Y}}{A}\right)^2 + 4\Big(1-2\frac{m(v)}{\mathcal{R}}\Big)}\right] \Bigg/ 2\Big(1-2\frac{m(v)}{\mathcal{R}}\Big)_{\Sigma}, \tag{3.1.18}$$

into (3.1.16b), the mass $m(v)$ function can be expressed in terms of the metric functions alone. The mass function is given by

$$m(v) = \left[\frac{Y}{2}\left(1+\frac{\dot{Y}^2}{A^2} - \frac{Y^{'2}}{B^2}\right)\right]_{\Sigma}. \tag{3.1.19}$$

The function $m(v)$ represents the total gravitational mass which is contained within the hypersurface Σ. Similar expressions for $m(v)$ have been obtained by other investigators [73, 74]. Upon substitution of (3.1.17) and (3.1.19) in (3.1.16b) we obtain

$$\dot{v}_{\Sigma} = \left(\frac{\dot{Y}}{A} + \frac{Y^{'}}{B}\right)^{-1}_{\Sigma}. \tag{3.1.20}$$

Differentiating (3.1.20) with respect to η and making use of (3.1.6a) results in an expression for $\ddot{v}_{\Sigma}$ given by

$$\ddot{v}_{\Sigma} = \left[-\frac{1}{A}\left(\frac{\dot{Y}}{A} + \frac{Y^{'}}{B}\right)^{-2}\left(\frac{\dot{Y}^{'}}{B} - \frac{\dot{B}Y^{'}}{B^2} - \frac{\dot{A}\dot{Y}}{A^2} + \frac{\ddot{Y}}{A}\right)\right]_{\Sigma}. \tag{3.1.21}$$

Then, by substituting (3.1.12b), (3.1.19), (3.1.20) and (3.1.21) into (3.1.16a) we arrive at the following expression

$$\left(-\frac{1}{B}\frac{A^{'}}{A}\right)_{\Sigma} = \left[\left(-\frac{\dot{Y}^{\prime}}{B} + \frac{\dot{B}Y^{\prime}}{B^2} + \frac{\dot{A}\dot{Y}}{A^2} - \frac{\ddot{Y}}{A} - \frac{\dot{Y}^2}{2AY} + \frac{A}{2Y}\left(\frac{Y^{\prime 2}}{B^2} - 1\right)\right) \times \left(\frac{\dot{Y}}{A} + \frac{Y^{'}}{B}\right)^{-1}\right]_{\Sigma}. \tag{3.1.22}$$

If we multiply both sides of the above equation by $\left(\frac{\dot{Y}}{A}+\frac{Y'}{B}\right)$, utilise Einstein field equations (2.6.1b) and (2.6.1d), and then simplify, we arrive at one of the most important equations describing gravitational collapse, i.e.

$$\left(p_r+\Pi+\frac{2}{3}\Omega+\epsilon\right)_\Sigma=\left(q_1B+\epsilon\right)_\Sigma. \tag{3.1.23}$$

3.1.5 Summary: The second junction condition

Therefore the necessary and sufficient conditions placed on the spacetimes, for the satisfying of the second junction condition (3.1.2), are

$$m(v) = \left[\frac{Y}{2}\left(1+\frac{\dot{Y}^2}{A^2}-\frac{Y'^2}{B^2}\right)\right]_\Sigma, \tag{3.1.24a}$$

$$\left(p_r+\Pi+\frac{2}{3}\Omega+\epsilon\right)_\Sigma = \left(q_1B+\epsilon\right)_\Sigma. \tag{3.1.24b}$$

It is worthwhile noting that the junction condition (3.1.24a) and (3.1.24b) are independent of any particular form for the metric functions A, B or Y, but rather has been established as a general result for spherically symmetric, shearing spacetimes. Since the radiation energy density ϵ appears on both sides of equation of (3.1.24b), we can re-write (3.1.24b) as

$$\left(p_r+\Pi+\frac{2}{3}\Omega\right)_\Sigma=\left(q_1B\right)_\Sigma. \tag{3.1.25}$$

According to [55], the left hand side of (3.1.25) can be regarded as an "effective" radial pressure. If we relax the bulk viscosity and but not the shear viscosity, we obtain the result (for shearing spacetime) of Naidu *et al* [37] viz. $\left(p_r\right)_\Sigma=\left(q_1B\right)_\Sigma$. The most general matching conditions for the spherically symmetric shearing spacetimes $\mathcal{Z}^+$ and $\mathcal{Z}^-$ are given by equations (3.1.12) and (3.1.24). Equation (3.1.24b) simply tells us that the effective radial pressure comprising of the radial pressure, the bulk viscous pressure and the shear stress, is proportional to the magnitude of the heat flow q_1B which is nonvanishing in general [55]. Thus, the radial pressure $\left(p_r\right)_\Sigma$ on the boundary can only be zero when the heat flow $\left(q_1B\right)_\Sigma$, the bulk viscosity Π and the shear viscosity Ω are

all zero. When this happens, no heat is radiated to the exterior spacetime and thus the exterior spacetime is no longer the Vaidya spacetime but becomes the Schwarzschild exterior spacetime.

3.1.6 Junction conditions: Shear–free limit

If we relax the bulk viscosity and the shear viscosity we obtain the Santos [16] junction conditions in the shear–free limit with isotropic pressure, given by

$$A(t,r_\Sigma)dt = \left(1-\frac{2m}{\mathsf{r}_\Sigma}+2\frac{d\mathsf{r}_\Sigma}{dv}\right)^{\frac{1}{2}}dv, \tag{3.1.26a}$$

$$r_\Sigma B(t,r_\Sigma) = \mathsf{r}_\Sigma(v), \tag{3.1.26b}$$

$$m(v) = \left(\frac{r^3B}{2A^2}{B_t}^2-r^2B_r-\frac{r^3}{2B}{B_r}^2\right)_\Sigma, \tag{3.1.26c}$$

$$p_\Sigma = (q_1B)_\Sigma. \tag{3.1.26d}$$

3.1.7 Physical interpretation of equation (3.1.24b)

There is a physical interpretation to equation (3.1.24b), which can be arrived at by taking into account the momentum flux across the boundary in the radial direction. With the knowledge that (3.1.19) represents the total energy for a sphere of radius r lying within the hypersurface Σ we are able to express the mass as a function of radial and time coordinates, viz.

$$m(t,r)=\left[\frac{Y}{2}\left(1+\frac{\dot{Y}^2}{A^2}-\frac{Y'^2}{B^2}\right)\right]_\Sigma.$$

Partial differentiation of $m(t,r)$ with respect to t yields

$$\left(\frac{\partial m}{\partial t}\right)_{\Sigma} = \left[\dot{Y}\left(\frac{\ddot{Y}Y}{A^2}+\frac{\dot{Y}^2}{2A^2}-\frac{Y'^2}{2B^2}-\frac{\dot{A}\dot{Y}Y}{A^3}+\frac{1}{2}\right)\right.$$

$$\left.-\frac{Y'\dot{Y}'Y}{B^2}+\frac{\dot{B}Y'^2Y}{B^3}\right]_{\Sigma}.$$

With the aid of the field equations (2.6.1b) and (2.6.1d) we are in a position to re–cast the expression $\left(\frac{\partial m}{\partial t}\right)_{\Sigma}$ as

$$\left(\frac{\partial m}{\partial t}\right)_{\Sigma} = \left[-\frac{Y^2}{2}\left(\dot{Y}\big(p_r+\Pi+\epsilon+\frac{2}{3}\Omega\big)+\frac{AY'}{B}\big(q_1B+\epsilon\big)\right)\right]_{\Sigma}. \tag{3.1.27}$$

Substitution of (3.1.24b) in (3.1.27) yields

$$\left(\frac{\partial m}{\partial t}\right)_{\Sigma} = \left[-\frac{AY^2}{2}\left(\frac{\dot{Y}}{A}+\frac{Y'}{B}\right)\Big(p_r+\Pi+\epsilon+\frac{2}{3}\Omega\Big)\right]_{\Sigma}. \tag{3.1.28}$$

The fact that the radial coordinate is comoving with respect to the hypersurface Σ enables us to write

$$\left(\frac{\partial m}{\partial t}\right)_{\Sigma} = \left(\frac{dm}{dt}\right)_{\Sigma} = \left(\frac{\dot{v}}{\dot{t}}\frac{dm}{dv}\right)_{\Sigma}. \tag{3.1.29}$$

If we consider (3.1.6), (3.1.12b), (3.1.28) and (3.1.29) we are able to show that

$$\left(-\frac{2}{\mathcal{R}^2}\frac{dm}{dv}\dot{v}^2\right)_{\Sigma} = \Big(p_r+\Pi+\epsilon+\frac{2}{3}\Omega\Big)_{\Sigma}. \tag{3.1.30}$$

From the initiatives of Lindquist *et al* [75] we know that the energy density of the radiation detected by an observer situated on the hypersurface Σ (having a four–velocity v^a) is expressed as

$$\epsilon = v^a v^b T_{ab}, \tag{3.1.31}$$

where the four–velocity expressed in component form is

$$v^a = (\dot{v}, \dot{\mathcal{R}}, 0, 0). \tag{3.1.32}$$

The Einstein tensor for the metric (2.8.1) is given by

$$G_{ab} = -\frac{2}{\mathcal{R}^2}\frac{dm}{dv}\delta^0_a\delta^0_b = T_{ab}. \tag{3.1.33}$$

Employing (3.1.33) and (3.1.32) in equation (3.1.31) we obtain the radiation energy density that an observer situated on the hypersurface Σ measures, i.e.

$$\epsilon = \left(-\frac{2}{\mathcal{R}^2}\frac{dm}{dv}\dot{v}^2 \right)_{\Sigma}. \tag{3.1.34}$$

If we consider the radial momentum flux in exterior spacetime Z^+ with an energy density given by (3.1.34), it becomes apparent that equation (3.1.30) implies the local conservation of momentum which takes into account bulk viscous effects, shear viscosity and null radiation. See Santos [16] for details.

3.1.8 Luminosity and surface redshift

The total luminosity detected or measured by an observer at rest at an infinite distance away from the surface of a star is given by

$$L_{\infty}(v) = -\frac{dm}{dv} = \lim_{\mathcal{R}\to\infty} \frac{\mathcal{R}^2}{2}\epsilon\frac{1}{\dot{v}^2}, \tag{3.1.35}$$

where $\frac{dm}{dv} \leq 0$ for the luminosity L_{∞} to be positive. The luminosity measured by an observer situated on Σ is given by

$$L_{\Sigma} = \left(\frac{\mathcal{R}^2\epsilon}{2} \right)_{\Sigma} = \left(\frac{Y^2\epsilon}{2} \right)_{\Sigma}. \tag{3.1.36}$$

The surface redshift z_{Σ}, which is in actual fact the change in the frequency of the radiation emitted from the hypersurface Σ of the star is expressed as

$$1 + z_{\Sigma} = \frac{dv}{d\eta} = \dot{v}_{\Sigma} = \left(\frac{\dot{Y}}{A} + \frac{Y'}{B} \right)^{-1}_{\Sigma}. \tag{3.1.37}$$

Note that as the star undergoes continued gravitational collapse, it will at some point reach the event horizon which is also referred to as the Schwarzschild radius, i.e. $\mathcal{R} = 2m(v)$. When the star's radius is less than Schwarzschild radius, signals from here take an infinitely long time to reach an observer on the outside. Thus, we can determine the time it takes for an event horizon to form. The above expressions allow us to write

$$L_{\infty} = -\frac{dm}{dv} = \left(\frac{\mathcal{R}^2}{2}\epsilon\frac{1}{\dot{v}^2} \right)_{\Sigma}. \tag{3.1.38}$$

We can rewrite (3.1.38), evaluated on the hypersurface Σ as:

$$L_\infty = -\frac{dm}{dv} = \left\{ \frac{Y^2}{2}\Big(p_r + \Pi + \epsilon + \frac{2}{3}\Omega\Big)\left[\frac{Y'}{B} + \frac{\dot{Y}}{A}\right]^2 \right\}_\Sigma . \tag{3.1.39}$$

It is worthwhile noting that equation (3.1.39) is a generalisation of the expression for L_∞ obtained by Naidu *el al* [37]. With the aid of (3.1.36), (3.1.37) and (3.1.12b), relation (3.1.38) can be recast in the form

$$\frac{L_\Sigma}{L_\infty} = \big(1 + z_\Sigma\big)^2, \tag{3.1.40}$$

which expresses the ratio of the luminosity on the hypersurface L_Σ to the luminosity an infinite distance away L_∞ in terms of the surface redshift.

Chapter 4

Perturbative framework

A perturbation is a small change that is made to a system (fluid distribution) which is initially in static equilibrium. This simply means that the fluid distribution is specified by quantities that have radial coordinate dependance only. These quantities are given a subscript zero to distinguish them from the perturbed quantities which are denoted by an over bar. We know from Chandrasekhar [76] that the adiabatic index Γ must be less than $\frac{4}{3}$ for the system to be stable against collapse. We will derive expressions for the static and perturbed quantities such as density, radial pressure, tangential pressure, etc., by following the treatment due to Chan *et al* [77]. In §4.1 we introduce the perturbative scheme that will be used in this study. This is followed by a derivation (for shearing spacetimes) of expressions for the static and perturbed matter variables as well the derivation of the Bianchi identities which concludes §4.2. In §4.3 we derive the temporal equation used in the perturbative scheme by imposing the results of the junction conditions obtained in Chapter 3. In §4.4 we discuss dynamical instabilities further, and summarise the work done on dynamical instabilities that will be relevant to Chapters 6 and 7 of this study.

4.1 Perturbative scheme

We assume that the metric functions $A(t,r)$, $B(t,r)$ and $Y(t,r)$, their perturbations, as well as the perturbations of the material functions all have the same time dependance [77]. Therefore, the metric functions and material functions are given by

$$A(t,r) = A_o(r) + \lambda T(t) a(r), \tag{4.1.1}$$

$$B(t,r) = B_o(r) + \lambda T(t) b(r), \tag{4.1.2}$$

$$Y(t,r) = Y_o(r) + \lambda T(t) y(r), \tag{4.1.3}$$

$$\rho(t,r) = \rho_o(r) + \lambda \overline{\rho}(t,r), \tag{4.1.4}$$

$$p_r(t,r) = p_{ro}(r) + \lambda \overline{p}_r(t,r), \tag{4.1.5}$$

$$p_t(t,r) = p_{to}(r) + \lambda \overline{p}_t(t,r), \tag{4.1.6}$$

$$m(t,r) = m_o(r) + \lambda \overline{m}(t,r), \tag{4.1.7}$$

$$\Theta(t,r) = \lambda \overline{\Theta}(t,r), \tag{4.1.8}$$

$$\sigma(t,r) = \lambda \overline{\sigma}(t,r), \tag{4.1.9}$$

$$q_1(t,r) = \lambda \overline{q}_1(t,r), \tag{4.1.10}$$

$$\epsilon(t,r) = \lambda \overline{\epsilon}(t,r), \tag{4.1.11}$$

where $0 < \lambda \ll 1$ is the perturbation amplitude and quantities with an 'over bar' represent perturbed quantities. We should point out that if one starts from spherical symmetry alone, one indeed has a very large gauge (coordinate) freedom to write the line element. However, once the line element is assumed as given by (2.5.1), all coordinate freedom is exhausted leaving only the possibility of rescaling the radial coordinate r and/or the time-like coordinate t. As it is evident by simple inspection, such rescaling would not change the form of equations (4.1.1) – (4.1.11). In essence, the choice of the perturbed variables as given in (4.1.1) – (4.1.11) is not unique. However, once the line element is prescribed, the choice of the perturbed variables cannot be changed to

produce the same physical results. The shear-free case within this perturbative scheme was studied by several authors [18],[19] and [77]. In all these investigations the static model was taken to be the isotropic Schwarzschild interior solution. An initially static configuration will start collapsing once perturbed. As the star collapses, a point is reached during the collapse process for which the density and temperature conditions are sufficiently suitable for neutrino emission and photon generation within the stellar core [77]. This gives rise to free–streaming radiation.

4.2 Perturbations for shearing spacetimes

In the absence of bulk viscosity, shear viscosity and free–streaming radiation the Einstein field equations (2.6.1a)–(2.6.1d) have the form:

$$\rho = \frac{1}{A^2}\left(2\frac{\dot{B}}{B}+\frac{\dot{Y}}{Y}\right)\frac{\dot{Y}}{Y}-\frac{1}{B^2}\left[2\frac{Y''}{Y}+\left(\frac{Y'}{Y}\right)^2-2\frac{B'}{B}\frac{Y'}{Y} - \left(\frac{B}{Y}\right)^2\right], \tag{4.2.1a}$$

$$p_r = -\frac{1}{A^2}\left[2\frac{\ddot{Y}}{Y}-\left(2\frac{\dot{A}}{A}-\frac{\dot{Y}}{Y}\right)\frac{\dot{Y}}{Y}\right]+\frac{1}{B^2}\left(2\frac{A'}{A}+\frac{Y'}{Y}\right)\frac{Y'}{Y}-\frac{1}{Y^2}, \tag{4.2.1b}$$

$$p_t = -\frac{1}{A^2}\left[\frac{\ddot{B}}{B}+\frac{\ddot{Y}}{Y}-\frac{\dot{A}}{A}\left(\frac{\dot{B}}{B}+\frac{\dot{Y}}{Y}\right)+\frac{\dot{B}}{B}\frac{\dot{Y}}{Y}\right] + \frac{1}{B^2}\left[\frac{A''}{A}+\frac{Y''}{Y}-\frac{A'}{A}\frac{B'}{B}+\left(\frac{A'}{A}-\frac{B'}{B}\right)\frac{Y'}{Y}\right], \tag{4.2.1c}$$

$$q_1 B = -\frac{2}{AB}\left(-\frac{\dot{Y}'}{Y}+\frac{\dot{B}}{B}\frac{Y'}{Y}+\frac{\dot{Y}}{Y}\frac{A'}{A}\right). \tag{4.2.1d}$$

Applying the perturbative scheme (4.1.1)–(4.1.11) to (4.2.1a)–(4.2.1d) we obtain the static configuration given by

$$\rho_o = -\frac{1}{B_o^2}\left(\frac{2Y_o''}{Y_o}+\frac{Y_o'^2}{Y_o^2}-\frac{2Y_o'B_o'}{Y_oB_o}-\frac{B_o^2}{Y_o^2}\right), \tag{4.2.2a}$$

$$p_{ro} = \frac{1}{B_o^2}\left(\frac{2A_o'Y_o'}{A_oY_o}+\frac{Y_o'^2}{Y_o^2}-\frac{B_o^2}{Y_o^2}\right), \tag{4.2.2b}$$

$$p_{to} = \frac{1}{B_o^2}\left[\frac{A_o''}{A_o}+\frac{Y_o''}{Y_o}-\frac{A_o'B_o'}{A_oB_o}+\frac{A_o'}{A_o}\left(\frac{Y_o'}{Y_o}-\frac{B_o'}{B_o}\right)\right], \tag{4.2.2c}$$

and from (4.2.1a)–(4.2.1d) we obtain for the perturbed quantities

$$\begin{aligned}\overline{\rho} = &-\frac{2bT\rho_o}{B_o}-\frac{2T}{{B_o}^2}\left[\left(\frac{y}{Y_o}\right)''-\frac{1}{Y_o}\left(\frac{b}{B_o}\right)'-\left(\frac{B_o'}{B_o}-\frac{3}{Y_o}\right)\left(\frac{y}{Y_o}\right)'\right.\\ &\left.-\left(\frac{B_o}{Y_o}\right)^2\left(\frac{b}{B_o}-\frac{y}{Y_o}\right)\right],\end{aligned} \tag{4.2.3a}$$

$$\begin{aligned}\overline{p}_r = &-\frac{2p_{ro}bT}{B_o}-\frac{2\ddot{T}y}{A_o^2Y_o}+\frac{2T}{Y_oB_o^2}\left[Y_o'\left(\frac{a}{A_o}\right)'+(\frac{y}{Y_o})'\left(Y_o'+\frac{A_o'Y_o}{A_o}\right)\right.\\ &\left.-\frac{B_o^2}{Y_o}\left(\frac{b}{B_o}-\frac{y}{Y_o}\right)\right],\end{aligned} \tag{4.2.3b}$$

$$\begin{aligned}\overline{p}_t = &-\frac{2bTp_{to}}{B_o}-\frac{\ddot{T}}{A_o^2}\left(\frac{b}{B_o}+\frac{y}{Y_o}\right)+\frac{T}{B_o^2}\left[\left(\frac{y}{Y_o}\right)''+\left(\frac{a}{A_o}\right)''\right.\\ &+\left(\frac{2A_o'}{A_o}-\frac{B_o'}{B_o}+\frac{Y_o'}{Y_o}\right)\left(\frac{a}{A_o}\right)'-\left(\frac{A_o'}{A_o}+\frac{Y_o'}{Y_o}\right)\left(\frac{b}{B_o}\right)'\\ &\left.+\left(\frac{A_o'}{A_o}-\frac{B_o'}{B_o}+\frac{2Y_o'}{Y_o}\right)\left(\frac{y}{Y_o}\right)'\right],\end{aligned} \tag{4.2.3c}$$

$$\overline{q}_1B_o = -\frac{2\dot{T}}{A_oB_o}\left[\frac{bY_o'}{B_oY_o}+\frac{y}{Y_o}\left(\frac{A_o'}{A_o}-\frac{Y_o'}{Y_o}\right)-\left(\frac{y}{Y_o}\right)'\right]. \tag{4.2.3d}$$

These equations generalize the recent work by Herrera *et al* [78] in which they considered a similar perturbative scheme with vanishing heat flux for the expansion–free condition. Surprisingly, they discovered that for expansion–free collapse, "*the range of the instability is defined by the local anisotropy of pressure and the energy density*

radial profile, but not by the adiabatic index Γ_1" in the Newtonian and post–Newtonian regimes. Expressions for the perturbed expansion coefficient and shear are given respectively by

$$\overline{\Theta} = \frac{\dot{T}}{A_o}\left(\frac{b}{B_o} + 2\frac{y}{Y_o}\right), \tag{4.2.4}$$

and

$$\overline{\sigma} = \frac{\dot{T}}{A_o}\left(\frac{b}{B_o} - \frac{y}{Y_o}\right). \tag{4.2.5}$$

The static and perturbed configuration for the mass function are respectively

$$m_o = \frac{Y_o}{2}\left[1 - \left(\frac{Y_o'}{B_o}\right)^2\right], \tag{4.2.6}$$

and

$$\overline{m} = -\frac{T}{B_o^2}\left[Y_o\left(Y_o' y' - \frac{{Y_o'}^2 b}{B_o}\right) + \frac{y}{2}\left({Y_o'}^2 - {B_o}^2\right)\right]. \tag{4.2.7}$$

The Bianchi identities (which include heat flow) (2.6.5) and (2.6.6) together with (4.1.1)–(4.1.11) yield for the collapsing static star

$$\left(p_{ro} + \rho_o\right)\frac{A_o'}{A_o} + 2\left(p_{ro} - p_{to}\right)\frac{Y_o'}{Y_o} + p_{ro}' = 0, \tag{4.2.8}$$

and the following equations for the perturbed configuration

$$\begin{aligned} 0 \;=\; & \dot{\overline{\rho}} + 2\left(\overline{q}_1 B_o\right)\left[\frac{A_o'}{B_o} + \frac{Y_o' A_o}{Y_o B_o}\right] + \frac{A_o}{B_o}\left(\overline{q}_1 B_o\right)' \\ & \frac{b\dot{T}}{B_o}\left(\rho_o + p_{ro}\right) + \frac{2y\dot{T}}{Y_o}\left(p_{to} + \rho_o\right), \end{aligned} \tag{4.2.9}$$

and

$$\begin{aligned} 0 \;=\; & \frac{B_o}{A_o}\left(B_o\dot{\overline{q}}_1\right) + \left(\overline{\rho} + \overline{p}_r\right)\frac{A_o'}{A_o} + \left(p_{ro} + \rho_o\right)T\left(\frac{a}{A_o}\right)' \\ & +2\left(p_{ro} - p_{to}\right)T\left(\frac{y}{Y_o}\right)' + \overline{p}_r{}' + 2\left(\overline{p}_r - \overline{p_t}\right)\frac{Y_o'}{Y_o}. \end{aligned} \tag{4.2.10}$$

4.3 The temporal equation employed in the perturbation scheme

Relation (3.1.24b) in the absence of bulk viscosity, shear viscosity, and null radiation, together with (4.2.3a) and $(p_{ro})_\Sigma = 0$ in (4.2.3b) determines the temporal evolution of the collapsing star and is given by

$$\alpha_\Sigma T - \ddot{T} = 2\beta_\Sigma \dot{T} > 0, \tag{4.3.1}$$

where

$$\alpha_\Sigma = \left\{ \frac{A_o^2}{B_o^2 y}\left[Y_o' \left(\frac{a}{A_o}\right)' + \left(\frac{y}{Y_o}\right)' \left(Y_o' + \frac{A_o' Y_o}{A_o}\right) - \frac{B_o^2}{Y_o}\left(\frac{b}{B_o} - \frac{y}{Y_o}\right)\right]\right\}_\Sigma, \tag{4.3.2}$$

and

$$\beta_\Sigma = \left\{ -\frac{A_o Y_o}{2B_o y}\left[\frac{bY_o'}{B_o Y_o} + \frac{y}{Y_o}\left(\frac{A_o'}{A_o} - \frac{Y_o'}{Y_o}\right) - \left(\frac{y}{Y_o}\right)'\right]\right\}_\Sigma. \tag{4.3.3}$$

Solutions of (4.3.1) include exponential functions (growth and decay) as well as oscillatory functions. In order to model collapse we will consider an exponentially decaying function which represents an initially static system at $t = -\infty$, ie. $T(-\infty) = 0$ with a decreasing luminosity radius as t increases. This temporal behaviour of our model is fulfilled if $\alpha_\Sigma > 0$ and $\beta \leq 0$. The temporal evolution of our model is then given by

$$T(t) = -e^{\left(-\beta_\Sigma + \sqrt{\alpha_\Sigma + {\beta_\Sigma}^2}\right)t}, \tag{4.3.4}$$

With the aid of (4.3.3), equation (4.2.3d) can be expressed as

$$\overline{q}_1 B_o = \frac{4y\beta}{A_o^2 Y_o}\dot{T}, \tag{4.3.5}$$

where $\beta = \beta(r)$. Note that when $\beta_\Sigma = 0$ (ie., no dissipation), the system continues to collapse.

4.4 Dynamical instabilities

The classic paper on instability by Chandrasekhar [76] in 1964 was based on an isotropic, perfect fluid model. Chandrasekhar showed the adiabatic index Γ (ratio of the

specific heats) must be less than $\frac{4}{3}$ for a system to be stable against gravitational collapse. The adiabatic index is a measure of the stiffness of a fluid. Intuition tells us that the squashing of a sponge ball (softer material) is easier to accomplish than of an identically sized orange (stiffer material). This is based on collapse from the outside directed inward. This analogy does not describe the stability index of a stellar fluid distribution, in which collapse is more dominant near the core regions (where the effects of gravitation would be the strongest) as opposed to the surface layers. We employ a novel "spring" analogy (a "toy" model) shown in Fig. 4.1, in which fluid particles are assumed to be connected to the centre of the spherical distribution of the fluid by means of "springs" whose spring constant or stiffness is a direct measure of Γ. For $\Gamma > \frac{4}{3}$, the "springs" become stiffer (more taut and responsive) thereby making it easier to pull the fluid towards the centre, which simply means that the fluid particles become more unstable against collapse. For $\Gamma < \frac{4}{3}$, the "springs" become weaker (softer, slack and less responsive) thereby making it much more difficult to pull the fluid particles towards the centre, which implies that the fluid becomes less unstable against collapse. This novel model allows us to directly understand the impact of the physical variables we are studying on the stiffness or softness of the fluid distribution.

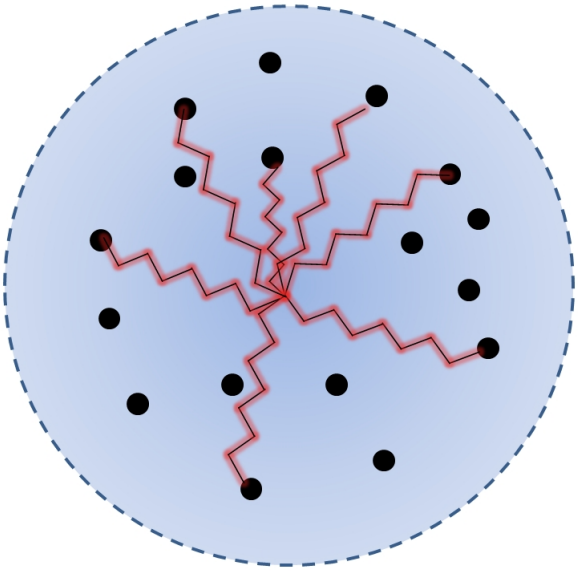

Figure 4.1: A spring model for Γ

Since the Chandrasekhar [76] paper, much work on dynamical instabilities has been conducted on imperfect fluids with heat flow (non–adiabatic) [18], radiation (free–streaming) and anisotropic pressures [77], as well as shear [19] to determine their impact on the stability index, Γ, and consequently on the unstable range of a collapsing stellar fluid. In this section we will only present the final results and analyses obtained by the various researchers. For details and derivations leading up to their final results, the reader is directed to the references [18]–[19]. We will consider the Newtonian limit where $A_o = 1, B_o = 1$ and $\rho_o \gg p_o$ for isotropic pressure or $\rho_o \gg p_{ro}, \rho_o \gg p_{to}$ for anisotropic pressure. For the Post–Newtonian limit we consider $A_o = 1 - m_o/r, B_o = 1 + m_o/r$ and allow for relativistic corrections up to the first order in m_o/r.

4.4.1 Non-adiabatic spherical collapse

Herrera *et al* [18] studied the impact of heat flow on the dynamical instability of a shear–free fluid distribution with isotropic pressure and no null radiation. After a marathon of calculations, they arrived at the expressions for the adiabatic index Γ for the Newtonian and the Post–Newtonian limits.

Newtonian limit

The limit is

$$\Gamma < \frac{4}{3} + \left[\frac{2}{3\kappa}\frac{\alpha_\Sigma \xi |f'|}{|p_o'|}\right]_{\text{MAX}}, \tag{4.4.1}$$

where $\alpha_\Sigma > 0$, κ is a constant, $\xi|f'|$ represents the contribution due to heat flow, p_o is the isotropic pressure and $|p_o'|$ is the absolute value of the derivative of the static pressure. It is evident from (4.4.1) that dissipative effects make the system more unstable by driving Γ above the value of $\frac{4}{3}$ required for stability.

Post–Newtonian limit

This limit is

$$\Gamma < \frac{4}{3} + \left[\frac{2}{3\kappa}\frac{\alpha_\Sigma \xi |f'|}{|p_o'|} + \frac{\kappa}{3}\frac{\rho_o p_o}{|p_o'|} - \frac{1}{3}\frac{\rho_o}{|p_o'|}\xi|f'|\right]_{\text{MAX}}, \tag{4.4.2}$$

where ρ_o is the static energy density. Upon analysing (4.4.2) it becomes evident that the unstable range of Γ is increased by the Newtonian term (first term within the square brackets) as well as by the relativistic corrections (second term within the square brackets) arising from the static fluid configuration. However, relativistic corrections as a result of heat flow (dissipation) (last term within square brackets) lowers the unstable range of Γ.

4.4.2 Radiating anisotropic collapse

Chan and co–workers [77] extended the work of Herrera *et al* [18] to a shear–free model with null radiation (free–streaming regime) as well as pressure anisotropy, i.e. unequal principal stresses.

Newtonian limit with $\bar{\epsilon} = 0$

In this case we have

$$\Gamma < \frac{4}{3} + \left[\frac{4}{3}\frac{(p_{to} - p_{ro})}{|p_{ro}'|r}\right]_{\text{MAX}}. \tag{4.4.3}$$

From (4.4.3) it quite clear that the anisotropy contribution to the unstable range of Γ is wholly dependant on the sign of difference between the static radial pressure p_{ro} and the static tangential pressure p_{to}. A difference $(p_{to} - p_{ro}) < 0$ will decrease the instability of the system, whilst a difference $(p_{to} - p_{ro}) > 0$ will increase the instability. Of course when $p_{ro} = p_{to}$ we have the isotropic case and the Newtonian classic limit, $\Gamma < \frac{4}{3}$, is achieved.

Post–Newtonian limit with $\bar{\epsilon} = 0$

We have the bound

$$\Gamma < \frac{4}{3} + \left[\frac{4}{3}\frac{(p_{to} - p_{ro})}{|p'_{ro}|r} + \frac{1}{3}\kappa\frac{\rho_o p_{ro}}{|p'_{ro}|}r\right]_{\text{MAX}}, \tag{4.4.4}$$

Relativistic corrections (second term within the square brackets) increase the unstable range of the adiabatic index, which results in configurations which are unstable.

4.4.3 Shearing viscous collapse

Chan *et al* [19] studied the role of shear viscosity on the dynamical instability of a stellar fluid configuration with isotropic pressure, no heat flow and no null radiation. They obtained the following results.

Newtonian limit

The limit is

$$\Gamma < \frac{4}{3} - \left[\frac{4}{9}\eta|s|\frac{\sqrt{\alpha_\Sigma}}{|p'_o|r}\right]_{\text{MAX}}, \tag{4.4.5}$$

From (4.4.5) it is evident that shear viscosity η diminishes the instability of system. In the absence of shear viscosity, either due to shear–free collapse ($s = 0$) or $\eta = 0$, the Newtonian classic result ($\Gamma < \frac{4}{3}$) is regained.

Post–Newtonian limit

$$\Gamma < \frac{4}{3} + \left[\frac{\kappa p_o \rho_o r}{3|p_o'|} - \frac{4}{9}\eta|s|\frac{\sqrt{\alpha_\Sigma}}{|p_o'|r} - \frac{1}{9}\kappa\rho_o r\eta|s|\frac{\sqrt{\alpha_\Sigma}}{|p_o'|} - \frac{2}{9}|s| - \frac{8}{9}|s|\frac{p_o}{|p_o'|r} - \frac{1}{3}|s|\frac{\rho_o r\alpha_\Sigma}{|p_o'|} \right]_{\rm MAX}, \tag{4.4.6}$$

The first term within the square brackets of (4.4.6) is the relativistic correction due to an increase in the effective energy density by the isotropic pressure. The rest of the contributions are all negative, thereby resulting in a decrease in the instability of the system. It is evident that the inclusion of shear viscosity leads to more stable (against collapse) stellar fluid configurations. Calculations based on a pre-supernova of about $15M_\odot$ having a core of $2M_\odot$, a temperature of $10^{10}K$ and a density $10^9 kg.m^{-3}$ (see [19] for details) yield the following values for the terms in (4.4.6):

- $\frac{\kappa p_o \rho_o r}{3|p_o'|} \approx 1.445 \times 10^{-5}$
- $\frac{4}{9}\eta|s|\frac{\sqrt{\alpha_\Sigma}}{|p_o'|r} \approx 3.824 \times 10^{-20}$
- $\frac{1}{9}\kappa\rho_o r\eta|s|\frac{\sqrt{\alpha_\Sigma}}{|p_o'|} \approx 4.458 \times 10^{-24}$
- $\frac{2}{9}|s| \approx 1.312 \times 10^{-4}$
- $\frac{8}{9}|s|\frac{p_o}{|p_o'|r} \approx 4.880 \times 10^{-5}$
- $\frac{1}{3}|s|\frac{\rho_o r\alpha_\Sigma}{|p_o'|} \approx 3.052 \times 10^{-7}$

Chan *et al* [19] analysed the relative magnitudes of these terms in detail.

Chapter 5

Thermodynamics

The evolution of a system such as a massive star undergoing gravitational collapse is critical in determining the temperature and luminosity profiles of the star. The Maxwell-Fourier law for heat conduction is adequate and appropriate in the classical regime. However, this law has to be modified to describe heat transport processes in the context of irreversible, relativistic thermodynamics. The Eckart theory [79], a relativistic analogue of the Maxwell-Fourier law includes an acceleration term which is responsible for producing heat flow (at constant temperature) directed opposite to the acceleration. The standard Fourier–Eckart type theories [79, 80], including Landau and Lifschitz [81], are plagued with features such as unstable equilibrium states and have thermal signals that travel at infinite propagation speed as soon as the temperature gradient is switched off as pointed out by Martínez [46]. In other words, the Eckart theory is a non–causal theory having zero relaxation time, i.e. instantaneous response, which is unrealistic. Herrera *et al* [82, 83] have estimated the relaxation time τ for neutron stars during stages of early formation to be approximately $10^{-4}s$ at a temperature of $10^{9}K$, and to be approximately $10^{2}s$ at a temperature of $10^{6}K$. These are much higher than the usually negligible $10^{-11}s$ for phonon–electron interactions and about $10^{-13}s$ for phonon–phonon interactions. This is a strong motivation for the inclusion of relaxational effects and the need for a causal theory.

The first non–relativistic causal theory for non–equilibrium thermodynamics was developed by Müller (see references within [84]) based on kinetic theory. Israel [23] extended the work of Müller to include relativistic effects. This was achieved by including second order terms in heat flux as well as viscous effects and this made the theory applicable to irreversible effects which are transient in nature and the theory was free of the pathological problems suffered by the non–causal theories of it predecessors. Much activity (Israel and Stewart [84] record the details) surrounded the development of a causal theory of non–equilibrium thermodynamics with relativistic effects taken into account. The reader is also referred to the work of Israel and Stewart [84] who extended Israel's [23] earlier work.

In this study we employ Cattaneo's [27] law for the heat transport to determine the temperature profile of stellar models. Our use of the Cattaneo [27] equation , or the Maxwell–Cattaneo equation, a truncated version of the Israel and Stewart [84] theory, is motivated in detail by Joseph and Preziosi [85]. For most part of the this chapter we will be following the formalism of Maartens [57] based on his review of "Causal thermodynamics in relativity", and provide a summarised version ranging from perfect fluids to extended irreversible causal thermodynamics.

We will now briefly review the notation used by Maartens [57]. Firstly he defines an instantaneous orthonormal frame (IOF) as the coordinates x^a that transforms an event P into orthonormal form, given by $g_{ab} \doteq \eta_{ab} \iff g_{ab}|_{IOF} = \eta_{ab}$. Covariant derivatives have a dot above the quantity e.g. the four–acceleration $\dot{V}^a$ is in fact $\dot{V}^a = V^a{}_{;b}V^b$. He gives a few examples of covariant spatial derivatives viz. $D_a f = h_a{}^b f_{,b}$, $D_a q_b = h_a{}^d h_b{}^e \nabla_d q_e$ and also $D_a \sigma_{bc} = h_a{}^d h_b{}^e h_c{}^f \nabla_d \sigma_{ef}$ etc., where $h_{ab} = g_{ab} + V_a V_b = h_{ba}$ is the projection tensor which splits the spacetime fabric into its temporal and three spatial components. In §5.1 we provide an overview of conservation laws for perfect fluids. An overview of irreversible thermodynamics is provided in §5.2. In §5.3 we review first–order standard irreversible thermodynamics focussing on the Eckart–type theories before discussing second–order causal thermodynamics for dissipative systems

in §5.4. We conclude the chapter with §5.5 by motivating our use of the Maxwell–Cattaneo heat flux equation used in the context of dissipative relativistic stellar fluids. In this chapter we will follow a similar approach to that adopted by Naidu [70], Fleming [71] and Govender [52].

5.1 Conservation laws for perfect fluids

The energy momentum tensor for a perfect fluid is given by

$$T_{ab} = \rho V_a V_b + p h_{ab}, \tag{5.1.1}$$

where V^a is the fluid four–velocity, ρ is the energy density, and p is the isotropic pressure. For a perfect fluid modeled as a continuum of particles described by an average timelike fluid four–velocity V^a, the particle number is given by

$$n_a = nV^a, \tag{5.1.2}$$

where n refers to the number density. If particle creation/annihilation processes are balanced then the particle number is conserved and this is expressed as

$$n^a{}_{;a} = 0 \iff \dot{n} + 3Hn = 0 \iff N \propto n\mathcal{A}^3 = \text{comoving constant}, \tag{5.1.3}$$

where $\mathcal{A}$ is a scale factor (comoving) which fully specifies the volume evolution, and H is a generalisation of the Newtonian expansion rate given by

$$H = \frac{\dot{\mathcal{A}}}{\mathcal{A}}. \tag{5.1.4}$$

Conservation of energy and momentum is obtained by setting the divergence of the energy momentum tensor equal to zero, i.e. $T^{ab}{}_{;b} = 0$. Consequently, we obtain equations describing, respectively, the conservation of energy and momentum

$$\dot{\rho} + 3H\big(\rho + p\big) = 0, \tag{5.1.5}$$

$$\big(\rho + p\big)\dot{V}_a + D_a p = 0. \tag{5.1.6}$$

Entropy S is conserved as well, and the expression for zero entropy flux is written as

$$S^{a}{}_{;a} = 0, \tag{5.1.7}$$

where

$$S^{a} = Sn^{a} \Rightarrow \dot{S} = 0. \tag{5.1.8}$$

The entropy S is not constant throughout the entire fluid, but is constant along the world lines of the fluid particles.

5.2 Overview of irreversible thermodynamics for dissipative relativistic fluids

While the perfect fluid model is sufficient to explain many processes in astrophysics, we know that gravitational collapse is a highly dissipative process and can only be understood in the context of a relativistic theory which takes into account dissipative fluids. When considering a dissipative fluid (heat flow and bulk viscous pressure) the particle four–current is described by (5.1.3) i.e.

$$N \propto n\mathcal{A}^{3} = \text{comoving constant},$$

which essentially amounts to selecting an average four–velocity, relative to which, the particle flux is zero. We anticipate that at any given event in spacetime, the fluids thermodynamic state is very close to the local equilibrium state at that particular point or event which is described by the following local equilibrium scalars, viz. $\overline{n}, \overline{\rho}, \overline{p}, \overline{S}, \overline{T}$ and four–velocity $\overline{V}^{d}$. With particular choice of $\overline{V}^{d}$ in the particle frame the number density n and energy density ρ could be made to correspond to the local equilibrium value, but the pressure differs from the local equilibrium value. Thus,

$$n = \overline{n}, \qquad \rho = \overline{\rho}, \qquad p = \overline{p} + \Pi \tag{5.2.1}$$

We rewrite the expression for pressure as

$$p_{eff} = p + \Pi \qquad \big(p \to p_{eff}, \overline{p} \to p\big), \tag{5.2.2}$$

where p_{eff} is the effective non-equilibrium pressure and Π is the bulk viscous pressure. Maartens [57] motivates for the following form of the energy momentum tensor, i.e.

$$T_{ab} = \rho V_a V_b + (p + \Pi)h_{ab} + q_a V_b + q_b V_a + \pi_{ab}. \tag{5.2.3}$$

Particle number is conserved here as was the case in the equilibrium limit (5.1.3), but the equations representing conservation of energy (5.1.5) and momentum (5.1.6) are modified to account for dissipative effects such as shear viscosity, heat flow and bulk viscosity. Thus we have

$$\dot{\rho} + 3H\big(\rho + p + \Pi\big) + D^a q_a + 2\dot{V}_a q^a + \sigma_{ab}\pi^{ab} = 0, \tag{5.2.4}$$

$$\begin{aligned}\big(\rho + p + \Pi\big)\dot{V}_a + D_a\big(p + \Pi\big) + D^b\pi_{ab} + \dot{V}^b\pi_{ab} \\ + h_a{}^b\dot{q}_b + \big(4Hh_{ab} + \sigma_{ab} + \omega_{ab}\big)q^b = 0,\end{aligned} \tag{5.2.5}$$

where ω_{ab} is the generalized vorticity. Entropy is not conserved in irreversible thermodynamics, but rather increases as predicted by the second law of thermodynamics. The rate at which entropy is produced is described by the divergence of the entropy–four current. We can write the second law of thermodynamics in its covariant form as

$$S^a{}_{;a} \geq 0. \tag{5.2.6}$$

The expression for S^a has to be modified, from its form in (5.1.8), to incorporate dissipative effects alluded to earlier. The new form of the entropy is

$$S^a = SnV^a + \frac{R^a}{\mathcal{T}}, \tag{5.2.7}$$

where $\mathcal{T}$ is the thermodynamic temperature. The entropy and temperature are equal to their respective local equilibrium values and are related through the Gibbs equation given by

$$\mathcal{T}dS = d\Big(\frac{\rho}{n}\Big) + pd\Big(\frac{1}{n}\Big). \tag{5.2.8}$$

It is worthwhile noting that the dissipative term R^a and S^a in (5.2.7) assumed to be a function of n_a and T_{ab}, and is expected to vanish at equilibrium, i.e. $\overline{R}^a = 0$. The assumption is well founded since it is known that non-equilibrium states are appropriately described by the hydrodynamic quantities n_a and T_{ab}.

5.3 First–order standard irreversible thermodynamics: Eckart–type theories

Standard Eckart theory models R^a (in 5.2.7) as a linear function of the dissipative quantities. A unique vector can be constructed from the dissipative quantities (viz. Π, q_a and π_{ab}) and the four–velocity is given by

$$R^a = f(n,a)\Pi V^a + g(\rho,n)q^a. \tag{5.3.1}$$

The entropy density $(-V_a S^a)$ is expected to reach its maximum value at equilibrium which implies that

$$\left[\frac{\partial}{\partial \Pi}(-V_a S^a)\right]_{equilibrium} = 0. \tag{5.3.2}$$

It can be shown that $f = 0$ when the entropy reaches its maximum at equilibrium. In an instantaneous orthonormal frame which is comoving, we find that $q_a/\mathcal{T} \doteq (0, \overrightarrow{q}/\mathcal{T})$, which represents the entropy flux as a result of heat flow. Note that $\overrightarrow{q}$ represents the heat flow vector. With $f = 0$ and $g = 1$, equation (5.3.1)becomes

$$R^a = q^a. \tag{5.3.3}$$

With the aid of (5.3.3), (5.2.7) now takes the form

$$S^a = SnV^a + \frac{q^a}{\mathcal{T}}. \tag{5.3.4}$$

By employing the Gibb's equation (5.2.8), the conservation equations (5.1.3) and the energy conservation equation (5.2.4), the divergence of (5.3.4) becomes

$$\mathcal{T}S^a{}_{;a} = -\left[3H\Pi + (D_a \ln \mathcal{T} + \dot{V}_a)q^a + \sigma_{ab}\pi^{ab}\right], \tag{5.3.5}$$

where $D_a \ln \mathcal{T}$ is the covariant spatial derivative of $\ln \mathcal{T}$. It is established from relativistic kinetic theory that at equilibrium the following conditions are true:

$$H = 0, \qquad \dot{V}_a = -D_a \ln \mathcal{T}, \qquad \sigma_{ab} = 0. \tag{5.3.6}$$

It follows from (5.3.5) and (5.3.6) that $S^{a}{}_{;a} = 0$. From (5.3.5) it seems that the easiest manner to ensure the validity of (5.2.6) is to assume linear relationships between the thermodynamic "fluxes" (Π, q_a, π_{ab}) and their corresponding thermodynamic "forces" $(H, \dot{V}_a + D_a \ln \mathcal{T}, \sigma_{ab})$. Consequently:

$$\Pi = -3\zeta H, \tag{5.3.7}$$

$$q_a = -\kappa\Big(D_a\mathcal{T} + \mathcal{T}\dot{V}_a\Big), \tag{5.3.8}$$

$$\pi_{ab} = -2\eta\sigma_{ab}, \tag{5.3.9}$$

where $\zeta(\rho, n) \equiv$ bulk viscosity, $\kappa(\rho, n) \equiv$ thermal conductivity and $\eta(\rho, n) \equiv$ shear viscosity. Equations (5.3.7)–(5.3.9) are the fundamental equations for dissipative quantities in the standard Eckart theory pertaining to relativistic irreversible thermodynamics and are, respectively, the relativistic generalisations of their corresponding Newtonian equations

$$\Pi = -3\zeta \overrightarrow{\nabla}.\overrightarrow{v} \quad \text{(Stokes)}, \tag{5.3.10}$$

$$q_a = -\kappa \overrightarrow{\nabla}\mathcal{T} \quad \text{(Fourier)}, \tag{5.3.11}$$

$$\pi_{ij} = -2\eta\sigma_{ij} \quad \text{(Newton)}. \tag{5.3.12}$$

This can be easily verified by employing a comoving instantaneous orthonormal frame in (5.3.7)–(5.3.9) above. Once again, we point out that the Eckart result (5.3.8) is a relativistic generalisation of Fourier result (5.3.11). However, it must be pointed out that in (5.3.8), there is an acceleration which is not present in the Fourier equation (5.3.11). This acceleration (of the matter) term, accounts for the inertia of heat energy which is able to produce a heat flux even in the absence of a temperature gradient, which is counterintuitive from a classical point of view. The isothermal heat flow is directed opposite to acceleration as highlighted in the introduction of this chapter.

Utilizing (5.3.7)–(5.3.9) in equation (5.3.5) the following expression for the divergence of entropy is obtain, viz.

$$S^{a}{}_{;a} = \frac{\Pi^2}{\zeta\mathcal{T}} + \frac{q_a q^a}{\kappa\mathcal{T}^2} + \frac{\pi_{ab}\pi^{ab}}{2\eta\mathcal{T}}. \tag{5.3.13}$$

We note from (5.3.13) that $S^a{}_{;a} \geq 0$ for $\zeta, \kappa, \eta \geq 0$. An equation describing the temporal evolution of the entropy is obtained by employing the Gibbs equation (5.2.8), the number conservation equation (5.1.3) as well as the energy conservation equation (5.2.4). It has the form

$$\mathcal{T} n \dot{S} = -3H\Pi - q^a{}_{;a} - \dot{V}_a q^a - \sigma_{ab}\pi^{ab}. \tag{5.3.14}$$

The Eckart theory of irreversible thermodynamics is adequate in the Newtonian regime. The theory, however, is plagued with causality violation which becomes evident when we suddenly "switch off" the thermodynamic force on the right hand side of equation (5.3.8), causing the heat flux to vanish instantaneously. This implies that thermal signals propagate at infinite speed, which is in direct violation of relativistic causality. See [46], [85] for details.

5.4 Second–order causal thermodynamics for dissipative systems

The Eckart assumption which is a linearisation of the contributions from the dissipative fluxes, uses a form of R^a that is oversimplified and ultimately results in the violation of causality and leads to model instabilities. Relativistic kinetic theory specifies that R^a be of second–order in the dissipative fluxes, and it is anticipated that this would yield a more stable model, and also one that satisfies relativistic causality. In keeping with this new idea, a form of R^a, that is of second–order in the dissipative fluxes is modeled by

$$S^d = Snu^d - \left(\beta_0\Pi^2 + \beta_1 q_e q^e + \beta_2 \pi_{ef}\pi^{ef}\right)\frac{V^d}{2\mathcal{T}} + \frac{\alpha_0 \Pi q^d}{\mathcal{T}} + \frac{\alpha_1 \pi^{de} q_e}{\mathcal{T}} + \frac{q^d}{\mathcal{T}} \tag{5.4.1}$$

where, $\beta_A(\rho, n) \geq 0$ are the thermodynamic coefficients for the dissipative contributions, and $\alpha_A(\rho, n)$ are the thermodynamic viscous/heat coupling coefficients. "Switching off" the viscous/heat coupling coefficients, i.e. $\alpha_0 = 0 = \alpha_1$ (a valid assumption, see

Maartens [57] for details), in (5.4.1) we find that the effective entropy density measured in a comoving reference frame to be

$$-u_d S^d = Sn - \frac{1}{2\mathcal{T}}\left(\beta_0 \Pi^2 + \beta_1 q_d q^d + \beta_2 \pi_{de}\pi^{de}\right). \tag{5.4.2}$$

The divergence of (5.4.1) with viscous/heat coupling coefficients set to zero, can be obtained by employing the Gibbs equation (5.2.8), as well the equations for the conservation of particle number (5.1.3), conservation of energy (5.2.4) and conservation of momentum (5.2.5). The expression for the divergence of (5.4.1) is given by:

$$\begin{aligned}
\mathcal{T} S^a{}_{;a} &= -\Pi\left[3H + \beta_0\dot{\Pi} + \frac{1}{2}\mathcal{T}\left(\frac{\beta_1}{\mathcal{T}}V^a\right)_{;a}\Pi\right] \\
&\quad -q^a\left[D_a \ln\mathcal{T} + \dot{V}_a + \beta_1\dot{q}_a + \frac{1}{2}\left(\frac{\beta_1}{\mathcal{T}}V^d\right)_{;d} q_a\right] \\
&\quad -\pi^{ad}\left[\sigma_{ad} + \beta_2\dot{\pi}_{ad} + \frac{1}{2}\mathcal{T}\left(\frac{\beta_2}{\mathcal{T}}V^e\right)_{;e}\pi_{ad}\right].
\end{aligned} \tag{5.4.3}$$

The second law of thermodynamics given by (5.2.6) is satisfied if we enforce a linear dependence of the thermodynamic fluxes on the dissipative forces. This yields the following transport equations,

$$\tau_0\dot{\Pi} + \Pi = -3\zeta H - \left[\frac{1}{2}\zeta\mathcal{T}\left(\frac{\tau_0}{\zeta\mathcal{T}}V^a\right)_{;a}\Pi\right], \tag{5.4.4}$$

$$\tau_1 h^b{}_a\dot{q}_b + q_a = -\kappa(D_a\mathcal{T} + \mathcal{T}\dot{V}_a) - \left[\frac{1}{2}\kappa\mathcal{T}^2\left(\frac{\tau_1}{\kappa\mathcal{T}^2}V^b\right)_{;b} q_a\right], \tag{5.4.5}$$

$$\tau_2 h^d{}_a h^e{}_b\dot{\pi}_{de} + \pi_{ab} = -2\eta\sigma_{ab} - \left[\eta\mathcal{T}\left(\frac{\tau_2}{2\eta\mathcal{T}}V^e\right)_{;e}\pi_{ab}\right], \tag{5.4.6}$$

where $\tau_A(\rho, n)$ represent the relaxational times, and are given by

$$\tau_0 = \zeta\beta_0, \qquad \tau_1 = \kappa\mathcal{T}\beta_1, \qquad \tau_2 = 2\eta\beta_2. \tag{5.4.7}$$

All terms contained within the square brackets in equations (5.4.4), (5.4.5) and (5.4.6) can be excluded since their contribution is negligible compared to that of the other terms, and the equations that result are referred to as the truncated Israel–Stewart equations. Assuming no viscous/heat coupling, the truncated Israel–Stewart equations

are of Maxwell–Cattaneo form and are covariant and relativistic. They are

$$\tau_0\dot{\Pi} + \Pi = -3\zeta H, \tag{5.4.8}$$

$$\tau_1 h^b{}_a \dot{q}_b + q_a = -\kappa(D_a\mathcal{T} + \mathcal{T}\dot{V}_a), \tag{5.4.9}$$

$$\tau_2 h^d{}_a h^e{}_b \dot{\pi}_{de} + \pi_{ab} = -2\eta\sigma_{ab}. \tag{5.4.10}$$

The Maxwell-Cattaneo equations (5.4.8)–(5.4.10) are first–order differential equations which describe the evolution of the dissipative fluxes as opposed to the Eckart transport equations (5.3.7)–(5.3.9) which were algebraic equations. The evolution terms having relaxation time coefficients τ_A, render the equations (5.4.8)–(5.4.10) casual in the context of relativistic irreversible thermodynamics. It is easy to see that upon setting the relaxational time coefficient τ_1 to zero in (5.4.9), the Eckart heat transport equation (5.3.8) is obtained.

5.5 Thermodynamics in relativistic stellar fluids

Gravitational collapse is a highly dissipative process [21] (and references therein) and thus any reasonable model of gravitational collapse has to include dissipation and relaxation time. Martínez [46] clearly highlights the effect of relaxation time especially for early and late stages of the collapse process. Di Prisco *et al* [28] have shown that relaxation time has a direct impact on the final mass, compactness and luminosity profile of a radiating star. Govender and co–workers have shown that relaxational effects can lead to higher core temperatures and enhanced cooling at the surface of the collapsing body [32, 86, 87, 88, 89]. In order to explore the contributions due to relaxational effects we employ the causal heat transport equation of the Maxwell-Cattaneo form (5.4.9). The Maxwell-Cattaneo form has many desirable features as pointed out by Joseph and Preziosi [85] since it satisfies the relativistic causality requirement and rate–type equations like it are "*extensively used in the theory of viscoelastic fluids and in relaxing gas dynamics*".

5.5.1 General case

The truncated form of the Israel–Stewart causal heat transport equation (5.4.5) is the Maxwell–Cattaneo equation (5.4.9) which is expressed as

$$\tau_r h_a{}^b \dot{q}_b + q_a = -\kappa\big(h_a{}^b \nabla_b \mathcal{T} + \mathcal{T}\dot{V}_a\big), \tag{5.5.1}$$

where $h_{ab} = g_{ab} + V_a V_b$ is the projection tensor, $\mathcal{T}(t, r)$ is the local equilibrium temperature, $\kappa(\geq 0)$ is the thermal conductivity, and $\tau_r(\geq 0)$ is the relaxation time-scale with which causal, stable behaviour is achieved. The non–causal Eckart heat transport equation is obtained by setting the relaxation time $\tau_r = 0$ in (5.5.1). With the aid of the metric (2.5.1), equation (5.5.1), with $\tau_r \neq 0$, becomes

$$\tau_r (qB)^{\cdot} + A(qB) = -\kappa \frac{(A\mathcal{T})'}{B}. \tag{5.5.2}$$

The thermodynamic coefficients associated with radiative transfer are well motivated in [32, 33, 46]. Following Martínez [46] we take the thermal conductivity to be

$$\kappa = \gamma \mathcal{T}^3 \tau_c, \tag{5.5.3}$$

where $\gamma = \frac{4}{3}b$ ($b = \frac{7}{8}a$ for neutrinos, with a being a radiation constant) and τ_c is the mean collision time. Martínez [46] finds the temperature dependance of the collision time, by assuming that the neutrinos generated as a consequence of thermal emission, to be $\tau_c \propto T^{-\frac{3}{2}}$. Based on his findings, we assume a power law relationship of the form

$$\tau_c = \left(\frac{\xi}{\gamma}\right) \mathcal{T}^{-\omega}, \tag{5.5.4}$$

where ξ and ω are positive constants, with $\omega = \frac{3}{2}$ for thermally generated neutrinos. It is easy to see that the case of $\omega = 0$ corresponds to constant collision time, which holds true for a limited temperature range. Martínez [46] assumes that the speed of the thermal and viscous signal to be comparable to the speed of sound in the fluid medium, which implies that it's reasonable to say that the relaxation time is proportional to the mean collision time. This is expressed as

$$\tau_r = \left(\frac{\psi\gamma}{\xi}\right) \tau_c, \tag{5.5.5}$$

where ψ (≥ 0) is a constant. Employing the definitions for τ_r and κ, it can be shown that equation (5.5.2) takes the form

$$\psi(qB)\dot{\mathcal{T}}^{-\omega} + A(qB) = -\xi\frac{\mathcal{T}^{3-\omega}(A\mathcal{T})'}{B}, \tag{5.5.6}$$

where ψ can be considered to be a 'causality index', that enables us to quantify the impact of relaxation effects on the system.

5.5.2 Non–causal solutions: $\psi = 0$

The non–causal solutions of (5.5.6) are obtained by setting $\psi = 0$. These solutions are due to Govinder and Govender [34] for shear–free radiating collapse, and are given by

$$(AT)^{4-\omega} = \frac{\omega-4}{\xi}\int A^{4-\omega}qB^2dr + F(t) \ \ ,\omega \neq 4 \tag{5.5.7}$$

$$\ln(AT) = -\frac{1}{\xi}\int qB^2dr + F(t) \ \ ,\omega = 4 \tag{5.5.8}$$

where $F(t)$ is an arbitrary integration function. The quantity $F(t)$ is obtained by applying the boundary condition, viz.

$$\Big(T^4\Big)_\Sigma = \Big(\frac{1}{r^2B^2}\Big)_\Sigma\Big(\frac{L_\infty}{4\pi\delta}\Big), \tag{5.5.9}$$

for the surface temperature, where L_∞ represents the total luminosity (3.1.39) observed at a very far distance and δ is a positive constant. Causal solutions of (5.5.6) are obtained by Govinder and Govender [34] for constant and non–constant collision time. These are given below.

5.5.3 Causal case: $\omega = 0$

The case of $\omega = 0$ in (5.5.4) corresponds to constant mean collision time. Upon integrating the causal transport equation (5.5.6) with $\omega = 0$, the following equation is obtained

$$\big(AT\big)^4 = -\frac{4}{\xi}\Big[\psi\int A^3B(qB)\dot{}dr + \int A^4qB^2dr\Big] + F(t). \tag{5.5.10}$$

5.5.4 Causal case: $\omega = 4$

Setting $\omega = 4$ in (5.5.4) produces a model that is valid for a specific range of temperatures as pointed out by Govinder and Govender [34]. The resulting equation has the form of a Bernoulli equation in AT and the solution to this equation has the form

$$\begin{aligned}(AT)^4 &= -\frac{4\psi}{\xi}\exp\Big(-\int\frac{4qB^2}{\xi}dr\Big)\int A^3B(qB)^{\cdot}\exp\Big(\int\frac{4qB^2}{\xi}dr\Big)\\ &\quad +F(t)\exp\big(-\int\frac{4qB^2}{\xi}dr\big).\end{aligned} \tag{5.5.11}$$

Temperature profiles (causal and non–causal) for (5.5.6) have been obtained for various models such as shear–free (horizon–free) collapse [36], radiating anisotropic collapse with shear [37], Euclidean star models [87, 88], dissipative collapse with cosmological constant [90], collapse involving first–order perturbations [39], shearing, radiative collapse with expansion and acceleration [1], models highlighting the effect of shear [40], as well as the role of anisotropy on the perturbed temperature profiles [91] .

Chapter 6

The role of shear in dissipative gravitational collapse

6.1 Introduction

In a fluid distribution, shear refers to the movement (sliding) or flow of adjacent layers of the fluid over each other with each pair of adjacent layers having a different relative velocity compared to the others. The relative velocity between these adjacent layers is lowest at the bottom of the fluid and it increases in the direction of the surface layers thereby creating a velocity gradient. Shear viscosity is defined as the resistance that a fluid offers to shearing flow and can be determined using the shear stress and the shear rate (velocity gradient). Shear viscosity is a characteristic property of a fluid. Shearing flow may possibly be initiated by the onset of turbulence in a fluid medium (see [19] and references therein). Bulk viscosity on the other hand is a measure of the resistance that a fluid layer will offer to pressure (bulk viscous stress) attempting to expand of contract its volume. The bulk viscous stress acts perpendicular to the fluid layers as opposed to the shear stress which acts parallel to the fluid layers. Bulk viscosity can be determined using the bulk viscous stress and the volume strain (fractional change in the volume of a fluid layer).

The inclusion of shear during the collapse process paved the way to study anisotropy in local systems. The first shearing model within this framework was obtained by Naidu *et al* [37]; this model was obtained by ad hoc assumptions on the metric functions. This model was later generalised by Rajah and Maharaj [38]. Various classes of radiating, shearing models of gravitational collapse were subsequently found, and they exhibit reasonable physical behaviour. Herrera and Santos [92] proposed the so-called Euclidean star model in which the proper radius equals the areal radius throughout the collapse process. Exact solutions for this case lead to physically reasonable models as shown by Govender *et al* [87]. Chan and co-workers carried out intensive investigations of the role of shear during dissipative collapse [93, 94, 95, 96, 97, 98]. They were able to show that the inclusion of bulk viscosity diminishes the effective adiabatic index within the stellar core thereby increasing the instability of the collapsing star. Recently, Thirukkanesh *et al* [1] were able to relax some of the assumptions and were able to provide various classes of shearing, radiating solutions. The simple analytical forms of the solutions allowed them to carry out a physical analysis of a particular model and they were able to show that this model was reasonably well behaved. Up to this point, all the exact models of radiating stars with shear did not have a shear-free limit, ie., the shear could not be switched off. As a result, it was not possible to highlight the effect of shear directly onto the collapse process. A particular solution of Thirukkanesh *et al* [1] (hereon referred to as *TRM*) exhibits the pleasant feature of a shear 'switch'.

The purpose of this chapter is to highlight the effect of shear on the temperature profiles of the collapsing matter distribution. By utilising the *TRM* solution and the causal heat transport equation of the Maxwell-Cattaneo form [27], given by equation (5.4.9), we are able to study the evolution of the temperature when the star leaves hydrostatic equilibrium. We also analyse how the stability of our model changes from shear–free conditions to shearing conditions by employing the shear 'switch'.

6.2 Interior spacetime

The line element for the interior of the collapsing star is described by the general spherically symmetric, shearing metric in comoving coordinates given by (2.5.1). The interior matter content is that of an imperfect fluid (2.5.7), which in the absence of bulk viscosity, free–steaming radiation and shear viscosity, is given by

$$T_{ab} = (\rho + p_t)V_aV_b + p_tg_{ab} + (p_r - p_t)\chi_a\chi_b + q_aV_b + q_bV_a. \tag{6.2.1}$$

where ρ is the energy density, p_r is the radial pressure, p_t is the tangential pressure, V^a is the comoving unit timelike fluid four–velocity, χ_a is a radial unit four–vector and q^a is the heat flux. The nonzero components of the Einstein field equations for the line element (2.5.1) and the energy momentum (6.2.1) are

$$\rho = \frac{1}{A^2}\left(2\frac{\dot{B}}{B} + \frac{\dot{Y}}{Y}\right)\frac{\dot{Y}}{Y} - \frac{1}{B^2}\left[2\frac{Y''}{Y} + \left(\frac{Y'}{Y}\right)^2 - 2\frac{B'}{B}\frac{Y'}{Y} - \left(\frac{B}{Y}\right)^2\right], \tag{6.2.2a}$$

$$p_r = -\frac{1}{A^2}\left[2\frac{\ddot{Y}}{Y} - \left(2\frac{\dot{A}}{A} - \frac{\dot{Y}}{Y}\right)\frac{\dot{Y}}{Y}\right] + \frac{1}{B^2}\Big(2\frac{A'}{A} + \frac{Y'}{Y}\Big)\frac{Y'}{Y} - \frac{1}{Y^2}, \tag{6.2.2b}$$

$$\begin{aligned} p_t = & -\frac{1}{A^2}\left[\frac{\ddot{B}}{B} + \frac{\ddot{Y}}{Y} - \frac{\dot{A}}{A}\left(\frac{\dot{B}}{B} + \frac{\dot{Y}}{Y}\right) + \frac{\dot{B}}{B}\frac{\dot{Y}}{Y}\right] \\ & + \frac{1}{B^2}\left[\frac{A''}{A} + \frac{Y''}{Y} - \frac{A'}{A}\frac{B'}{B} + \left(\frac{A'}{A} - \frac{B'}{B}\right)\frac{Y'}{Y}\right], \end{aligned} \tag{6.2.2c}$$

$$q_1B = \frac{2}{AB}\Big(\frac{\dot{Y}'}{Y} - \frac{\dot{B}}{B}\frac{Y'}{Y} - \frac{\dot{Y}}{Y}\frac{A'}{A}\Big). \tag{6.2.2d}$$

6.3 Exterior spacetime and junction conditions

The exterior spacetime is taken to be the Vaidya solution which is given by (2.8.1). The necessary conditions for the smooth matching of the interior spacetime (2.5.1) to the exterior spacetime (2.8.1) have been dealt with in detail in Chapter 3. We present

the main results that are necessary for modeling a radiating star. The continuity of the intrinsic and extrinsic curvature components of the interior and exterior spacetimes across a timelike boundary yielded an equations (3.1.24a) and (3.1.24b). In the absence of bulk viscosity, free–steaming radiation and shear viscosity, junction condition (3.1.24a) remains the same, i.e.

$$m(v) = \left[\frac{Y}{2}\left(1 + \frac{\dot{Y}^2}{A^2} - \frac{Y'^2}{B^2}\right)\right]_\Sigma,$$

although junction condition (3.1.24b) becomes

$$\left(p_r\right)_\Sigma = \left(q_1 B\right)_\Sigma. \tag{6.3.1}$$

We point out that relation (6.3.1) determines the temporal evolution of the collapsing star.

6.4 Temporal evolution

With the aid of equation (6.2.2b) for the radial pressure p_r and equation (6.2.2d) for the heat flow $(q_1 B)$, the junction condition $(p_r)_\Sigma = (q_1 B)_\Sigma$ yields

$$\begin{aligned}\dot{B} = \left(\frac{Y}{2AY'}\right)\left[2\frac{\ddot{Y}}{Y} + \left(\frac{\dot{Y}}{Y}\right)^2 - 2\frac{\dot{A}}{A}\frac{\dot{Y}}{Y} + \frac{A^2}{Y^2}\right]B^2 \\ + \left[\frac{\dot{Y}'}{Y'} - \frac{A'}{A}\frac{\dot{Y}}{Y'}\right]B - \frac{A}{2}\left[\frac{Y'}{Y} + 2\frac{A'}{A}\right],\end{aligned} \tag{6.4.1}$$

which is a Riccati equation, given in terms of the gravitational potential B, of the form

$$\dot{B} = \mathcal{C}_0(t)B^2 + \mathcal{C}_1(t)B + \mathcal{C}_2(t). \tag{6.4.2}$$

Thirukkanesh *et al* [1] have provided various classes of exact solutions to (6.4.1). Setting

$$\frac{\dot{Y}'}{Y'} - \frac{A'}{A}\frac{\dot{Y}}{Y'} = 0, \tag{6.4.3}$$

equation (6.4.1) reduces to an inhomogeneous Riccati equation. Integrating this equation we get

$$A = \alpha(t)\dot{Y}, \tag{6.4.4}$$

where $\alpha(t)$ is an integration constant. In this case (6.4.1) becomes

$$\dot{B} = \left[\frac{\dot{Y}(1+\alpha^2)}{2YY'\alpha} - \frac{\dot{\alpha}}{\alpha^2 Y'}\right] B^2 - \left[\dot{Y}'\alpha + \frac{\dot{Y}Y'\alpha}{2Y}\right]. \tag{6.4.5}$$

This is an inhomogeneous Riccati equation which is difficult to analyse in general.

We take α as a constant and Y to be the separable function

$$Y(t,r) = K(r)C(t), \tag{6.4.6}$$

where $K(r)$ and $C(t)$ are arbitrary functions of r and t respectively. Then (6.4.5) can be written as

$$\dot{B} = \left[\frac{(1+\alpha^2)}{2\alpha K'}\frac{\dot{C}}{C^2}\right] B^2 - \frac{3}{2}\alpha K'\dot{C}. \tag{6.4.7}$$

For $\alpha = -2$, Thirukkanesh *et al* [1] were able to provide a simple exact solution to (6.4.7) of the form

$$A(r,t) = -2K\dot{C}, \tag{6.4.8}$$

$$B(r,t) = \frac{2K'C[3C^4 + f(r)]}{5C^4 - f(r)}, \tag{6.4.9}$$

$$Y(t,r) = K(r)C(t), \tag{6.4.10}$$

where C, K and f are arbitrary functions. In the limit $f(r) \to 0$ (6.4.9) becomes

$$B(r,t) = \frac{6}{5}K'C. \tag{6.4.11}$$

Simple calculations reveal that

$$\frac{\dot{Y}}{Y} = \frac{\dot{C}}{C} = \frac{\dot{B}}{B}. \tag{6.4.12}$$

Employing (6.4.12) in the expression (2.5.16) for shear

$$\sigma = \frac{1}{A}\Big(\frac{\dot{B}}{B} - \frac{\dot{Y}}{Y}\Big),$$

we find that the shear σ vanishes. The function $f(r)$ is the 'shear switch' since $f(r) \to 0$ causes the shear σ to vanish. With an insightful choice of $f(r)$ we can investigate the role played by shear directly on the collapse process. This will be taken up in the next

section. It is remarkable that we can write down the kinematical and thermodynamical quantities in compact, closed form. The acceleration, collapse rate and shear are given by

$$a = \frac{K'(r)}{K(r)}, \tag{6.4.13}$$

$$\Theta = -\frac{3f^2(r)+26f(r)C^4(t)-45C^8(t)}{2f^2(r)K(r)C(t)-4f(r)K(r)C^5(t)-30K(r)C^9(t)}, \tag{6.4.14}$$

$$\sigma = -\frac{16f(r)C^3(t)}{K(r)[f(r)-5C^4(t)][f(r)+3C^4(t)]}. \tag{6.4.15}$$

The Einstein field equations (6.2.2a)-(6.2.2d) yield

$$\rho = -\frac{l(r,t)}{2K^2(r)C^2(t)([f(r)-5C^4(t)][f(r)+3C^4(t)]^3K'(r)}, \tag{6.4.16a}$$

$$p_r = q_1 B = -\frac{f^2(r)+30f(r)C^4(t)-15C^8(t)}{2K^2(r)C^2(t)\left[f(r)+3C^4(t)\right]^2}, \tag{6.4.16b}$$

$$p_t = \frac{4C^2(t)g(r,t)}{K^2(r)[f(r)-5C^4(t)]^2[f(r)+3C^4(t)]^3K'(r)}, \tag{6.4.16c}$$

where we have defined

$$\begin{aligned} g(r,t) &= K(r)[f(r)-5C^4]^3f'(r)-[f(r)+3C^4(t)][13f^3(r)+45f^2(r)C^4(t) \\ &\quad +95f(r)C^8(t)-25C^{12}(t)]K'(r), \end{aligned} \tag{6.4.17}$$

$$\begin{aligned} l(r,t) &= -3f^4(r)K'(r)-52f^3(r)C^4(t)K'(r)+20f(r)C^8(t)[-4K(r)f'(r) \\ &\quad +7C^4(t)K'(r)]+5C^{12}(t)[40K(r)f'(r)+57C^4(t)K'(r)] \\ &\quad +2f^2(r)[4K(r)C^4(t)f'(r)-57C^8(t)K'(r)]. \end{aligned} \tag{6.4.18}$$

6.5 A particular radiating model

In order to extract the physics of the collapse process we select a particular model in which the radial and temporal evolution are specified as follows

$$C(t) = 1+at^2, \tag{6.5.1}$$

$$K(r) = 1+br^2, \tag{6.5.2}$$

$$f(r) = \frac{\gamma}{r^2+c^2}, \tag{6.5.3}$$

where a, b, c and γ are constants. It can be easily seen that the constant γ is a toggle (on/off) for $f(r)$ which, as seen earlier, is the shear switch. Consequently the metric functions become

$$A(r,t) = -4a(1+br^2)t, \tag{6.5.4}$$

$$B(r,t) = \frac{4br(1+at^2)\left[3(1+at^2)^4+\frac{\gamma}{c^2+r^2}\right]}{5(1+at^2)^4-\frac{\gamma}{c^2+r^2}}, \tag{6.5.5}$$

$$Y(r,t) = (a+br^2)(1+at^2). \tag{6.5.6}$$

For the line element (6.2.1) the kinematical quantities (6.4.13)-(6.4.15) yield

$$a = \frac{2br}{1+br^2}, \tag{6.5.7}$$

$$\Theta = -\frac{2+\frac{\left[5(1+at^2)^4-\frac{\gamma}{c^2+r^2}\right]\left[15(1+at^2)^8-\frac{30(1+at^2)^4\gamma}{c^2+r^2}-\frac{\gamma^2}{(c^2+r^2)^2}\right]}{\left[-5(1+at^2)^4+\frac{\gamma}{c^2+r^2}\right]^2\left[3(1+at^2)^4+\frac{\gamma}{c^2+r^2}\right]}}{2(1+br^2)(1+at^2)}, \tag{6.5.8}$$

$$\sigma = \frac{\left[16(c^2+r^2)(1+at^2)^3\gamma\right]}{\left[(1+br^2)\left(5(c^2+r^2)(1+at^2)^4-\gamma\right)\left(3(c^2+r^2)(1+at^2)^4+\gamma\right)\right]}. \tag{6.5.9}$$

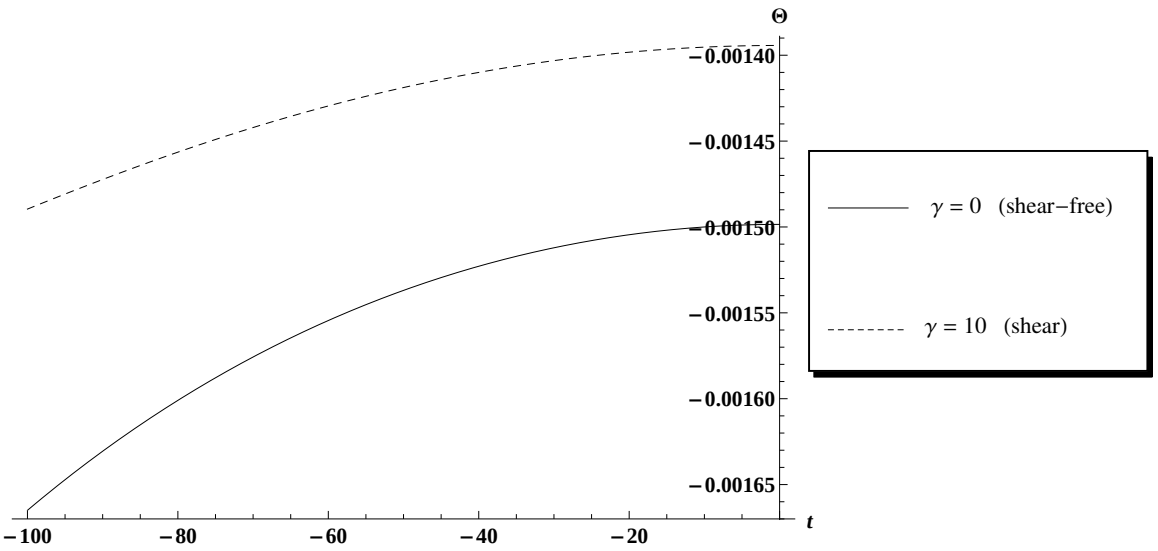

Figure 6.1: Collapse rate Θ (at the surface) as a function of time.

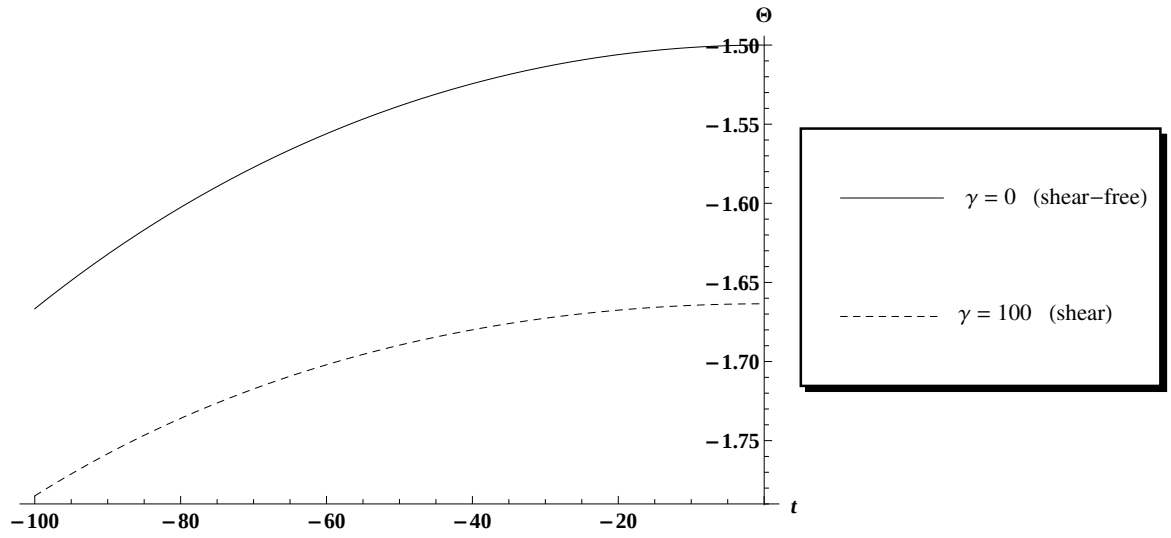

Figure 6.2: Collapse rate Θ (at the centre) as a function of time.

Our work clearly demonstrates the impact of shear on observable properties of a radiating, collapsing star. We were able to achieve this because our model allows us to switch off the shear and compare the physics in both the shearing and shear-free limits. In addition, Fig. 6.1 shows that the collapse rate at the boundary of the star is higher in the shearing model as compared to its shear-free counterpart. The opposite trend is observed at the centre of the collapsing star, ie., the collapse rate in the presence of shear is lower than the collapse rate in the shear-free case as evidenced in Fig. 6.2. It is well known that shear-free collapse proceeds at the slowest possible rate [99]. It is worthwhile noting that the effect of shear on the collapse rate at the boundary is of the order of 10^3 times smaller that that at the centre. The matter variables assume the following form

$$\rho = \frac{\left[\frac{8(1+at^2)^4\gamma\left[-5(c^2+r^2)(1+at^2)^4+\gamma\right]}{b}+\frac{w(r,t)}{\left[5(c^2+r^2)(1+at^2)^4-\gamma\right]}\right]}{2(1+br^2)^2(1+at^2)^2\left[3(c^2+r^2)(1+at^2)^4+\gamma\right]^3}, \tag{6.5.10a}$$

$$p_r = q_1 B = -\frac{-15(1+at^2)^8+\frac{30(1+at^2)^4}{c^2+r^2}+\frac{\gamma^2}{(c^2+r^2)^2}}{2(1+br^2)^2(1+at^2)^2\left[3(1+at^2)^4+\frac{\gamma}{c^2+r^2}\right]^2}, \tag{6.5.10b}$$

$$p_t = \frac{z_1(r,t)}{\left[b(1+br^2)^2(-5r^2(1+at^2)^4+\gamma)^2(3r^2(1+at^2)^4+\gamma)^3\right]}, \tag{6.5.10c}$$

where the function $w(r,t)$ is defined as

$$\begin{aligned} w(r,t) &= \Big[285c^8(1+at^2)^{16}+285r^8(1+at^2)^{16}-60r^2(1+at^2)^{12}\gamma \\ &\quad -34r^4(1+at^2)^8\gamma^2-60r^2(1+at^2)^4\gamma^3-3\gamma^4+20c^6(1+at^2)^{12} \\ &\quad \times(57r^2(1+at^2)^4+7\gamma)+2c^4(1+at^2)^8\Big[855r^4(1+at^2)^8 \\ &\quad +110r^2(1+at^2)^4\gamma-57\gamma^2\Big]+4c^2(1+at^2)^4\times\Big[285r^6(1+at^2)^{12} \\ &\quad +5r^4(1+at^2)^8\gamma-37r^2(1+at^2)^4\gamma^2-13\gamma^3\Big]\Big], \end{aligned} \tag{6.5.11}$$

and $z_1(r,t)$ is defined as

$$\begin{aligned} z_1(r,t) &= \Big[4(1+at^2)^2\Big[(5r^2(1+at^2)^4-\gamma)^3\gamma+br^2\Big[75r^8(1+at^2)^{16} \\ &\quad -135r^6(1+at^2)^{12}\gamma-305r^4(1+at^2)^8\gamma^2-69r^2(1+at)^4\gamma^3 \\ &\quad -14\gamma^4\Big]\Big]\Big]. \end{aligned} \tag{6.5.12}$$

The thermodynamical quantities at the centre of the star are given by

$$q_0 = -\frac{-15(1+at^2)^8+\frac{30(1+at^2)^4\gamma}{c^2}+\frac{\gamma^2}{c^4}}{2(1+at^2)^2\Big[3(1+at^2)^4+\frac{\gamma}{c^2}\Big]^2}, \tag{6.5.13a}$$

$$(p_r)_0 = \frac{-5+\frac{3\Big[-5(1+at^2)^4+\frac{\gamma}{c^2}\Big]^2}{\Big[3(1+at^2)^4+\frac{\gamma}{c^2}\Big]^2}}{4(1+at^2)^2}, \tag{6.5.13b}$$

$$\rho_0 = \frac{\Big[\frac{8(1+at^2)^4\Big(-5c^2(1+at^2)^4+\gamma\Big)}{b}+\frac{w(0,t)}{\Big(5c^2(1+at^2)^4-\gamma\Big)}\Big]}{2(1+at^2)^2\Big[3c^2(1+at^2)^4+\gamma\Big]^3}, \tag{6.5.13c}$$

$$(p_t)_0 = -\frac{4(1+at^2)^2}{b\gamma}, \tag{6.5.13d}$$

where $w(0,t)$ is given by

$$\begin{aligned} w(0,t) &= 285c^8(1+at^2)^{16}+140c^6(1+at^2)^{12}\gamma-114c^4(1+at^2)^8\gamma^2 \\ &\quad -52c^2(1+at^2)^4\gamma^3-3\gamma^4, \end{aligned} \tag{6.5.14}$$

and subscripts denote the quantities evaluated at $r=0$.

6.6 Causal thermodynamics

Causal heat flow in dissipative collapse has received widespread attention since the pioneering work by Herrera and co-workers [55, 100, 101, 102] on radiating stars. Many of the early stellar models described shear-free, dissipative collapse in the form of a radial heat flow in the free-streaming or diffusion approximation. Results obtained show that relaxational effects are prominent during the latter stages of collapse. In particular, it was shown that relaxational effects lead to higher temperatures within the stellar interior with cooling being enhanced closer to the surface of the collapsing body. The effect of shear and pressure anisotropy were recently highlighted within the Eckart framework. It is well known that the Eckart formalism of dissipative processes has several shortcomings as pointed out in numerous studies as highlighted in Chapter 5. The non–causal nature of the theory as well as its prediction of unstable equilibrium states has warranted the use of casual transport equations of the Maxwell-Cattaneo form. The study of relaxational effects during radiating, shearing collapse using a causal heat transport equation was first carried out by Di Prisco *et al* [28]. Their results show that the luminosity profiles obtained for nonvanishing relaxation times are different from those obtained when the relaxation times are ignored. The details are discussed further in Chapter 5. The relativistic version of the Cattaneo equation (5.5.1) given below is employed for the heat transport. Note that (5.5.1) is essentially the unpacked version of the Maxwell–Cattaneo form (5.4.9):

$$\tau_r h_a{}^b \dot{q}_b + q_a = -\kappa\big(h_a{}^b \nabla_b \mathcal{T} + \mathcal{T}\dot{u}_a\big).$$

The evolution terms (5.5.1) with the relaxation time coefficients τ_r are needed for relativistic causality, as well as for modelling high frequency or transient phenomena, where 'fast' variables and relaxation effects are important [29, 57, 85, 103, 104]. It has been shown for spherically symmetric stars with radial heat flow, the temperature gradient which appears as a result of the perturbation, and hence the luminosity, are highly dependent on the product of the relaxation time by the period of the oscillation

of the star.

We utilize the causal heat transport (5.5.6) equation to describe the evolution of the heat flux. In the case of constant mean collision time, corresponding to $\omega = 0$, we obtain the following expression for the causal temperature profile, i.e.

$$\begin{aligned} T^4(r,t) &= \frac{1}{16K^4(r)}\Bigg(-1/(\psi_1 C^2(t))64\Big(\beta\int\Big[K(r)(f^3(r)-15f^2(r)C^4(t) \\ &+315f(r)C^8(t)-45C^{12}(t)\Big]K'(r)/\Big[[f(r)-5C^4(t)][f(r)+3C^4(t)]^2\Big]dr \\ &+\Big(\int\frac{K^2(r)[f^2(r)+30f(r)C^4(t)-15C^8(t)]K'(r)}{[f(r)-5C^4(t)][f(r)+3C^4(t)]}dr\Big)C(t)\Big) \\ &+\frac{F(t)}{[C'(t)]^4}\Bigg), \end{aligned} \tag{6.6.1}$$

where ψ_1 is a constant. The function $F(t)$ is evaluated by invoking the boundary condition

$$\left(T^4\right)_\Sigma = \left(\frac{1}{r^2B^2}\right)_\Sigma\left(\frac{L_\infty}{4\pi\delta}\right), \tag{6.6.2}$$

where L_∞ is the total luminosity at infinity and δ (>0) is a constant. In the absence of bulk viscosity, radiation and shear viscosity, the expression (3.1.39) for L_∞ becomes

$$\begin{aligned} \left(T^4\right)_\Sigma &= -\left(5\left(at^2+1\right)^4-\frac{\gamma}{c^2+r^2}\right)\Bigg(30\gamma\left(at^2+1\right)^4\left(c^2+r^2\right)-15\Big(at^2+1\Big)^8 \\ &\times\left(c^2+r^2\right)^2+\gamma^2\Bigg)\times\Bigg(64\pi b\delta r^3\left(at^2+1\right)\times\Bigg(3\left(at^2+1\right)^4\left(c^2+r^2\right)+\gamma\Bigg)^2 \\ &\times\left(3\left(at^2+1\right)^4+\frac{\gamma}{c^2+r^2}\right)\Bigg)^{-1}. \end{aligned} \tag{6.6.3}$$

Fig. 6.3 clearly shows that the inclusion of shear leads to a higher core temperature.

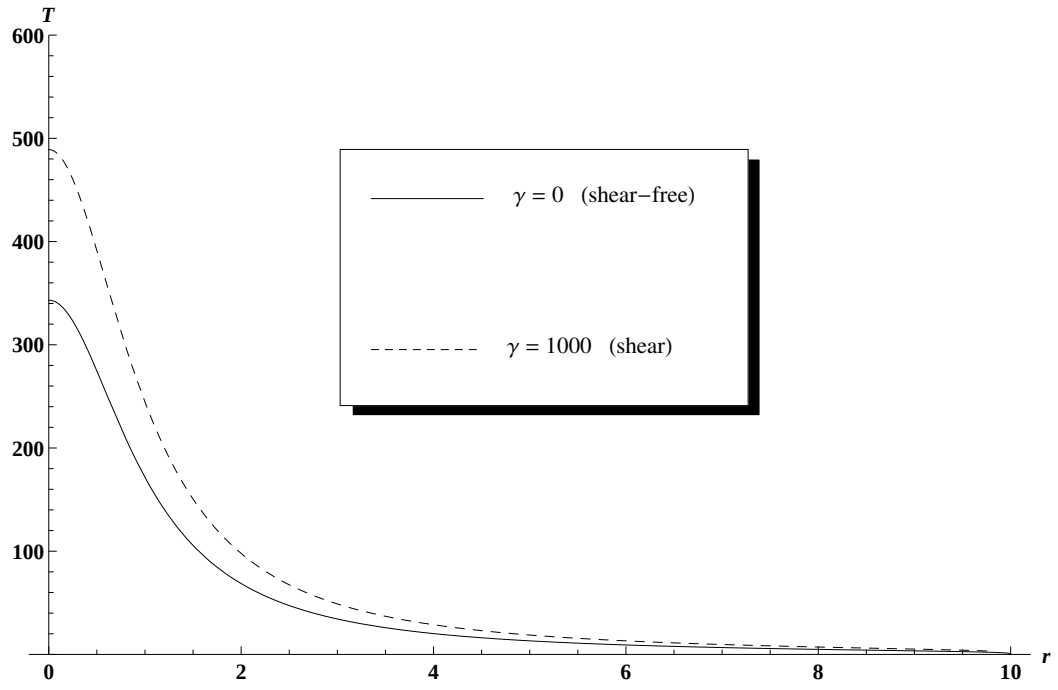

Figure 6.3: Non–causal temperature vs radial coordinate.

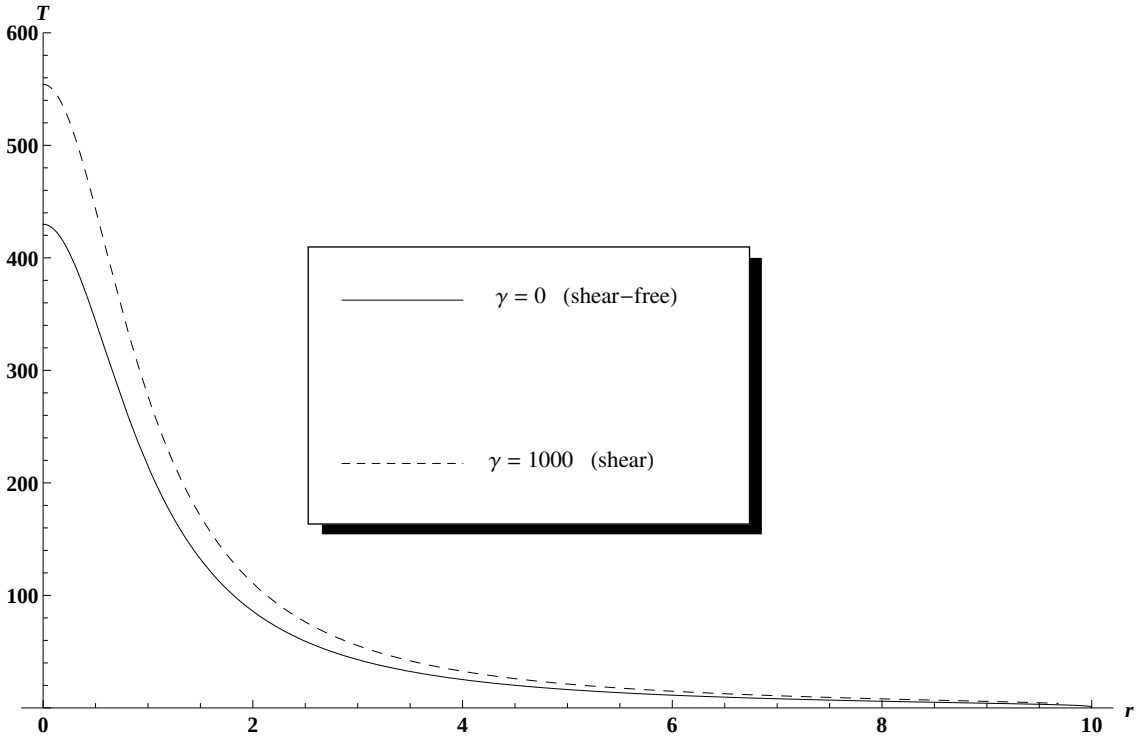

Figure 6.4: Causal temperature vs radial coordinate.

As with previous investigations [32, 33, 35, 69], Fig. 6.4 shows that relaxational

effects predict a higher temperature than its non–causal counterpart. The interesting feature in our investigation is the enhancement of the relaxational effects brought about by the inclusion of shear. We can understand the increased temperature within the stellar core on the basis that the shear is responsible for the internal friction between the layers of the stellar fluid. This interaction between the layers at each interior point of the collapsing body leads to the generation of heat within the core. Furthermore, we expect the generation of heat due to friction to be more pronounced closer to the centre of the star as the density and pressure here are maximum.

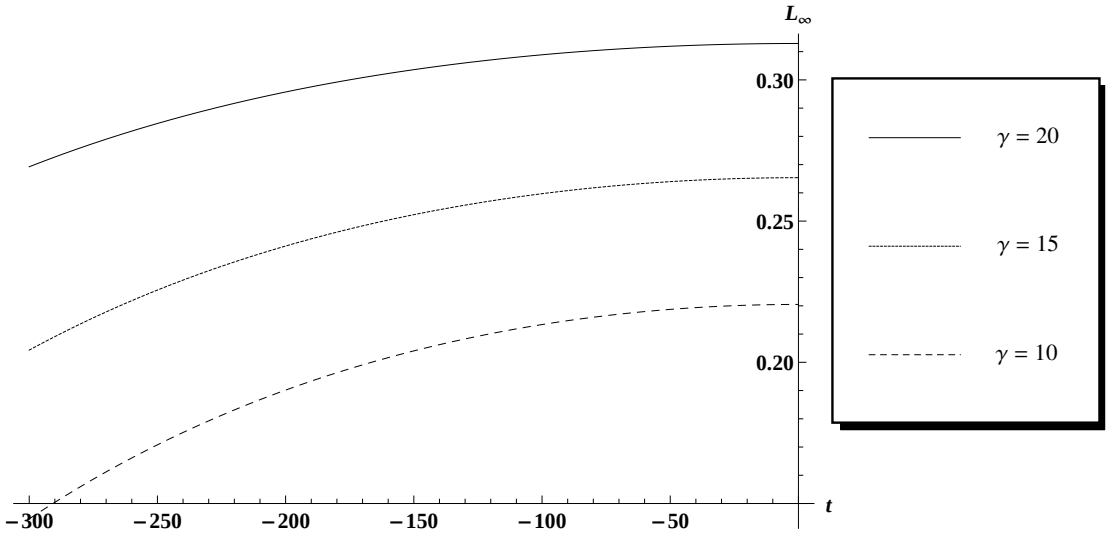

Figure 6.5: Luminosity at infinity vs time.

Fig. 6.5 illustrates the trend in the luminosity at infinity as a function of time. For our particular model, the luminosity is independent of time in the shear-free limit. This implies that in the shear-free model the horizon is never encountered. In this case the rate of energy dissipation is equal to the collapse rate of the core. Similar models were studied by Banerjee *et al* [105], Naidu and Govender [36] and Maharaj *et al* [106]. Fig. 6.5 shows that the luminosity increases as the shear increases. We note that in our model there is no direct link between the luminosity and the product $\sigma\eta$ where η is the shear viscosity coefficient. The trend in the luminosity profile, in relation to the shear, can be understood in terms of the deviations from the shear-free profile.

These deviations are obtained from the evolution equation describing the shear and are related to a scalar function

$$Y_{TF} = 16\pi\eta\sigma + \frac{4\pi}{R^3}\int_0^R R^3\left(D_R\rho - 3q\frac{U}{RE}\right)dR, \tag{6.6.4}$$

where ρ is the energy density, $D_R = \frac{1}{R'}\frac{\partial}{\partial r}$ is the proper radial derivative, $D_T = \frac{1}{A}\frac{\partial}{\partial t}$ is the proper time derivative, $U = D_T R < 0$ and

$$E = \left(1 + U^2 - \frac{2m}{R}\right)^{1/2}.$$

is the mass function which measures the stability of the shear-free condition [107]. Y_{TF} is a combination of localized pressure anisotropy, inhomogeneities of the energy density, dissipative fluxes such as heat flow and shear viscosity. It is quite clear from (6.6.4) that even in the absence of shear viscosity η (if we ignore the internal friction between the layers of the collapsing fluid) there can be an increase in the absolute value of the shear scalar due to the presence of density inhomogeneity and heat flux. From (6.6.4) we see that energy density inhomogeneity is responsible for deviations from an initial shear-free profile. These deviations can be enhanced in the presence of heat dissipation within the stellar core. The role of energy density inhomogeneity during dissipative collapse was highlighted by Herrera [50] in which it was shown that the factors responsible for the generation of energy density inhomogeneities depend on the nature of the fluid distribution. Our results confirm the findings of Herrera in that both shear and dissipative fluxes (in our case heat flow) lead to the generation of energy density inhomogeneities. It has been shown that sufficiently dominant shearing effects in the neighbourhood of the singularity can delay the formation of the apparent horizon [108]. This dispersive effect of shear can lead to the singularity being exposed to an external observer.

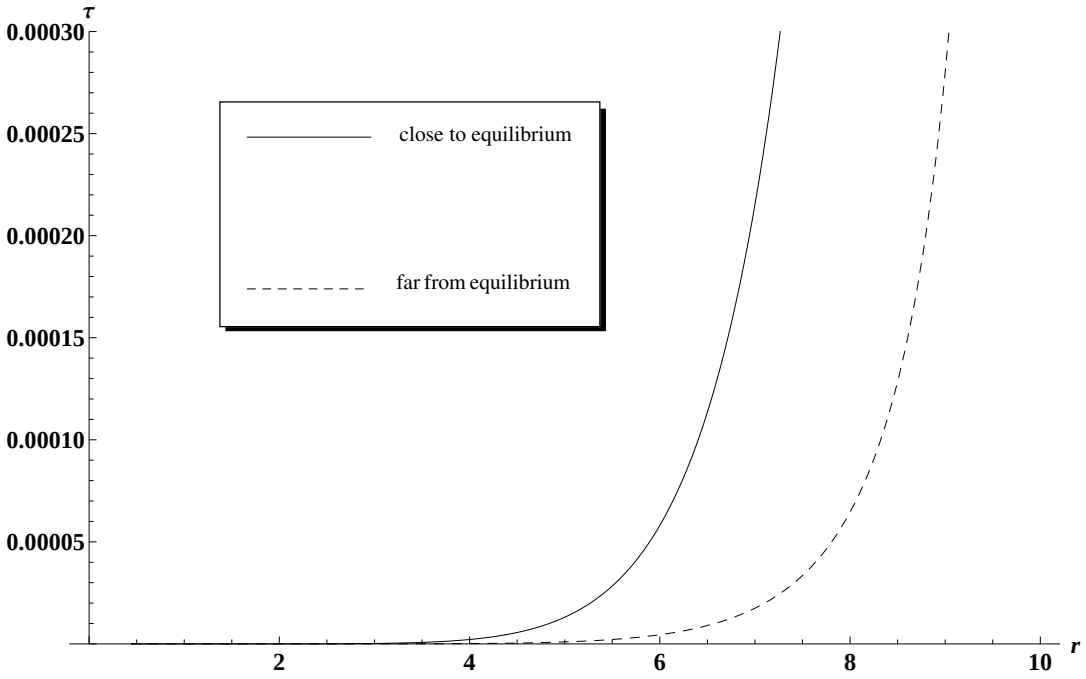

Figure 6.6: Relaxation time τ_r as a function of the radial coordinate.

Fig. 6.6 shows the behaviour of the relaxation time as a function of the radial coordinate. The relaxation time for the shear stress exhibits substantially different behaviour when the fluid is close to hydrostatic equilibrium as opposed to late-time collapse. In particular, our results confirm earlier findings by Naidu *et al* [37] in which they showed that

$$\frac{(\tau_1)_{early}}{(\tau_1)_{late}} \approx 100. \tag{6.6.5}$$

In their model, the acceleration vanishes and the particle trajectories are geodesics.

6.7 Proper radius

The proper radius R_p for the model employed in this chapter, can be obtained by integrating the gravitational potential $B(t, r)$ with respect to the radial coordinate r.

Utilizing (6.5.5) we obtain

$$\begin{aligned} R_p &= \int_0^{r_\Sigma} B(t,r)\,dr \qquad (6.7.1)\\ &= \frac{2b\left(8\gamma\log\left(5c^2\left(at^2+1\right)^4+5\left(r_\Sigma\right)^2\left(at^2+1\right)^4-\gamma\right)+15\left(r_\Sigma\right)^2\left(at^2+1\right)^4\right)}{25\left(at^2+1\right)^3}, \end{aligned}$$

With suitable choices for a, b, c and γ in (6.7.1) we find that the proper radius R_p decreases with time, which is reasonable since the star is undergoing gravitational collapse and losing mass and energy.

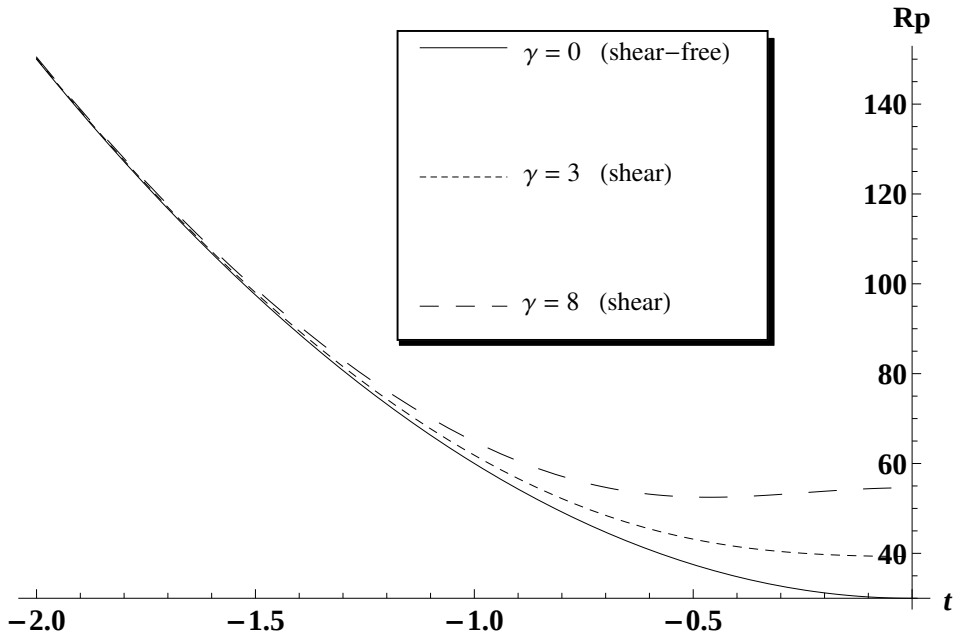

Figure 6.7: Proper radius profiles versus time.

In Fig. 6.7 we plot the profiles for the proper radius against time, for shear–free conditions ($\gamma = 0$) as well with shear switched on $\gamma \neq 0$. It is evident that shear plays a significant role during the late stages of collapse and in actual fact delays gravitational collapse. For high values of γ we find that after a particular time the radius of the star begins to increase which implies that the star is starting to expand. A possible explanation is that the high degree of shear (through γ) produces such intense internal friction that the stellar fluid heats up considerably resulting in enormous heat flow and hydrodynamic pressure which is able to significantly overcome the gravitational force.

6.8 Stability analysis of the model

We are studying a system in which two major forces are at play, viz. the gravitational forces attempting to contract the fluid as well as the hydrodynamic forces trying to overcome gravity. The authors in [109] point out that the study of the "resistance of a given material to be compressed (its compressibility)" is critical to the study of gravitational collapse. For the adiabatic scenario, i.e. one in which there is no heat flow, the adiabatic index (a measure of a fluids resistance to compression) is quite easily obtained. The adiabatic index Γ is given by the relationship

$$\Gamma = \frac{d\ln P}{d\ln \rho}, \tag{6.8.1}$$

where $\Gamma < \frac{4}{3}$ is required for stability against gravitational collapse. Chan [49] looked at the collapse of a radiating, anisotropic star with heat flow and utilized an effective adiabatic index given by

$$\Gamma_{eff} = \frac{d\ln P_r}{d\ln \rho}. \tag{6.8.2}$$

We utilize equation (6.8.2) to investigate the stability of our model near the centre of the star as well as on an arbitrarily chosen hypersurface (r_Σ). It is evident from Fig. 6.8 that the presence of shear induces instabilities (asymptotic behavior) that are very pronounced near the core region. For late stages of collapse, we find the core region to be stable.

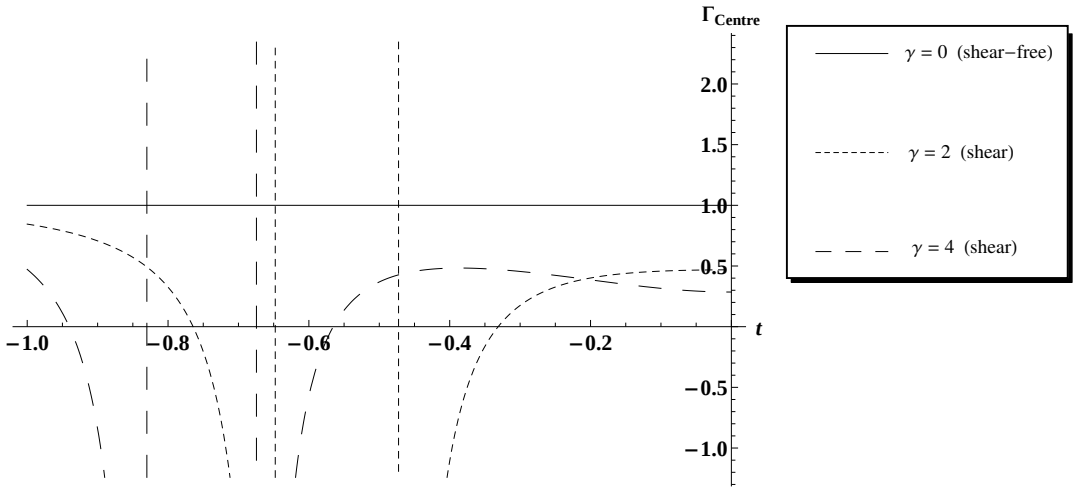

Figure 6.8: Adiabatic index profiles versus time at the centre.

The stability index on the hypersurface ($r_\Sigma = 5$) shown in Fig. 6.9 appears to be independent of shear during the early stages of collapse, but during the late stages the impact of shear is quite evident. In fact, the presence of shear appears to be slowing down (during the latter stages of collapse) the collapse process thereby decreasing the instability of the system. In other words, the presence of shear during the latter stages of collapse renders the fluid 'softer' and thus less susceptible to gravitational collapse. At the boundary the shear is contributing positively to the hydrodynamical forces which are competing with the gravitational forces to keep the stellar fluid stable.

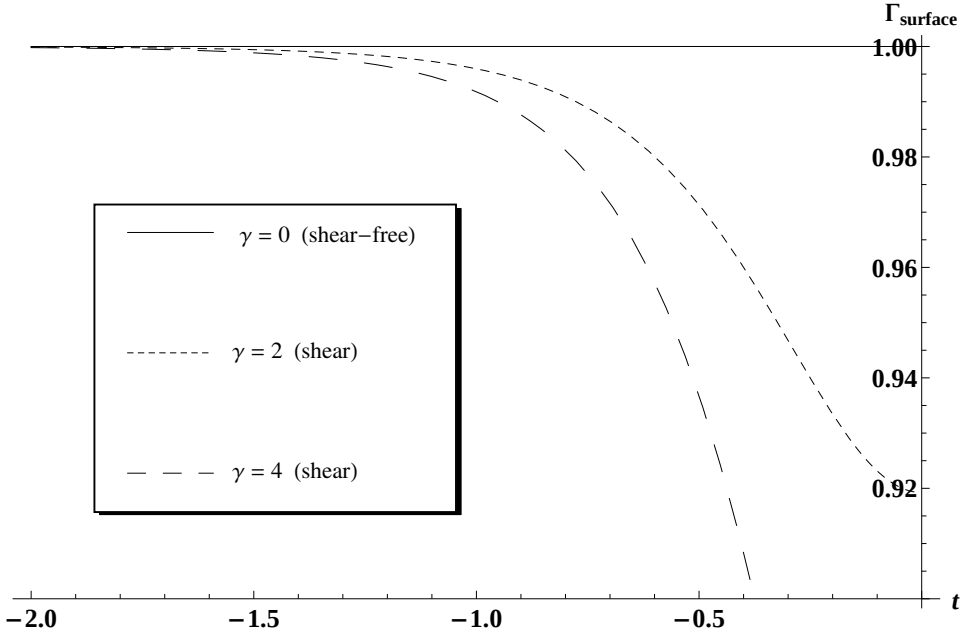

Figure 6.9: Adiabatic index profiles versus time at the surface.

The results yielded by our model, in particular for the very late stages of the collapse shown in Figs. 6.8 and 6.9, are in excellent agreement with the findings of Chan *et al* [19]. They report that shearing viscous collapse results in much more stable configurations compared to shear–free collapse (with either $\eta = 0$ or $s = 0$ in (4.4.5)) for both the Newtonian limit (4.4.5),

$$\Gamma < \frac{4}{3} - \left[\frac{4}{9}\eta|s|\frac{\sqrt{\alpha_\Sigma}}{|p_o'|r}\right]_{\rm MAX},$$

as well as for the Post–Newtonian limit (4.4.6),

$$\Gamma < \frac{4}{3} + \left[\frac{\kappa p_o \rho_o r}{3|p_o'|} - \frac{4}{9}\eta|s|\frac{\sqrt{\alpha_\Sigma}}{|p_o'|r} - \frac{1}{9}\kappa\rho_o r\eta|s|\frac{\sqrt{\alpha_\Sigma}}{|p_o'|} - \frac{2}{9}|s| - \frac{8}{9}|s|\frac{p_o}{|p_o'|r} - \frac{1}{3}|s|\frac{\rho_o r\alpha_\Sigma}{|P_o'|}\right]_{\rm MAX}.$$

Relativistic corrections due to an increased effective energy density driven by the isotropic pressure is the only term in (4.4.6) that is positive, which decreases the unstable range of Γ, and thereby attempts to make the fluid stiffer and more susceptible

to collapse. The rest of the terms in (4.4.6) are negative and have a collective effect that is greater than the only positive term, which implies that the inclusion of shear is successful in stabilizing the stellar fluid distribution against collapse. In terms of our "spring" model, shear viscosity makes the fluid to become softer, i.e. the "spring constant" of the fluid Γ is lowered making the fluid distribution less susceptible to gravitational collapse and consequently more stable.

We also employ another technique [110, 111, 112] to investigate the stability of our model near the centre ($r \approx 0$) and on some arbitrary hypersurface ($r = r_\Sigma$). Herrera points out that stability occurs for those regions in which the radial speed of sound exceeds the transverse speed of sound, i.e.

$$v_{st}^2 - v_{sr}^2 < 0, \tag{6.8.3}$$

where

$$v_{sr}^2 = \frac{dp_r}{d\rho} \qquad \text{and} \qquad v_{st}^2 = \frac{dp_t}{d\rho} \tag{6.8.4}$$

We plot graphs of $v_{st}^2 - v_{sr}^2$ for the shear–free case and for small deviations (small γ) near the centre in Fig. 6.10 and on an arbitrarily chosen hypersurface ($r_\Sigma = 5$) in Fig. 6.11 for the star.

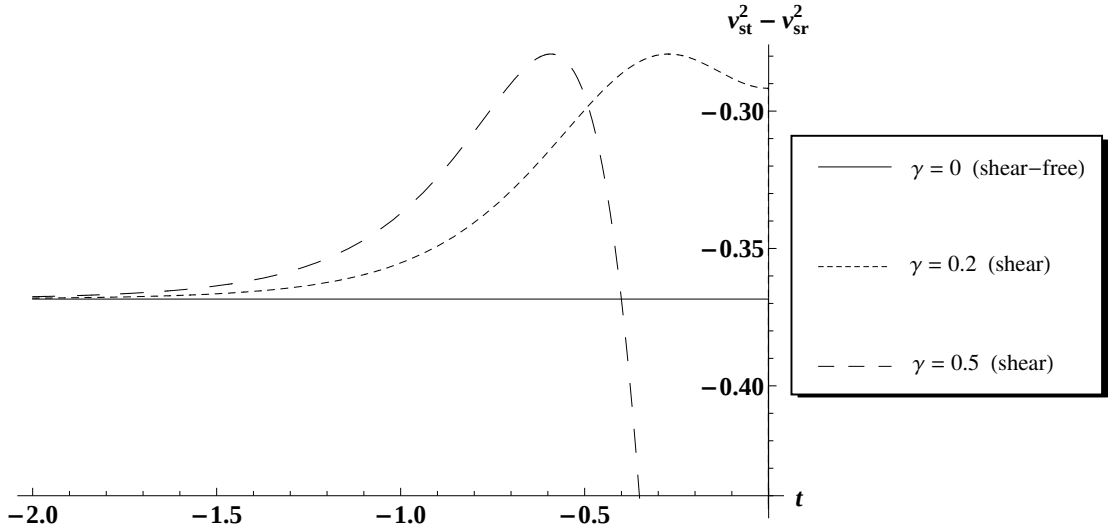

Figure 6.10: $v_{st}^2 - v_{sr}^2$ profiles versus time near the centre ($r \approx 0$).

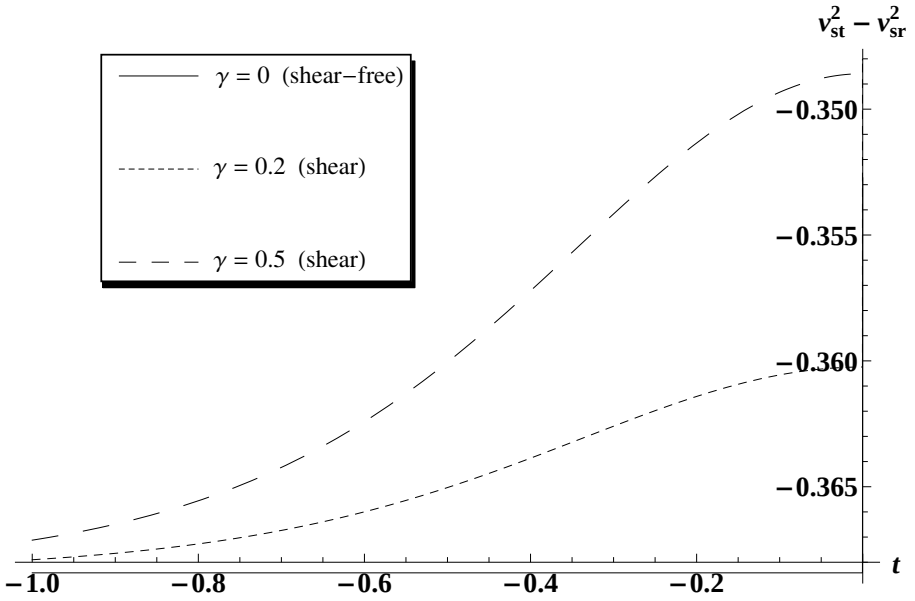

Figure 6.11: $v_{st}^2 - v_{sr}^2$ profiles versus time on the hypersurface ($r_\Sigma = 5$)

We find that for late time collapse, $-1 \leq v_{st}^2 - v_{sr}^2 \leq 0$ near the centre and boundary for the shear–free case as well as for small γ. According to [111] this corresponds to the existence of potentially stable (rather than cracking) regions. Cracking "refers only to

the tendency of the configuration to split (or to compress) at a particular point within the distribution but not to collapse or to expand" [111].

6.9 Conclusion

Utilising a solution recently discovered by Thirukkanesh *et al* [1] which describes a radiating sphere undergoing dissipative collapse we were able to clearly demonstrate the effect of shear on observable quantities such as the temperature and luminosity profiles. The simple nature of this particular exact solution allows the shear to be switched off which makes it possible (for the first time) to compare the dynamics of the collapse process both in the shearing and shear-free limits. We were able to show that the shear leads to an enhancement of the temperature at each interior point of the collapsing body. Also for the first time, we are able to show that relaxational effects are pronounced in the presence of shear. These effects are strengthened during late stages of gravitational collapse. We were able to confirm that the presence of shear delays the collapse process and highlighted this directly by utilising expressions for the stability index used by Chan [19]. We have comprehensively explored the extent of this model and in particular the pleasant feature of the shear 'switch'.

Chapter 7

Impact of anisotropic stresses during dissipative gravitational collapse

7.1 Introduction

Anisotropy in a fluid distribution simply implies unequal principle stresses, i.e. the radial pressure is not equal to the tangential pressure. The origin of anisotropy has been extensively researched and much of the pioneering work in this area has been reviewed by Herrera and Santos [45]. Anisotropic particle transport arises from turbulence caused by differential rotation within the stellar core [113]. It is a widely accepted view that pressure anisotropy is a characteristic feature of superdense (in excess of nuclear densities) stars, and it has been used to model the behaviour of quintessence stars [114]. In a recent paper Ivanov [115] presents strong arguments for a model having anisotropy and heat flow, as a general model for relativistic fluids. The stability of anisotropic fluids has been investigated by Chan [49] and Chan *et al* [77].

In this work we employ the Bowers and Liang [2] static solution as a seed model to investigate the role played by anisotropy for highly dense matter of the order of

$10^{15} g.cm^{-3}$. We employ a linear perturbative scheme to analyse the subsequent dissipative collapse starting from the initially static Bowers and Liang [2] model. Our investigation centres around the impact of the variation in the anisotropic parameter on the static property variables as well the perturbed quantities, viz. radial and tangential pressures, heat flow, energy density, expansion scalar and temperature profiles. The model allows us to directly measure the behaviour of the above mentioned physical properties starting with the isotropic case and then seeing the departure from isotropy as the radial pressure gradually begins to dominate the tangential pressure. Using the Bowers and Liang [2] model, we essentially merge the idea of varying the anisotropic factor [51] with the idea of temperature perturbation (shear–free and isotropic pressure) [39]. We arrive at a model that allows us to investigate the effect of the anisotropic factor (varying degree) on the static properties as well as a variety of perturbed properties of a spherically symmetric collapsing star possessing shear, radial heat flow and pressure anisotropy.

This chapter is organised as follows. In §7.2 we present the field equations describing the geometry and matter content for a star undergoing shearing gravitational collapse. In §7.3 we discuss the perturbative scheme as well as the static and perturbed quantities including the expansion coefficient, shear and mass functions. In §7.4 we present the junction conditions for the smooth matching of the interior spacetime with Vaidya's exterior solution across a timelike boundary. In §7.5 we present the temporal equation employed in the perturbative scheme that begins with an initially static star that is perturbed and the perturbations decay exponentially with time. In §7.6 we give the results obtained for the static core, and in §7.7 the results for the nonstatic model is presented. In §7.8 stability analysis of our model, based on the work of Chan [49], is investigated. In §7.9 motivation for using a causal heat transport equation is given. In §7.10 the perturbations to the temperature are obtained and analysed and the chapter concludes with §7.11.

7.2 Shearing spacetimes

The interior spacetime of the collapsing sphere is described by the general spherically symmetric, shearing metric in comoving coordinates given by (2.5.1). The energy momentum tensor describing the interior matter composition is given by (6.2.1). The heat flow vector q^a and the fluid four–velocity V^a are given by (2.5.9). The fluid four–velocity (V^a), radial unit four–vector (χ^a) and the heat flux (q^a) satisfy (2.5.8). The magnitude of the heat flow is given by (2.6.2) and can be expressed as (2.6.3). The collapse rate is given by (2.5.13) and the magnitude of the fluid four–acceleration is given by (2.5.12). The shear tensor σ_{ab} by (2.5.14) and shear σ is given by (2.5.16). The mass function $m(t,r)$ is given by (2.6.4). The nonzero components of the Einstein field equations, for the line element are given by (6.2.2a)–(6.2.2d).

7.3 Perturbative scheme

We begin with an initially static fluid described by quantities that are only dependant on the radial coordinate. We represent such quantities with a zero subscript and we also assert that the metric functions $A(t,r)$, $B(t,r)$ and $Y(t,r)$ and matter functions have the same time dependence when perturbed. The metric functions and thermodynamic variables are given by (4.1.1)–(4.1.11).

The shear-free case within this perturbative scheme was studied by several authors [18], [19] and [77]. In all these investigations the static model was taken to be the isotropic Schwarzschild interior solution. Taking into consideration (4.1.1)–(4.1.11), we obtain the relationships for the static configuration ρ_o given by (4.2.2a), p_{ro} given by (4.2.2b) and p_{to} given by (4.2.2c). Using (4.1.1)–(4.1.6) and (4.1.11) as well as (6.2.2a)–(6.2.2d) we obtain the perturbed energy density $\overline{\rho}$ given by (4.2.3a), the perturbed radial pressure $\overline{p}_r$ given by (4.2.3b), perturbed tangential (transverse) pressure $\overline{p}_t$ given by (4.2.3c) and perturbed heat flow given by (4.2.3d). Expressions for the

perturbed expansion $\overline{\Theta}$ coefficient and shear $\overline{\sigma}$ are given respectively by (4.2.4) and (4.2.5). The static and perturbed configurations for the mass function are respectively (4.2.6) and (4.2.7).

7.4 Exterior spacetime and junction conditions

The exterior spacetime is taken to be the Vaidya solution [15] given by (2.8.1). The necessary conditions for the smooth matching of the interior spacetime (2.5.1) to the exterior spacetime (2.8.1) have been extensively reviewed in Chapter 3. We present the main results that are necessary for modeling a radiating star. The continuity of the intrinsic and extrinsic curvature components of the interior and exterior spacetimes across a timelike hypersurface (Σ) yields the necessary and sufficient junction conditions given (3.1.12a),(3.1.12b), (3.1.24a) and (3.1.25) (in the absence of bulk viscosity and shear viscosity):

$$\begin{aligned} A\left(t, r_{\Sigma}\right) dt &= \left(1-\frac{2m(v)}{\mathcal{R}_{\Sigma}}+2\frac{d\mathcal{R}_{\Sigma}}{dv}\right)^{\frac{1}{2}} dv, \\ Y(t, r_{\Sigma}) &= \mathcal{R}_{\Sigma}(v), \\ m(v)_{\Sigma} &= \left\{\frac{Y}{2}\left[\left(\frac{\dot{Y}}{A}\right)^{2}-\left(\frac{Y'}{B}\right)^{2}+1\right]\right\}_{\Sigma}, \\ (p_r)_{\Sigma} &= (q_1 B)_{\Sigma}. \end{aligned} \tag{7.4.1}$$

7.5 The temporal equation employed in the perturbation scheme

Relation (3.1.25), together with (4.2.3d) and $(p_{ro})_{\Sigma} = 0$ in (4.2.3b), determines the temporal evolution of the collapsing star, and is given by

$$\alpha_{\Sigma} T - \ddot{T} = 2\beta_{\Sigma}\dot{T} > 0,$$

where α_{Σ} is given by (4.3.2) and β_{Σ} is given by (4.3.3). For a collapsing model it is necessary to have an exponential decaying function which represents a star that

is initially static at $t = -\infty$, i.e. $T(-\infty) = 0$ and then decreases with time. This temporal behaviour of our model is satisfied if $\alpha_\Sigma > 0$ and $\beta \leq 0$. Taking these factors into account, the temporal evolution equation of our model is then given by

$$T(t) = -e^{\left(-\beta_\Sigma + \sqrt{\alpha_\Sigma + \beta_\Sigma{}^2}\right)t}.$$

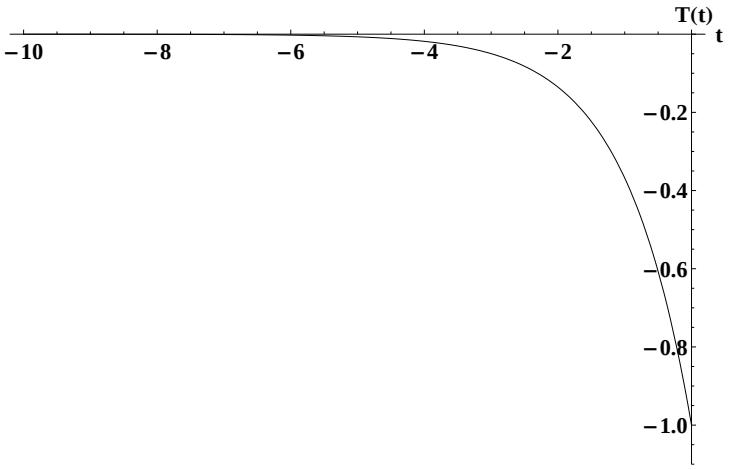

Figure 7.1: Temporal evolution.

7.6 The static core

We take the interior static solution to be the Bowers and Liang [2] model with constant density. This model is the generalisation of the interior Schwarzschild solution to include anisotropic pressures. This model was used to investigate the role played by local anisotropy in highly dense matter distributions typically of the order of $10^{15} g.cm^{-3}$. If we denote the fractional anisotropy by $\Delta_f = \frac{p_t - p_r}{p_r}$ then the Bowers and Liang model exhibits the following features:

(a) $\Delta_f > 0$: The maximum equilibrium mass and surface redshift are greater than their corresponding isotropic ($\Delta_f = 0$) counterparts.

(b) $\Delta_f < 0$: The maximum mass and surface redshift are less than their corresponding isotropic values.

Moreover, the anisotropy allows for arbitrarily large surface redshifts as observed in quasars.

The Bowers and Liang metric is

$$\begin{aligned} ds^2 &= -\left[\frac{3\big(1-2M/r_\Sigma\big)^{h/2}-\big(1-2m/r\big)^{h/2}}{2}\right]^{2/h} dt^2+\Big(1-\frac{2m}{r}\Big)^{-1}dr^2 \\ &\quad +r^2\big(d\theta^2+\sin^2\theta d\phi^2\big), \end{aligned} \tag{7.6.1}$$

where $0 \le r \le R$. From the metric (7.6.1) it is clear that

$$A_o^2 = \left[\frac{3\big(1-2M/r_\Sigma\big)^{h/2}-\big(1-2m/r\big)^{h/2}}{2}\right]^{2/h}, \tag{7.6.2}$$

$$B_o^2 = \Big(1-\frac{2m}{r}\Big)^{-1}, \tag{7.6.3}$$

and

$$Y_o^2 = r^2, \tag{7.6.4}$$

where h is a constant. In the physical analysis that follows we take

$$y = \Big(1-\frac{2m}{r}\Big)^{-1/2}, \quad a = 1, \quad b = r, \quad m = \frac{r^3 M}{R^3}. \tag{7.6.5}$$

Using (7.6.2)–(7.6.5), equations (4.2.2a)–(4.2.2c) become, respectively,

$$\rho_o = 6M/R^3, \tag{7.6.6}$$

$$\begin{aligned} p_{ro} &= -\rho_o\left[\Big(1-\frac{2Mr^2}{R^3}\Big)^{h/2}-\Big(1-\frac{2M}{R}\Big)^{h/2}\right]\times\left[\Big(1-\frac{2Mr^2}{R^3}\Big)^{h/2}\right. \\ &\quad \left.-3\Big(1-\frac{2M}{R}\Big)^{h/2}\right]^{-1}, \end{aligned} \tag{7.6.7}$$

$$\begin{aligned} p_{to} &= -6M\left(2\left(1-\frac{2M}{R}\right)^{h/2}\left(1-\frac{2Mr^2}{R^3}\right)^{h/2}\big((h+3)Mr^2-2R^3\big)\right. \\ &\quad +3\left(1-\frac{2M}{R}\right)^{h}\big(R^3-2Mr^2\big)+\big(R^3-2Mr^2\big)\left(1-\frac{2Mr^2}{R^3}\right)^{h}\Bigg) \\ &\quad \times\left(R^3\big(R^3-2Mr^2\big)\left(\left(1-\frac{2Mr^2}{R^3}\right)^{h/2}-3\left(1-\frac{2M}{R}\right)^{h/2}\right)^2\right)^{-1}. \end{aligned} \tag{7.6.8}$$

The anisotropy parameter $\Delta = p_t - p_r$ is expressed (for the static case) as

$$\begin{aligned}\Delta &= -12(h-1)M^2r^2\left(1-\frac{2M}{R}\right)^{h/2}\left(1-\frac{2Mr^2}{R^3}\right)^{h/2} \\ &\times\left(R^3\left(R^3-2Mr^2\right)\left(\left(1-\frac{2Mr^2}{R^3}\right)^{h/2}-3\left(1-\frac{2M}{R}\right)^{h/2}\right)^2\right)^{-1}. \quad (7.6.9)\end{aligned}$$

We point out that equations (7.6.10)-(7.6.16) below, including their derivation, can be found in a review article by Herrera and Santos [45]. We simply state the equations here, and discuss the relationship between the anisotropy parameter Δ and the anisotropic factor C. Δ can also be written as

$$\Delta = \frac{4}{3}\pi Cr^2\Big(\rho_o + p_{ro}\Big)\Big(\rho_o + 3p_{ro}\Big)\Big(1-\frac{2m}{r}\Big)^{-1}, \quad (7.6.10)$$

where the anisotropic factor C, measures the degree of anisotropy and is given by

$$h = 1 - 2C. \quad (7.6.11)$$

It follows from equation (7.6.10) that the anisotropic parameter can be recast as $\Delta = C\chi(r)$, where $\chi(r) = \frac{4}{3}\pi r^2\big(\rho_o + p_{ro}\big)\big(\rho_o + 3p_{ro}\big)\big(1-\frac{2m}{r}\big)^{-1}$. We also point out that $\chi(r) > 0$ for all r, implying that Δ is directly proportional (and of similar sign) to C. From (7.6.11) it is clear that $h = 1$ corresponds to $C = 0$ which is the isotropic case, while $h = 2$ and $h = 4$ correspond respectively to $C = -\frac{1}{2}$ and $C = -\frac{3}{2}$ which imply that the radial pressure dominates the tangential pressure. The model has a limiting case of $h = 0$ which corresponds to the Florides [116] solution which is not considered in our analysis.

The critical value of $2M/r_\Sigma$, resulting in infinite central pressure, is given by

$$\left(\frac{2M}{r_\Sigma}\right)_{crit} = 1 - \Big(\frac{1}{3}\Big)^{2/h}, \quad (7.6.12)$$

and the associated critical mass is given by

$$M_{crit} = \left(\frac{3}{32\pi\rho_o}\right)^{1/2}\left[1-\Big(\frac{1}{3}\Big)^{2/h}\right]^{3/2}. \quad (7.6.13)$$

It is also worthwhile to note that the ratio of the anisotropic critical mass to that of the isotropic case is given by

$$\frac{(M_{ani})_{crit}}{(M_{iso})_{crit}} = \frac{8}{9}\left[1 - \left(\frac{1}{3}\right)^{2/h}\right]^{3/2}. \tag{7.6.14}$$

The redshift z at the star's surface is expressed as

$$z = \left(1 - \frac{2M}{r_\Sigma}\right)^{-1/2} - 1. \tag{7.6.15}$$

Using equation (7.6.15), the critical value of the red shift is

$$z_{crit} = 3^{1/h} - 1. \tag{7.6.16}$$

From Fig. 7.2 we note that static radial pressure is a monotonically decreasing function of the radial coordinate r. In addition, the radial pressure is enhanced at each interior point of the stellar distribution as the relative anisotropy increases (larger h values). We observe similar behaviour for the tangential pressure (see Fig. 7.3). We note that p_{to} does become negative for $h = 4$ for a certain range of values during the collapse process.

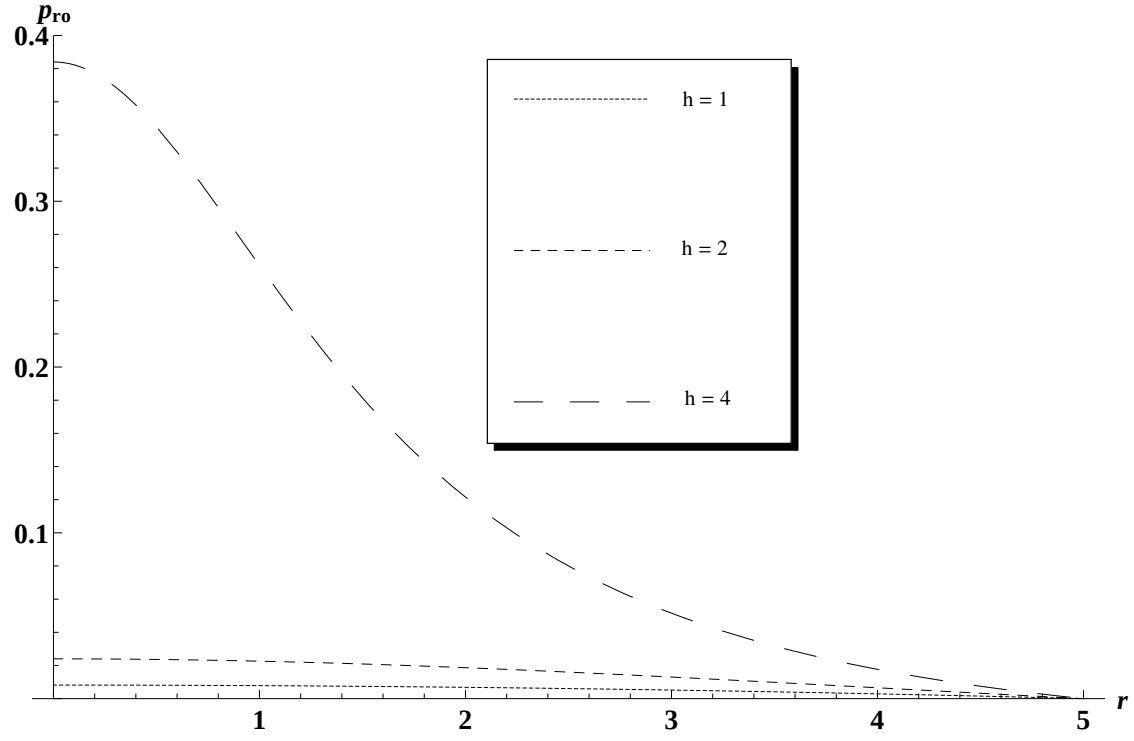

Figure 7.2: Static radial pressure p_{ro} profiles versus radial coordinate.

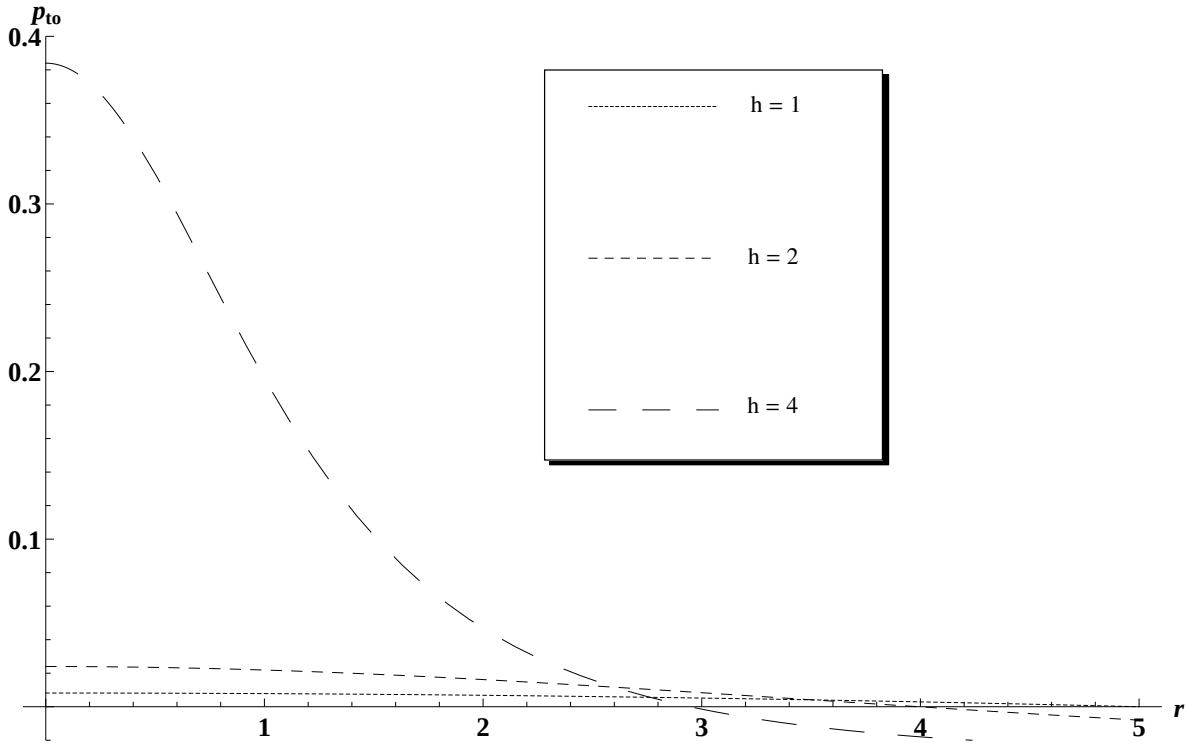

Figure 7.3: Static tangential pressure p_{to} profiles versus radial coordinate for $M = 1$ and $R = 5$.

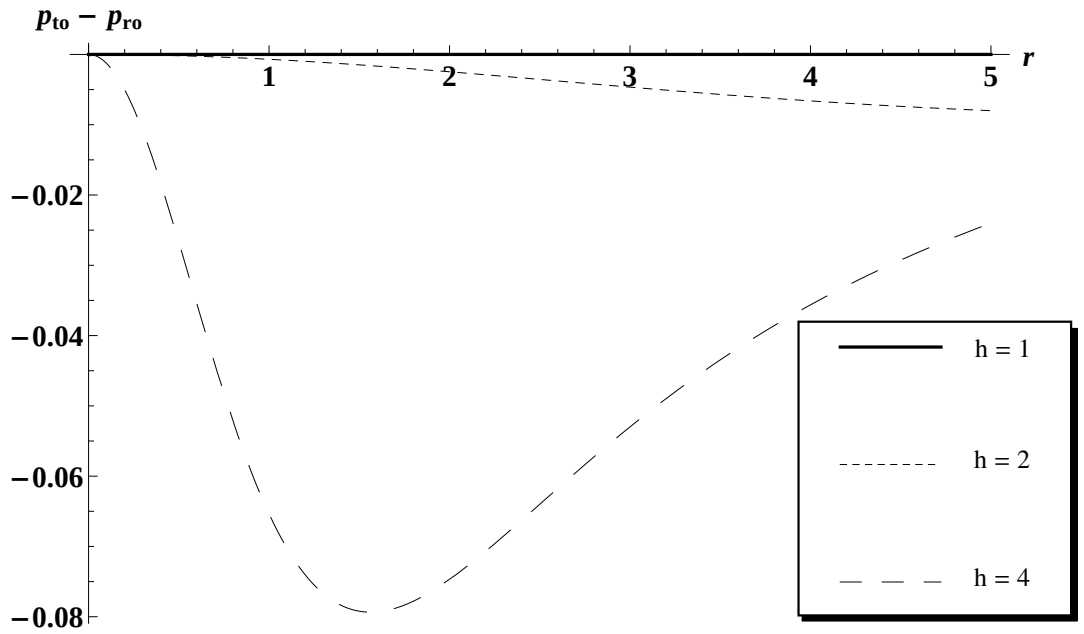

Figure 7.4: $p_{to} - p_{ro}$ against radial coordinate.

7.7 The nonstatic model

Using equations (4.2.3a)–(4.2.5) we obtain the perturbation in the density, radial pressure, tangential pressure, heat flow, collapse rate and shear respectively. These have the forms

$$\overline{\rho} = \frac{4T(t)\left(-20M^3r^6+4M^2r^2\left(6r^2+1\right)R^3-M\left(9r^2+4\right)R^6+R^9\right)}{rR^6\sqrt{1-\frac{2Mr^2}{R^3}}\left(R^3-2Mr^2\right)}, \tag{7.7.1}$$

$$\begin{aligned}
\overline{p}_r \;=\; & -\frac{2\left(3\left(1-\frac{2M}{R}\right)^{h/2}-\left(1-\frac{2Mr^2}{R^3}\right)^{h/2}\right)^{-\frac{h+1}{h}}}{rR^6\sqrt{1-\frac{2Mr^2}{R^3}}\left(R^3-2Mr^2\right)}\times\Bigg[-2^{\frac{1}{h}+2}M^2r^3R^3 \\
& \times\left(1-\frac{2Mr^2}{R^3}\right)^{\frac{h+1}{2}}+2^{\frac{1}{h}+1}MrR^6\left(1-\frac{2Mr^2}{R^3}\right)^{\frac{h+1}{2}} \\
& -3\left(3\left(1-\frac{2M}{R}\right)^{h/2}-\left(1-\frac{2Mr^2}{R^3}\right)^{h/2}\right)^{\frac{1}{h}} \\
& \times\left(1-\frac{2M}{R}\right)^{h/2}\left(2Mr^2-R^3\right)\left(4M^2r^4-4M\left(r^2+1\right)R^3+R^6\right) \\
& +\left(3\left(1-\frac{2M}{R}\right)^{h/2}-\left(1-\frac{2Mr^2}{R^3}\right)^{h/2}\right)^{\frac{1}{h}}\left(1-\frac{2Mr^2}{R^3}\right)^{h/2} \\
& \times\left(24M^3r^6-4M^2r^2\left(7r^2+4\right)R^3+2M\left(5r^2+3\right)R^6-R^9\right)\Bigg]T(t) \\
& -\left(2^{\frac{h+2}{h}}\ddot{T}(t)\left(3\left(1-\frac{2M}{R}\right)^{h/2}-\left(1-\frac{2Mr^2}{R^3}\right)^{h/2}\right)^{-2/h}\right) \\
& \times\left(r\sqrt{1-\frac{2Mr^2}{R^3}}\right)^{-1},
\end{aligned} \tag{7.7.2}$$

$$
\begin{aligned}
\overline{p}_t &= -\frac{2\left(3\left(1-\frac{2M}{R}\right)^{h/2}-\left(1-\frac{2Mr^2}{R^3}\right)^{h/2}\right)^{-\frac{h+1}{h}}}{rR^6\sqrt{1-\frac{2Mr^2}{R^3}}\left(R^3-2Mr^2\right)}\times T(t)\Bigg(-3\left(1-\frac{2M}{R}\right)^{h/2} \\
&\times\left(2Mr^2-R^3\right)\left(4M^2r^4-4M\left(r^2+1\right)R^3+R^6\right)\Bigg(3\left(1-\frac{2M}{R}\right)^{h/2} \\
&-\left(1-\frac{2Mr^2}{R^3}\right)^{h/2}\Bigg)^{\frac{1}{h}}-2^{\frac{1}{h}+2}M^2r^3R^3\Big(1-\frac{2Mr^2}{R^3}\Big)^{\frac{h+1}{2}}+\Big(24M^3r^6 \\
&-4M^2r^2\left(7r^2+4\right)R^3+2M\left(5r^2+3\right)R^6-R^9\Big)\Bigg(3\left(1-\frac{2M}{R}\right)^{h/2}- \\
&\left(1-\frac{2Mr^2}{R^3}\right)^{h/2}\Bigg)^{\frac{1}{h}}\Big(1-\frac{2Mr^2}{R^3}\Big)^{h/2}+2^{\frac{1}{h}+1}MrR^6\left(1-\frac{2Mr^2}{R^3}\right)^{\frac{h+1}{2}}\Bigg) \\
&-2^{\frac{h+2}{h}}\ddot{T}(t)\left(3\left(1-\frac{2M}{R}\right)^{h/2}-\left(1-\frac{2Mr^2}{R^3}\right)^{h/2}\right)^{-2/h} \\
&\times\left(r\sqrt{1-\frac{2Mr^2}{R^3}}\right)^{-1}, \qquad (7.7.3)
\end{aligned}
$$

$$
\begin{aligned}
\overline{q}_1B_o &= -2^{\frac{1}{h}+1}\dot{T}(t)\left(3\left(1-\frac{2M}{R}\right)^{h/2}-\left(1-\frac{2Mr^2}{R^3}\right)^{h/2}\right)^{-1/h} \\
&\times\left(M\left(\frac{2\left(\frac{1}{3\left(1-\frac{2M}{R}\right)^{h/2}\left(1-\frac{2Mr^2}{R^3}\right)^{-h/2}-1}-1\right)}{R^3-2Mr^2}-\frac{2r^2}{R^3}\right)+1\right), \qquad (7.7.4)
\end{aligned}
$$

$$
\begin{aligned}
\overline{\Theta} &= 2^{\frac{1}{h}}\left(r\sqrt{1-\frac{2Mr^2}{R^3}}+\frac{2}{r\sqrt{1-\frac{2Mr^2}{R^3}}}\right)\dot{T}(t)\Bigg(3\left(1-\frac{2M}{R}\right)^{h/2} \\
&-\left(1-\frac{2Mr^2}{R^3}\right)^{h/2}\Bigg)^{-1/h}, \qquad (7.7.5)
\end{aligned}
$$

$$
\begin{aligned}
\overline{\sigma} &= 2^{\frac{1}{h}}\left(r\sqrt{1-\frac{2Mr^2}{R^3}}-\frac{1}{r\sqrt{1-\frac{2Mr^2}{R^3}}}\right)\dot{T}(t)\Bigg(3\left(1-\frac{2M}{R}\right)^{h/2} \\
&-\left(1-\frac{2Mr^2}{R^3}\right)^{h/2}\Bigg)^{-1/h}. \qquad (7.7.6)
\end{aligned}
$$

We note that the perturbed density in (7.7.1) does not depend on the anisotropic factor h. For our particular model we find that the perturbation to the energy density

is negative during the collapse process, and strongest near the centre of the star, as shown in Fig. 7.5. We note that the overall energy density $\rho(t, r)$, given by (4.1.4), is positive.

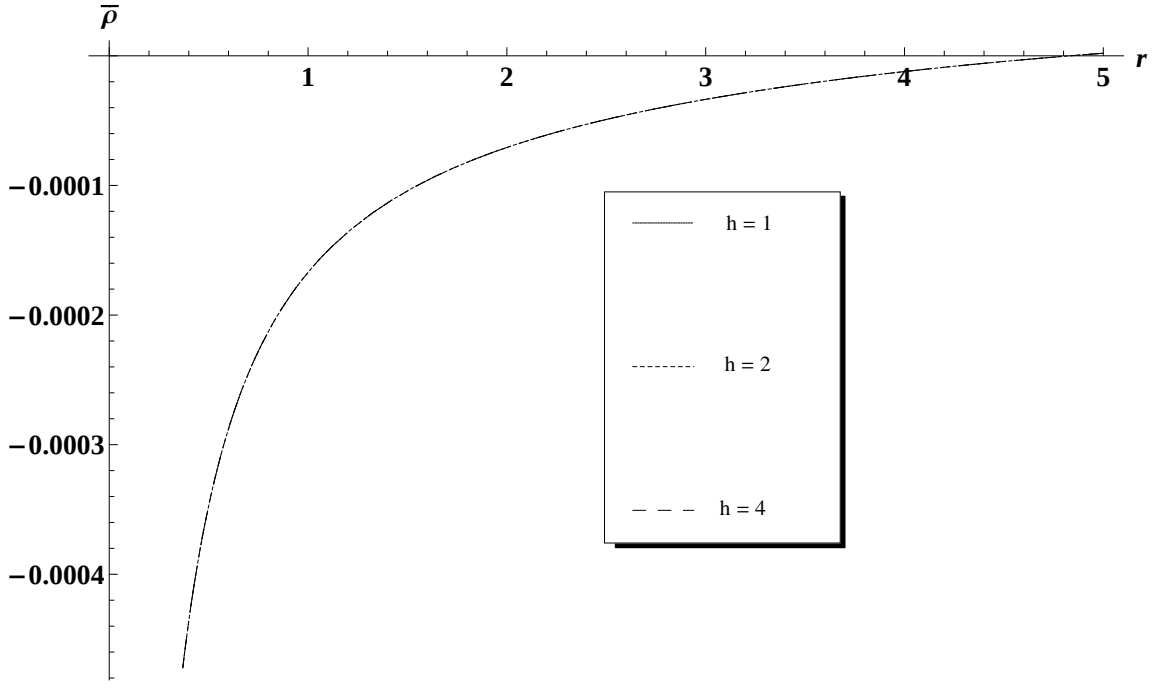

Figure 7.5: Perturbed energy density $\overline{\rho}$ profile versus radial coordinate ($M = 1$, $R = 5$ and $t = -10$).

From Fig. 7.6 we can conclude that the perturbation to the radial pressure is highest at the centre of the star and gradually drops off as we move away from the centre. This behaviour is expected as the heat generation is the highest in the core regions. It is also clear that the degree of anisotropy enhances the perturbations to the radial pressure and this effect is more pronounced near the centre of the stellar fluid.

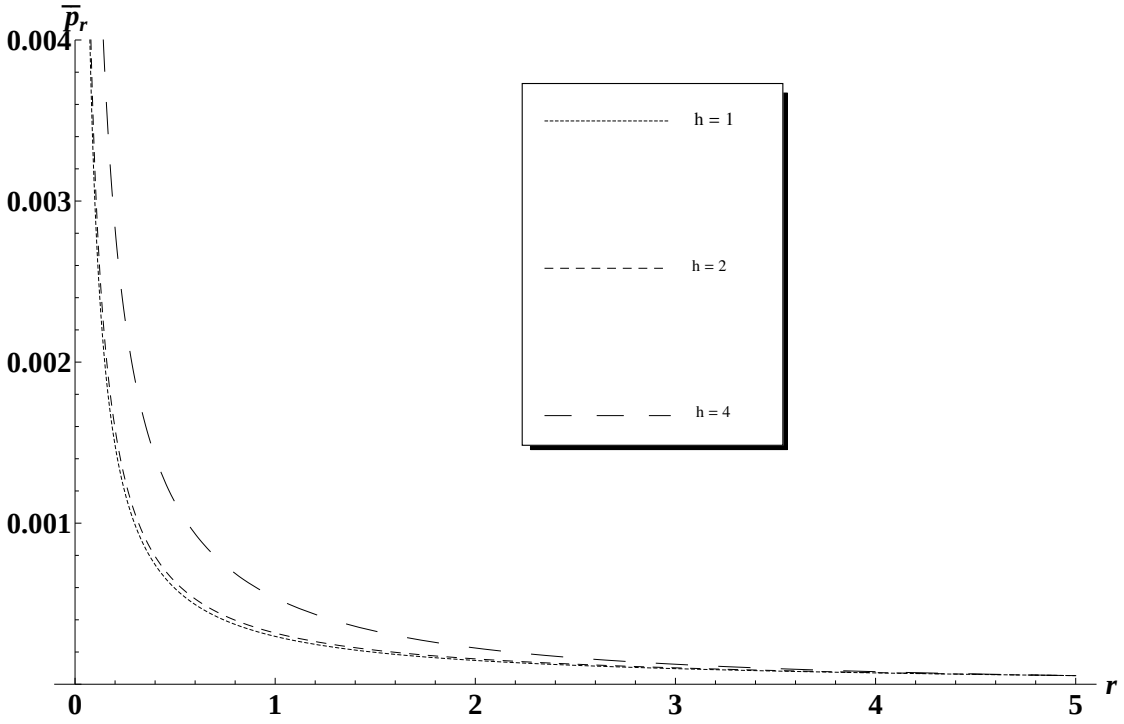

Figure 7.6: Perturbed radial pressure $\overline{p}_r$ profiles versus radial coordinate ($M = 1$, $R = 5$ and $t = -10$).

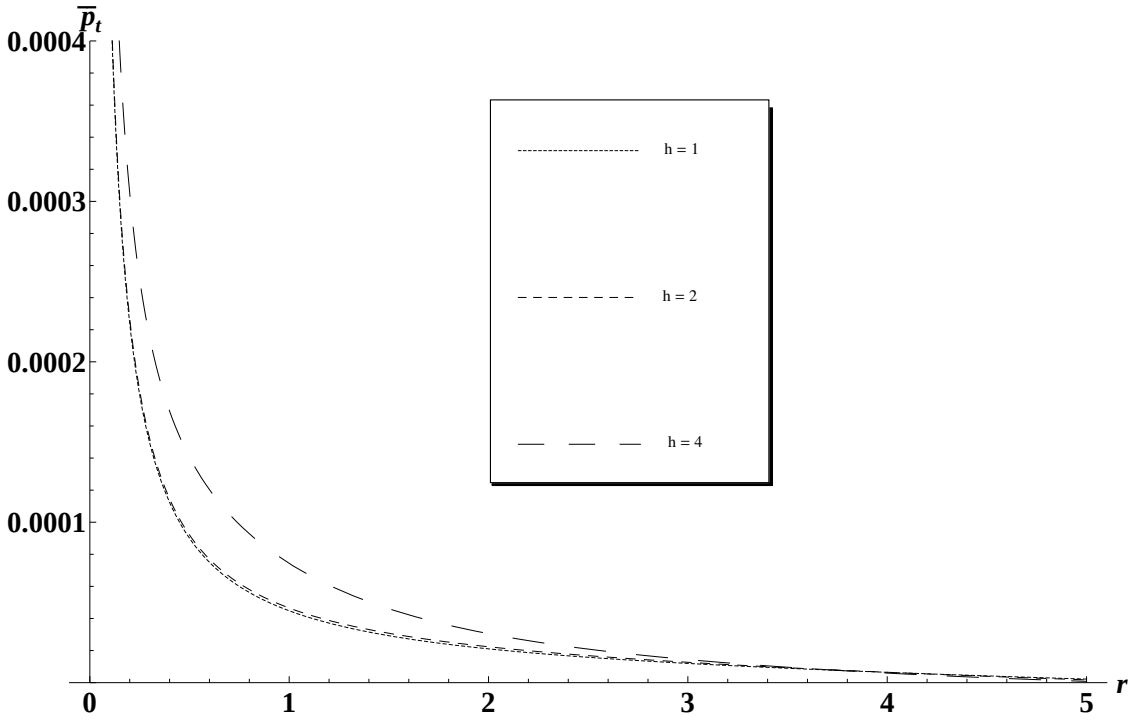

Figure 7.7: Perturbed tangential pressure $\overline{p}_t$ profiles versus radial coordinate ($M = 1$, $R = 5$ and $t = -10$).

Comparing Fig. 7.6 and Fig. 7.7 we observe that the perturbations in the radial pressure dominate the perturbations in the tangential pressure throughout the interior of the stellar distribution. Again we note that the perturbations in the tangential pressure grow with an increasing deviation (larger h) from isotropy ($h = 1$). Furthermore, the perturbations in the tangential pressure decrease more rapidly than the perturbations in the radial pressure as we move towards the stellar surface.

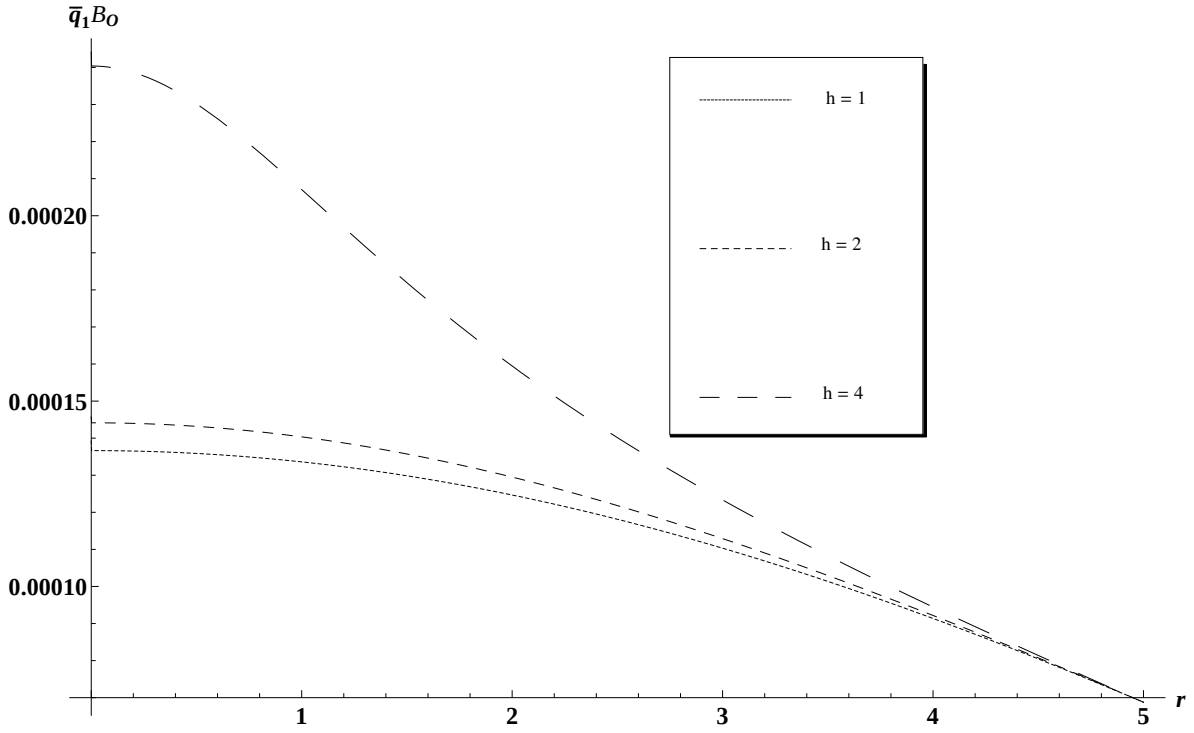

Figure 7.8: Perturbed heat flow $\bar{q}_1 B_o$ profiles versus radial coordinate ($M = 1$, $R = 5$ and $t = -10$).

From Fig. 7.8 we see that the heat flux is maximum at the centre where the pressure is the highest, and then gradually drops off towards the surface. Heat generation is enhanced in the central regions of the collapsing star as the anisotropy increases. It is clear that the anisotropy makes no significant contribution to the heat generation closer to the stellar surface. Our analysis of the physics at play here is supported by Figs. 7.11–7.12, where it is clear that the perturbations to the shear close to the core are enhanced as the anisotropy increases. An increase in the perturbation to the shear is likely to result in greater internal friction between adjacent layers of stellar fluid and this mechanism is expected to enhance the temperature and heat flow near the core region, which is vividly apparent from Figs. 7.8 and 7.14.

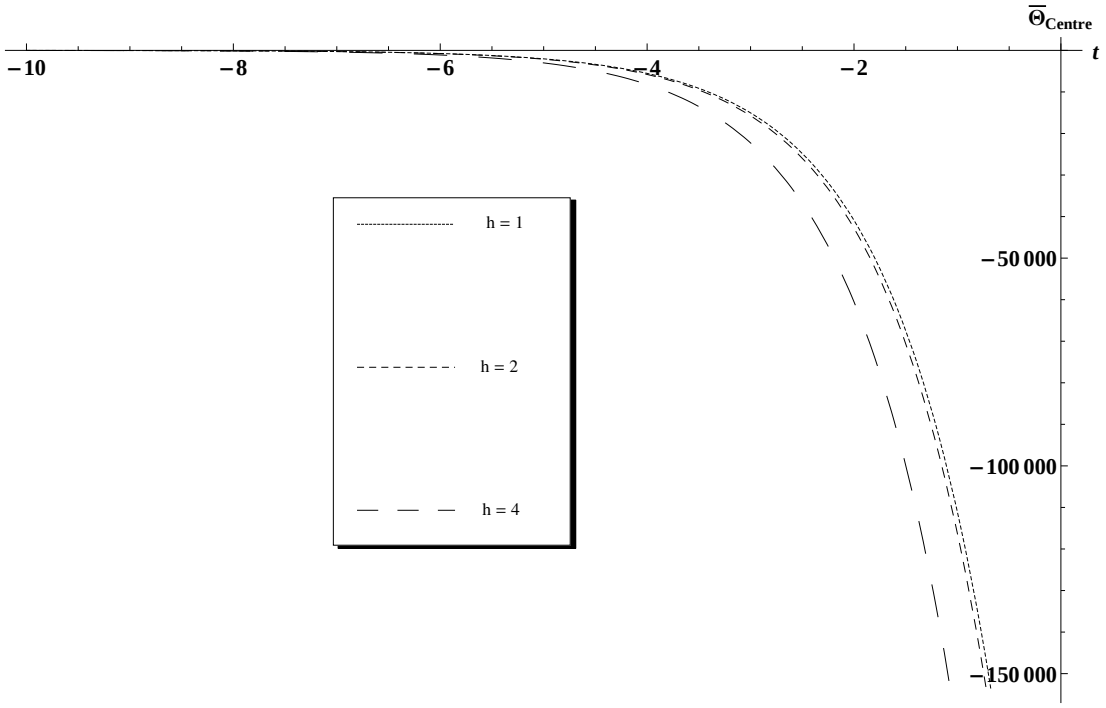

Figure 7.9: Perturbed collapse rate profiles versus time at the centre ($M = 1$, $R = 5$ and $r \approx 0$).

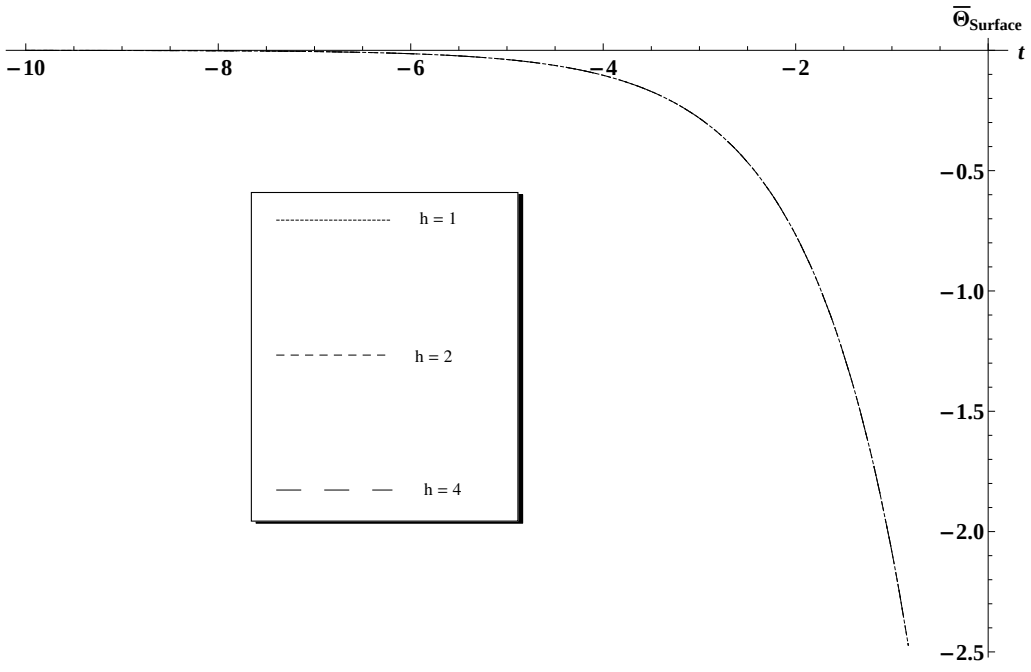

Figure 7.10: Perturbed collapse rate profiles versus time at the surface ($M = 1$, $R = 5$ and $r \approx 5$).

Figures 7.9 and 7.10 illustrate the behaviour of the perturbations in the collapse rate at the centre and at the surface respectively.

We observe that

$$\frac{\bar{\Theta}_{\text{centre}}}{\bar{\Theta}_{\text{surface}}} \approx 10^4, \tag{7.7.7}$$

which means that the core collapses at a much greater rate than the cooler surface layers.

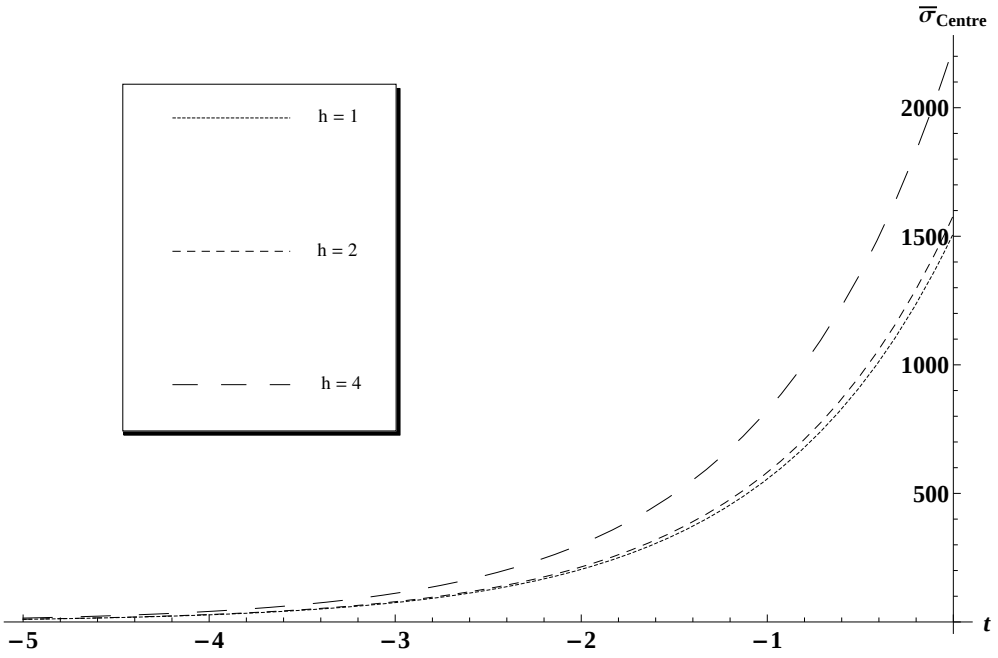

Figure 7.11: Perturbed shear profiles versus time at the centre ($M = 1$, $R = 5$ and $r \approx 0$).

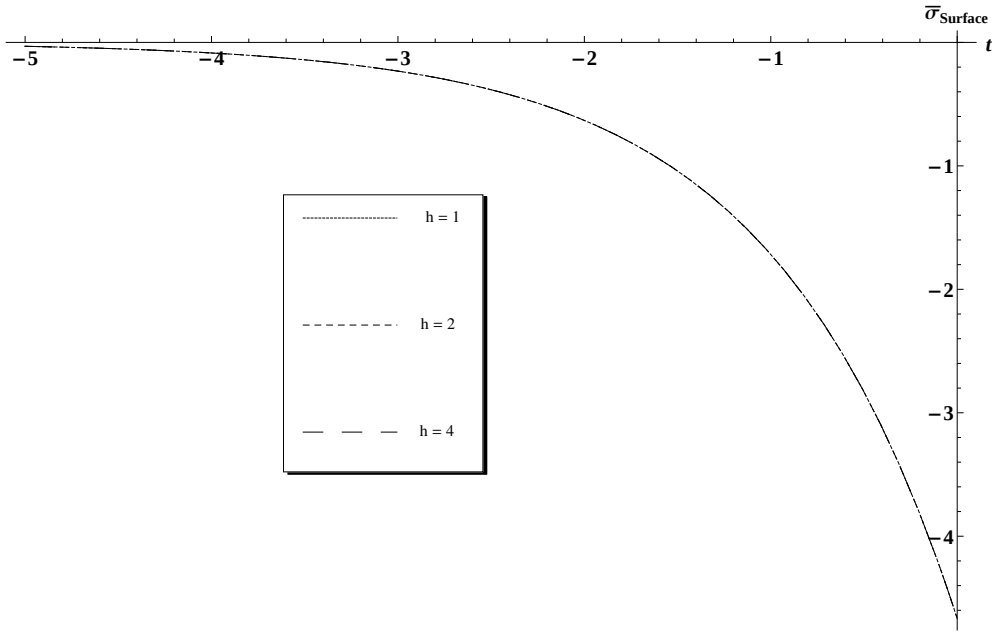

Figure 7.12: Perturbed shear profiles versus time at the surface ($M = 1$, $R = 5$ and $r \approx 5$).

7.8 Stability analysis

Stability analysis of models is critical to the understanding of gravitational collapse, in particular to the final fate of the stellar fluid. In a self–gravitating system, hydrodynamic forces oppose the contracting pull of gravity in order to stabilize the stellar fluid against collapse. Radial pressure plays a critical role in stability. The effective adiabatic index (which takes into account dissipative effects) is given by Chan [49], viz.

$$\Gamma_{eff} = \frac{dp_r}{d\rho},$$

which is used to investigate the stability of our model after being perturbed from an initially static configuration at $t = -\infty$, We study the behaviour of the effective adiabatic index Γ_{eff} near the centre of stellar fluid as well as on an arbitrarily chosen

hypersurface ($r_\Sigma = \text{const.}$). We utilize the equations

$$\begin{aligned} p_r(t,r) &= p_{ro}(r) + \lambda \overline{p}_r(t,r), \\ \rho(t,r) &= \rho_o(r) + \lambda \overline{\rho}(t,r). \end{aligned}$$

With the aid of (4.2.2a)–(4.2.2c) and (4.2.3a)–(4.2.3c) and $\lambda = 0.001$ in (6.8.2) we obtain plots of difference between Γ_{eff} at the centre and the boundary, for varying degrees of the anisotropic factor h, as shown in Fig. 7.13.

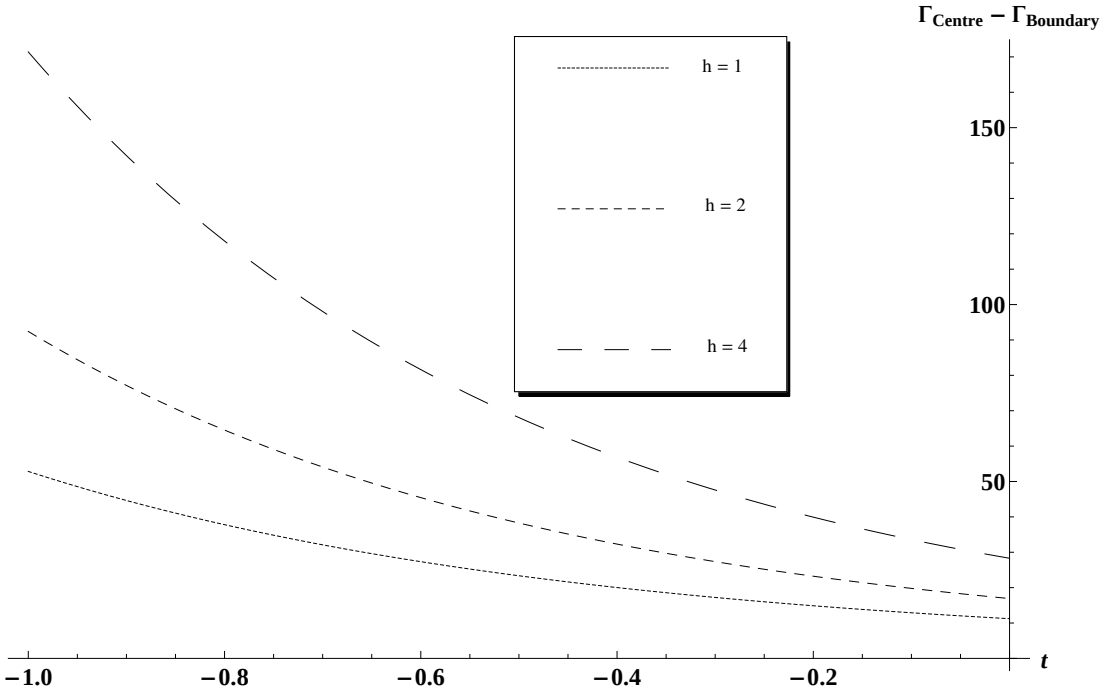

Figure 7.13: $\Gamma_{\text{Centre}} - \Gamma_{\text{Boundary}}$ against time, for varying degrees of anisotropic parameter.

It is evident from Fig. 7.13 that $\Gamma_{\text{Centre}} - \Gamma_{\text{Boundary}} > 0$ which implies that $\Gamma_{\text{Centre}} > \Gamma_{\text{Boundary}}$. This indicates that the core region of the star is less stable than the cooler boundary layers. It is also clear from Fig. 7.13 that the difference between the effective adiabatic index at the centre and boundary grows with anisotropic factor h. So, in fact, pressure anisotropy renders the core regions even more unstable than it was under isotropic conditions.

It is unfortunate that we could not use our $(p_{to} - p_{ro})$ expression to directly study the impact of pressure (static) anisotropy on the stability index given by (4.4.3) for the Newtonian limit and by (4.4.4) for the post–Newtonian limit (see Chan *et al* [77]) for vanishing shear. This is due to the fact that a transformation of the Bowers and Liang metric from curvature coordinates to comoving isotropic coordinates is required. This requires a difficult integration which we will leave for future work. It will also be worthwhile to study the effect of the anisotropic factor on the relativistic contributions to the stability or adiabatic index.

7.9 Thermal behaviour

The thermal behaviour of a star undergoing dissipative gravitational collapse cannot be described by the Einstein field equations. To this end, several thermodynamic theories involving irreversible processes have been proposed. The Eckart theory [22] forecasts propagation velocities, for the thermal signals, that lie outside the causal cone of propagation, and the theory is additionally plagued with unstable equilibrium states. The "pathological problems" inherent in the Eckart model were addressed, in the context of extended irreversible thermodynamics, by several authors [23, 24, 25, 26] by taking the relaxation time of the heat flux into account. These models yield hyperbolic heat transport equations that are of Cattaneo [27] form (see Maartens [57] for details), resulting in thermal signals obeying the causality principle, i.e. the velocity of the thermal signals do not exceed the speed of light. Di Prisco *et al* [28] have estimated the relaxation times for neutron star matter, in early stages of gravitational collapse, to be as small as $0.1ms$ for a core temperature of $10^9 K$and as large as $100s$ at $10^6 K$. Work done by Anile *et al* [29] also indicates that relaxational effects are significant, and Herrera and Martinez [30] show explicitly that thermal relaxation time has a direct impact on the luminosity profiles as well as the compactness of the star.

Causal relativistic heat transport equations without shear and acceleration have

been studied at by Govender *et al* [32, 33]. Their results, for constant collision time, indicate that causal temperature profiles are higher than their non–causal counterparts throughout the star, except for the boundary where they are equal. Thirukkanesh *et al* [1] have studied the impact of causality for "shearing, radiative collapse with expansion and acceleration" and report that the causal temperature profiles are higher than those in the non–causal case, and their work generalises the Naidu *et al* model [37].

Up to this point, the only nonzero accelerating models with shear are the so-called Euclidean stars which were first investigated by Herrera *et al* [92]. The first exact model of a Euclidean star was presented by Govender *et al* [87]. This model has been generalised by Govender and Govinder [88] in which the thermal behaviour and stability of Euclidean stars were investigated. The thermal behaviour of these models were studied within the context of extended irreversible thermodynamics. For both shear-free models and shearing, geodesic models it was shown that relaxational effects due to heat dissipation lead to higher interior temperatures in the Euclidean stellar core. To this end, Govender *et al* [39] have investigated the causal and non–causal profiles of the perturbed temperature in the linear regime of the perturbation. Their results reveal that the perturbed temperature is higher in the causal case implying that relaxational effects enhances the temperature contributions due to perturbation. Recently Govender *et al* [40] have demonstrated that shear enhances both the causal and non–causal temperature profiles, and that the causal profiles are higher than the non–causal case in both shearing and shear–free cases.

The importance of relaxational effects during dissipative gravitational collapse has been highlighted by several researchers. Govender and co-workers have shown that relaxational effects can lead to higher core temperatures and enhanced cooling at the surface of the collapsing body [32, 86, 87, 88, 89]. In order to explore the contributions from relaxational effects as the fluid exits hydrostatic equilibrium we will employ a causal heat transport equation of Cattaneo [27] form (see Maartens [57] for details). The truncated causal transport equation in the absence of rotation and viscous heat

coupling is given by

$$\tau_r h_a{}^b \dot{q}_b + q_a = -\kappa\big(h_a{}^b \nabla_b \mathcal{T} + \mathcal{T}\dot{V}_a\big),$$

where all quantities are discussed in Chapter 5. With the aid of the metric (2.5.1), equation (5.5.1) for non–zero relaxation time τ_r becomes

$$\tau_r (qB)^{\cdot} + A(qB) = -\kappa \frac{(A\mathcal{T})'}{B}.$$

The thermodynamic coefficients associated with radiative transfer are well motivated in [32, 33, 46]. The thermal conductivity κ and mean collision time τ_c are given by (5.5.4) and the relaxation time τ_r is given by (5.5.5). Equation (5.5.6) of the form

$$\psi(qB)^{\cdot}\mathcal{T}^{-\omega} + A(qB) = -\xi \frac{\mathcal{T}^{3-\omega}(A\mathcal{T})'}{B},$$

is integrated for the causal case ($\omega = 0$) with constant collision time ($\psi \neq 0$) to yield equation

$$\big(A\mathcal{T}\big)^4 = -\frac{4}{\xi}\Big[\psi \int A^3 B(qB)^{\cdot} dr + \int A^4 qB^2 dr\Big] + F(t).$$

7.10 Perturbation of the temperature

Equation (5.5.10) is perturbed with the aid of (4.1.1)–(4.1.3) and

$$\mathcal{T} = \mathcal{T}_o + \lambda \overline{\mathcal{T}} T, \tag{7.10.1}$$

where $\mathcal{T}_o$ is the equilibrium temperature and $\overline{\mathcal{T}}$ represents the perturbation in the temperature which is a function of radial coordinate only. Using (7.10.1) and (5.5.10) we obtain the following expression for the perturbed temperature

$$\begin{aligned}
\overline{\mathcal{T}}(r) \;=\; & -\frac{2\psi}{\xi A_o}\frac{\ddot{T}}{T}\int \frac{1}{A_o}\mathcal{T}_o^{-3}\Big[\Big(\frac{y}{Y_o}\Big)' - \frac{bY_o'}{B_o Y_o} - \frac{y}{Y_o}\Big(\frac{A_o'}{A_o} - \frac{Y_o'}{Y_o}\Big)\Big]dr \\
& -\frac{2}{\xi A_o}\frac{\dot{T}}{T}\int A_o \mathcal{T}_o^{\omega-3}\Big[\Big(\frac{y}{Y_o}\Big)' - \frac{bY_o'}{B_o Y_o} - \frac{y}{Y_o}\Big(\frac{A_o'}{A_o} - \frac{Y_o'}{Y_o}\Big)\Big]dr \\
& -\frac{a\mathcal{T}_o}{A_o} + \frac{C_1}{A_o},
\end{aligned} \tag{7.10.2}$$

where C_1 is an integration constant. Relation (7.10.2) is a generalisation of the temperature perturbation obtained by Maharaj *et al* [39] in which they investigated the

collapse of a shear-free distribution of matter. Using our static model parameters (7.6.2)–(7.6.4) in (7.10.2) we obtain an expression for the perturbed temperature in terms of the anisotropic scale factor h, given by

$$\begin{aligned}
\overline{\mathcal{T}} \;=\; & C_1 2^{\frac{1}{h}}\left(3\left(1-\frac{2M}{R}\right)^{h/2}-\left(1-\frac{2Mr^2}{R^3}\right)^{h/2}\right)^{-1/h}-\frac{1}{\mathrm{C}_o{}^3\xi T(t)}2^{1-\frac{1}{h}}\psi\ddot{T}(t)\times \\
& \Big(3\left(1-\frac{2M}{R}\right)^{h/2}-\big(1-\frac{2Mr^2}{R^3}\big)^{h/2}\big)^{-1/h}\Big(\int\Big(3\left(1-\frac{2M}{R}\right)^{h/2}- \\
& \big(1-\frac{2Mr^2}{R^3}\big)^{h/2}\Big)^{2/h}\Bigg[\Bigg(-2Mr\left(1-\frac{2Mr^2}{R^3}\right)^{\frac{h}{2}-1}\times\Big(R^3\Big(3\left(1-\frac{2M}{R}\right)^{h/2}- \\
& \left(1-\frac{2Mr^2}{R^3}\right)^{h/2}\Big)\Big)^{-1}-\frac{1}{r}\Bigg)\times\Big(r\sqrt{1-\frac{2Mr^2}{R^3}}\Big)^{-1}+\frac{2M}{R^3\left(1-\frac{2Mr^2}{R^3}\right)^{3/2}}- \\
& \sqrt{1-\frac{2Mr^2}{R^3}}-\frac{1}{r^2\sqrt{1-\frac{2Mr^2}{R^3}}}\Bigg]dr\Big)-\Bigg[2\dot{T}(t)\Big(3\left(1-\frac{2M}{R}\right)^{h/2}- \\
& \Big(1-\frac{2Mr^2}{R^3}\big)^{h/2}\Big)^{-1/h}\Big(\int\Big(3\left(1-\frac{2M}{R}\right)^{h/2}-\Big(1-\frac{2Mr^2}{R^3}\Big)^{h/2}\Big)^{\frac{1}{h}}\times \\
& \Bigg(-\Bigg[\Bigg(2Mr\left(1-\frac{2Mr^2}{R^3}\right)^{\frac{h}{2}-1}\Bigg)\times\Big(R^3\Big(3\left(1-\frac{2M}{R}\right)^{h/2}-\Big(1- \\
& \frac{2Mr^2}{R^3}\Big)^{h/2}\Big)\Big)^{-1}\big)-\frac{1}{r}\Bigg]\times\Big(r\sqrt{1-\frac{2Mr^2}{R^3}}\Big)^{-1}+\frac{2M}{R^3\left(1-\frac{2Mr^2}{R^3}\right)^{3/2}}- \\
& \sqrt{1-\frac{2Mr^2}{R^3}}-\frac{1}{r^2\sqrt{1-\frac{2Mr^2}{R^3}}}\Bigg)\Big(\mathrm{C}_o 2^{\frac{1}{h}}\Big(3\Big(1-\frac{2M}{R}\Big)^{h/2}- \\
& \Big(1-\frac{2Mr^2}{R^3}\Big)^{h/2}\Big)^{-1/h}\Big)^{\omega-3}dr\Big)\Bigg]\big(\xi T(t)\big)^{-1}+\mathrm{C}_o\left(-2^{2/h}\right)\times \\
& \Big(3\Big(1-\frac{2M}{R}\Big)^{h/2}-\left(1-\frac{2Mr^2}{R^3}\right)^{h/2}\Big)^{-2/h}. \qquad (7.10.3)
\end{aligned}$$

The zeroth order perturbation of (5.5.10) yields

$$\mathcal{T}_o{}' = -\frac{A_o'}{A_o}\mathcal{T}_o, \qquad (7.10.4)$$

which can be easily expressed as

$$\Big(A_o\mathcal{T}_o\Big)' = 0. \qquad (7.10.5)$$

Equation (7.10.5) easily integrates to give

$$\mathcal{T}_o = \frac{C_o}{A_o}, \tag{7.10.6}$$

where C_o is a positive constant of integration. Herrera and Santos [83] and Maharaj *et al* [39] provide a discussion of the physical significance of equation (7.10.4), which was first obtained by Tolman in 1930. They point out that equation (7.10.4) alludes to the existence of a temperature gradient which prohibits the movement of heat flux along the gradient of the gravitational field. This is the mechanism that is responsible for the thermal equilibrium being maintained in the presence of a gravitational field.

The profiles of the perturbed temperature for varying degrees of anisotropic parameter are shown in Fig. 7.14.

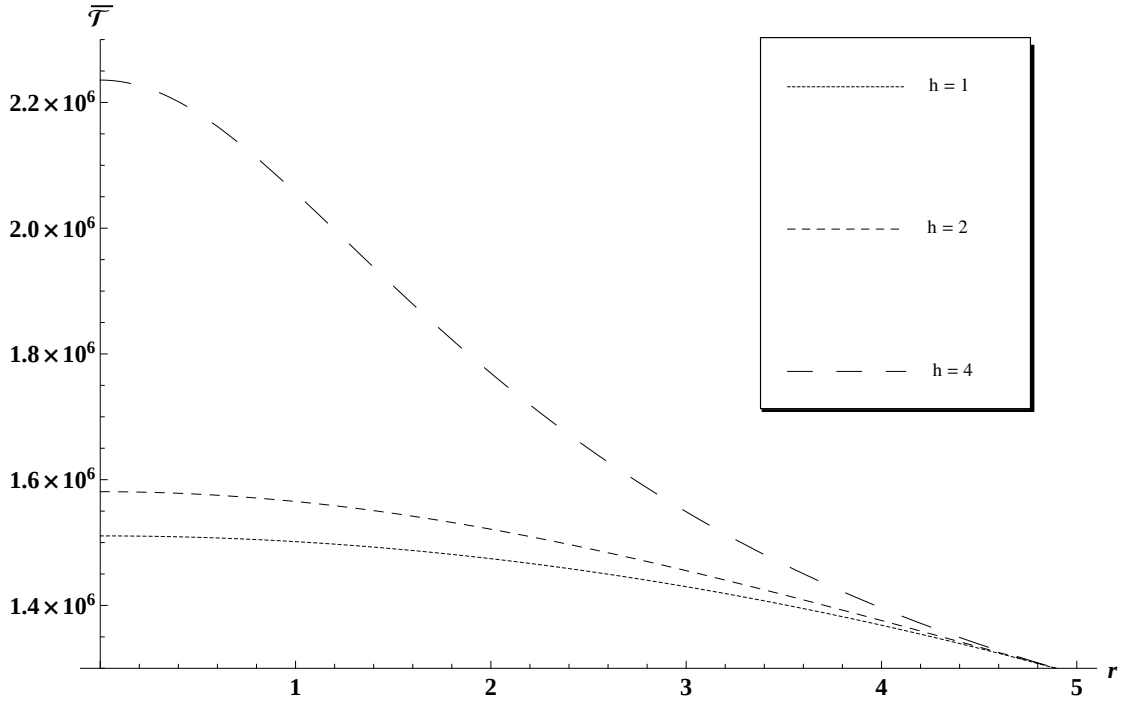

Figure 7.14: Perturbed temperature $\overline{\mathcal{T}}$ profiles versus radial coordinate ($M = 1$, $R = 5$, $t = -10$, $C_o = 1 \times 10^5$, $C_1 = 1 \times 10^7$, $\xi = 1 \times 10^4$, $\psi = 1 \times 10^5$).

From Fig. 7.14 we note that the perturbations in the temperature are greatest when there is a greater divergence from isotropy with p_r dominating p_t. This is in keeping with a greater generation of heat within the core due to internal friction between

the neighbouring layers of the stellar fluid. An interesting and surprising result is that the causal and non–causal temperatures are identical for this particular epoch of the collapse which is markedly different from the shear–free case [39]. The possible explanation for the independence of the perturbed temperature on the causality index ψ is that for this particular model, and choice of values that produced physically reasonable results, the Eckart temperature appears to dominate the thermal behaviour. It is highly unlikely that the inclusion of shear is producing this behaviour.

7.11 Conclusion

We have investigated the impact of anisotropy on the physical behaviour of a spherically symmetric stellar fluid undergoing shearing dissipative collapse. Our system is initially static and is then subjected to linear perturbations that drive the system away from hydrostatic equilibrium. The initial static core is described by the Bowers and Liang [2] model which is an anisotropic generalisation of the Schwarzschild uniform density sphere. The effect of pressure anisotropy on the collapse process is clearly evidenced on the perturbations to the energy density, radial pressure, tangential pressure, heat flow, collapse rate and shear. We have shown that the perturbations are enhanced with growing anisotropy. An interesting finding in our work is that the perturbations to the temperature profiles in both the Eckart and causal regimes are identical. This is in contrast to the shear-free, isotropic models studied in [39]. We must point out that the causal temperature perturbations were obtained by using a truncated heat transport equation of Maxwell-Cattaneo form [27]. It would be interesting to investigate the evolution of these perturbations by invoking the full causal heat transport equation.

Chapter 8

Conclusion

As a first step in the research process, we began by developing an understanding of relativistic stars in general. We provided a brief overview describing the evolution of a star originating as separate gas molecules and then pulled so close together by gravitational attraction that nuclear fusion ensues, followed by the production of new nuclei and the release of huge amounts energy as well as subatomic particles. As highlighted the final fate of a star in general could be a white dwarf, a neutron star, a singularity contained within a black hole or a naked singularity. Our study is based on very massive stars that are not able to reach a stable configuration (as a neutron star or a white dwarf) but undergo continual gravitational collapse resulting ultimately in a singularity at the stellar centre.

We highlighted that the theory of general relativity, which is essentially a geometric theory of gravitation, leads ultimately to Einstein's field equations which are essential to the study of relativistic collapsing stars. To this end, we derived in detail the most general Einstein field equations for spherically symmetric shearing spacetimes. The matter distribution is described by an imperfect fluid possessing heat flow, pressure anisotropy, shear, bulk viscosity and null radiation.

Several solutions [6, 13, 14, 15] to Einstein's field equations have been obtained for the interior and the exterior of a star. We have shown that the smooth matching of

these spacetimes into a single model is essential to gaining a complete understanding of gravitational collapse. The matching process, which was reviewed in detail in Chapter 3, essentially entails the matching (interior–to–hypersurface–to–exterior) of the metrics and the spacetime curvature. We have considered the junction conditions for a matter distribution that includes bulk viscosity, shear, null radiation, in addition to heat flux.

The framework for perturbative analysis was generated for a shearing line element to yield the static and perturbed physical properties of a star for the general spherical metric. This provides the basic framework to understand the features related to the dynamical instability of a system having heat flow [18], anisotropic pressure and radiation [77] and shear viscosity [19]. The use of the Maxwell-Cattaneo [27] (in the truncated version of the Israel–Stewart theory) form for the heat transport used in this study is motivated [85] in Chapter 5, where an overview of thermodynamics is presented based primarily on the Maartens [57] formalism.

We are able to directly study the impact of shear on the temperature profile, the luminosity profile, the collapse rate as well as on the relaxation time by utilising a 'shear switch' built into our model. Our results in Chapter 6 clearly illustrate that the inclusion of shear results in higher temperature which is more pronounced in the core regions of the star as opposed to the surface layers. These results are reasonable since the inclusion of shear is expected to cause internal friction between fluid layers which is expected to raise the temperature. We were able to show that causal thermodynamics with relaxational effects predicts higher core temperatures; relaxational effects seem to have little effect on the temperature profile of a star at its surface. Stability analysis reveals that the inclusion of shear makes the system more stable and this is more pronounced at the surface layers for late time collapse. The core is very unstable as revealed by erratic behaviour of the adiabatic index.

The Bowers and Liang [2] model was considered in Chapter 7. This made it possible to directly study the impact of pressure anisotropy on the static and perturbed physical properties of the collapsing model via the anisotropic factor built into the Bowers and

Liang [2] model. Perturbation to the heat flow is enhanced as the anisotropic factor increases, and this effect is very pronounced near the core regions; this relationship is almost completely absent at the boundary. Perturbations to the causal temperature profiles behave in a similar manner to the heat flow, as expected. We conclude that the perturbations to the collapse rate are sensitive to the anisotropic factor at the core of the star but not close to the boundary, and that the star is more stable near the surface as compared to the core. An interesting point to pick up on is that the perturbed temperature profiles are independent of the causality index, meaning that the non–causal and causal perturbed temperature profiles are identical. This is the first time that perturbed temperature profiles have been done with shear and anisotropy, especially for the Bowers and Liang [2] model. It will be interesting to analyse the perturbed thermal behaviour with varying degrees of anisotropy using the Israel–Stewart theory including second order terms. It may be possible that the Maxwell–Cattaneo [27] form for the heat flux will not able to show the differences. This, however, is left for future work, where we hope to be able to directly highlight the effects of higher order relativistic effects on the relaxation time and hence on the perturbed temperature profiles. Another possible avenue for future work is to be develop a model to investigate the dynamical instability of a system having anisotropic pressure, heat flow, radiation as well as shear.

We believe that gravitational collapse still holds many secrets that we have yet to uncover. There is a need for more realistic modelling and the use of data sets to update and tweak current collapse models to have better agreement with experimental results. We also foresee the need for a multidisciplinary approach, i.e. the integration of fluid mechanics, particle physics, nuclear physics as well as plasma physics into general relativity to help construct more realistic models describing gravitational collapse to an even greater degree than is currently being done.

Bibliography

[1] S Thirukkanesh, S S Rajah and S D Maharaj, *Shearing radiative collapse with expansion and acceleration*, J. Math. Phys. **53**, 032506, 2012

[2] R L Bowers and E P T Liang, *Anisotropic spheres in general relativity*, Astrophys. J. **188** 657, 1974

[3] S Chandrasekhar, *The highly collapsed configurations of a stellar mass*, Mon. Not. R. Astron. Soc. **95**, 207, 1935

[4] J R Oppenheimer and G Volkoff, *On massive neutron cores*, Phys. Rev. **55**, 374, 1939

[5] J V Narlikar, *From black clouds to black holes*, World Scientific, Singapore, 1985

[6] J R Oppenheimer and H Snyder, *On continued gravitational contraction*, Phys. Rev. **56**, 455, 1939

[7] R Penrose, *Gravitational collapse: The role of general relativity*, Riv. Nuovo Cimento **1**, 252, 1969

[8] P S Joshi, *Cosmic censorship: A current perspective*, arXiv: gr-qc/0206087v1, 2002

[9] P S Joshi and D Malafarina, *Recent developments in gravitational collapse and spacetime singularities*, Int. J. Mod. Phys. D **20**, 2641, 2011

[10] T P Singh, *Gravitational collapse, black holes and naked singularities*, J. Astrophys. Astron. **20**, 221, 1999

[11] M Patil and P S Joshi, *Naked singularities as particle accelerators*, Phys. Rev. D **82**, 104049, 2010

[12] P S Joshi, D Malafarina and R Narayan, *Distinguishing black holes from naked singularities through their accretion disk properties*, Class. Quantum Grav. **31**, 015002, 2014

[13] K Schwarzschild, *Uber das Gravitationsfeld eines Massenpunktes nach der Einsteinschen Theorie*, Sitzber. Deut. Akad. Wiss. Berlin, Kl. Math.–Phys. Tech, 189, 1916a

[14] K Schwarzschild, *Uber da Gravitationsfeld einer Kugel aus inkompressibler Flussgkeit nach der Einsteinschen Theorie*, Sitzber. Deut. Akad. Wiss. Berlin, Kl. Math.–Phys. Tech, 424, 1916b

[15] P C Vaidya, *The gravitational field of a radiating star*, Proc. Indian Acad. Sc. A **33**, 264, 1951

[16] N O Santos, *Non-adiabatic radiating collapse*, Mon. Not. R. Astron. Soc. **216**, 403, 1985

[17] A K G de Oliveira and N O Santos, *Nonadiabatic gravitational collapse*, Astrophys. J. **312**, 640, 1987

[18] L Herrera, G Le Denmat and N O Santos, *Dynamical instability for non-adiabatic spherical collapse*, Mon. Not. R. Astron. Soc. **237**, 257, 1989

[19] R Chan, L Herrera and N O Santos, *Dynamical instability for shearing viscous collapse*, Mon. Not. R. Astron. Soc. **267**, 637, 1994

[20] R Chan, *Radiating gravitational collapse with shearing motion and bulk viscosity*, Astron. Astrophys. **368**, 325, 2001

[21] A Di Prisco, L Herrera, G Le Denmat, M A H MacCallum and N O Santos, *Nonadiabatic charged spherical gravitational collapse*, Phys. Rev. D **76**, 064017, 2007

[22] C Eckart, *The Thermodynamics of Irreversible Processes. III. Relativistic Theory of the Simple Fluid*, Phys. Rev. **58**, 919, 1940

[23] W Israel, *Nonstationary irreversible thermodynamics: A causal relativistic theory*, Ann. Phys. **100**, 310, 1976

[24] W Israel and J Stewart, *Thermodynamics of nonstationary and transient effects in a relativistic gas*, Phys. Lett. A **58**, 213, 1976

[25] W Israel and J Stewart, *Transient relativistic thermodynamics and kinetic theory*, Ann. Phys. **118**, 341, 1979

[26] D Pavón, D Jou and J Casas-Vázquez, *On a covariant formulation of dissipative phenomena*, Ann. Inst. H. Poincaré A **36**, 79, 1982

[27] C Cattaneo, *Sulla conduzione de calore*, Atti del Semin. Mat. e Fis. Univ. Modena **3**, 3, 1948

[28] A Di Prisco, L Herrera and M Esculpi, *Radiating gravitational collapse before relaxation*, Class. Quantum Grav. **13**, 1053, 1996

[29] A M Anile, D Pavon and V Romano, *The case for hyperbolic theories of dissipation in relativistic fluids*, arXiv: gr-qc/9810014v2, 1998

[30] L Herrera and J Martínez, *Gravitational collapse: A case for thermal relaxation*, Gen. Relativ. Gravit. **30**, 445, 1998

[31] A Di Prisco, L Herrera, N Falcon, M Esculpi and N O Santos, *Pre-relaxation processes in a radiating relativistic sphere*, Gen. Relativ. Gravit. **29**, 1391, 1997

[32] M Govender, S D Maharaj and R Maartens, *A causal model of radiating stellar collapse*, Class. Quantum Grav. **15**, 323, 1998

[33] M Govender, R Maartens and S D Maharaj, *Relaxational effects in radiating stellar collapse*, Mon. Not. R. Astron. Soc. **310**, 557, 1999

[34] K S Govinder and M Govender, *Causal solutions for radiating stellar collapse*, Phys. Lett. A **283**, 71, 2001

[35] M Govender and K S Govinder, *Temperature evolution during radiative gravitational collapse*, Int. J. Theor. Phys. **41**, 1797, 2002

[36] N F Naidu and M Govender, *Causal temperature profiles in horizon-free collapse*, J. Astrophys. Astr. **28**, 167, 2007

[37] N F Naidu, M Govender and K S Govinder, *Thermal evolution of a radiating anistropic star with shear*, Int. J. Mod. Phys. D **15**, 1053, 2006

[38] S S Rajah and S D Maharaj, *A Riccati equation in radiative stellar collapse*, J. Math. Phys. **49**, 012501, 2008

[39] S D Maharaj, G Govender and M Govender, *Temperature evolution during dissipative collapse*, Pramana - J. Phys. **77**, 469, 2011

[40] M Govender, K P Reddy and S D Maharaj, *The role of shear in dissipative gravitational collapse*, Int. J. Mod. Phys. D **23**, 1450013, 2014

[41] M Ruderman, *Pulsars: Structure and dynamics*, Ann. Rev. Astr. Ap. **10**, 427, 1972

[42] V Canuto, *Neutron stars: General review*, Solvay Conference on Astrophysics and Gravitation, Bruxelles, 1973

[43] V V Uslov, *Electric fields at the quark surface of strange stars in the color-flavor locked phase*, Phys. Rev. D **70**, 067301, 2004

[44] F Weber, *Pulsars and astrophysical observatories for nuclear and particle physics*, Institute of Physics, Bristol, 1999

[45] L Herrera and N O Santos, *Local anisotropy in self-gravitating systems*, Phys. Rep. **286**, 53, 1997

[46] J Martínez, *Transport processes in anisotropic gravitational collapse*, Phys. Rev. D **53**, 6921, 1996

[47] K Dev and M Gleiser, *Anisotropic stars: Exact solutions*, Gen. Relativ. Gravit. **34**, 1793, 2002

[48] K Dev and M Gleiser, *Anisotropic stars II: Stability*, Gen. Relativ. Gravit. **35**, 1435, 2003

[49] R Chan, *Collapse of a radiating anisotropic star*, Astrophys. Space Sci. **206**, 219, 1993

[50] L Herrera, *Physical causes of energy density inhomogenization and stability of energy density homogeneity in relativistic self-gravitating fluids*, Int. J. Mod. Phys. D **20**, 1689, 2011

[51] R Sharma and S Das, *Collapse of a relativistic self-gravitating star with radial heat flux: Impact of anisotropic stresses*, Journal of Gravity **2013**, 659605, 2013

[52] M Govender, *Heat transport in relativistic astrophysics and cosmology*, PhD dissertation: University of Natal, 1998

[53] C W Misner, K S Thorne and J A Wheeler, *Gravitation*, W H Freeman, San Francisco, 1973

[54] J B Hartle, *Gravity – An introduction to Einstein's general relativity*, Addison Wesley, San Francisco, 2003

[55] L Herrera, A Di Prisco, E Fuenmayor and O Troconis, *Dynamics of viscous dissipative collapse: A full causal approach*, Int. J. Mod. Phys. D **18**, 129, 2009

[56] L Herrera, *Relativistic Fluids and the Physics of Gravitational Collapse*, arXiv: 0909.3474v2, 2011

[57] R Maartens, *Causal thermodynamics in relativity*, arXiv: astro-ph/9609119v1, 1996

[58] F Fayos, X Jaén, E Llanta and J M M Senovilla, *Interiors of Vaidya's radiating metric: Gravitational collapse*, Phys. Rev. D **45**, 2732, 1992

[59] C W Misner and D Sharp, *Relativistic equations for adiabatic, spherically symmetric gravitational collapse*, Phys. Rev. B **136**, 571, 1964

[60] G Darmois, *Les équations de la gravitation einsteinenne*, Mémorial des sciences mathématiques, fascicule **25**, 1, 1927

[61] A Lichnerowicz, *Théories relativistes de la gravitation et de ĺ electromagnetism*, Masson, Paris, 1955

[62] S O'Brien and J L Synge, *Jump conditions at discontinuities in general relativity*, Commun. Dublin Inst. Ad. Stud. **9A**, 1952

[63] W B Bonner and P A Vickers, *Junction conditions in general relativity*, Gen. Relativ. Gravit **13**, 29, 1981

[64] C W Misner, *Relativistic equations for spherical gravitational collapse with escaping neutrinos*, Phys. Rev. B **137**, 1360, 1965

[65] W Israel, *Singular hypersurfaces and thin shells in general relativity*, Il Nuovo Cimento B **44**, 1, 1966

[66] N A Tomimura and F C P Nunes, *Radiating spherical collapse with shear and heat flow*, Astrophys. Space Sci. **199**, 215, 1993

[67] R Chan, *Radiating gravitational collapse with shear viscosity*, Mon. Not. R. Astron. Soc. **316**, 588, 2000

[68] L Herrera, N O Santos and A Wang, *Shearing expansion–free spherical anisotropic collapse*, Phys. Rev. D. **78**, 084026, 2008

[69] S D Maharaj and M Govender, *Collapse of a charged radiating star with shear*, Pramana - J. Phys. **54**, 715, 2000

[70] N Naidu, *Dynamics of dissipative gravitational collapse*, MSc dissertation: University of KwaZulu-Natal, 2008

[71] D Fleming, *Dissipative gravitating systems*, MSc dissertation: University of KwaZulu-Natal, 2011

[72] K Lake, V^{th} *Brazilian School of Cosmology and Gravitation*, Edited by M Novello, World Scientific, Singapore, 1987

[73] M E Cahill and G C McVittie, *Spherical symmetry and mass-energy in general relativity. I. General theory*, J. Math. Phys. **11**, 1382, 1970

[74] W C Hernandez and C W Misner, *Observer time as a coordinate in relativistic spherical hydrodynamics*, Astrophys. J. **143**, 452, 1966

[75] R W Lindquist, R Schwartz and C W Misner, *Vaidya's radiating Schwarzschild metric*, Phys. Rev. B **137**, 1364, 1965

[76] S Chandrasekhar, *The dynamical instability of gaseous masses approaching the Schwarzschild limit in general relativity*, Astrophys. J. **140**, 417, 1964

[77] R Chan, L Herrera and N O Santos, *Dynamical instability for radiating anisotropic collapse*, Mon. Not. R. Astron. Soc. **265**, 533, 1993

[78] L Herrera, G Le Denmat and N O Santos, *Dynamical instability and the expansion-free condition* Gen. Relativ. Gravit. **44**, 1143, 2012

[79] C Eckart, *The thermodynamics of irreversible processes III. Relativistic theory of the simple fluid*, Phys. Rev. **58**, 919, 1940

[80] G A Kluitenberg, S R De Groot and P Mazur, *Relativistic thermodynamics of irreversible processes i: Heat conduction, diffusion, viscous flow and chemical reactions; formal part*, Physica **19**, 689, 1953

[81] L Landau and E Lifshitz, *Fluid mechanics*, Butterworth-Heinemann, Oxford, 1959.

[82] L Herrera and N Falcón, *Convection theory before relaxation*, Astrophys. Space Sci. **234**, 139, 1995

[83] L Herrera and N O Santos, *Thermal evolution of compact objects and relaxation time*, Mon. Not. R. Astron. Soc. **287**, 161, 1997

[84] W Israel and J M Stewart, *On transient relativistic thermodynamics and kinetic theory, II*, Proc. R. Soc. Lond. A. **365**, 43, 1979

[85] D D Joseph and L Preziosi, *Heat Waves*, Rev. Mod. Phys. **61**, 41, 1989

[86] M Govender, K S Govinder, S D Maharaj, R Sharma, S Mukherjee and T K Dey, *Radiating spherical collapse with heat flow*, Int. J. Mod. Phys. D **12**, 667, 2003

[87] G Govender, M Govender and K S Govinder, *Thermal behaviour of Euclidean stars*, Int. J. Mod. Phys. D **19**, 1773, 2010

[88] K S Govinder and M Govender, *A general class of Euclidean stars*, Gen. Relativ. Grav. **44**, 147, 2012

[89] M Govender, *Non-adiabatic spherical collapse with a two-fluid atmosphere* Int. J. Mod. Phys. D **22**, 1350049, 2013

[90] S Thirukkanesh, S Moopanar and M Govender, *The final outcome of dissipative collapse in the presence of Lambda*, Pramana - J. Phys. **79**, 223, 2012

[91] K P Reddy, M Govender and S D Maharaj, *Impact of anisotropic stresses during dissipative gravitational collapse*, Gen. Relativ. Gravit. in press, 2014

[92] L Herrera and N O Santos, *Collapsing spheres satisfying an Euclidean condition*, Gen. Relativ. Gravit. **42**, 2383, 2010

[93] R Chan, *Radiating gravitational collapse with shear revisited*, Int. J. Mod. Phys. D **12**, 1131, 2003

[94] P C Nogueira and R Chan, *Radiating gravitational collapse with shear viscosity and bulk viscosity*, Int. J. Mod. Phys. D, **13**, 1727, 2004

[95] G Pinheiro and R Chan, *Radiating gravitational collapse with shear viscosity*, Gen. Relativ. Grav. **40**, 2149, 2008

[96] G Pinheiro and R Chan, *Radiating gravitational collapse with shearing motion and bulk viscosity revisited*, Int. J. Mod. Phys. D **19**, 1797, 2010

[97] L Herrera, G Le Denmat and N O Santos, *Cavity evolution in relativistic self–gravitating fluids*, Class. Quantum Grav. **27**, 135017, 2010

[98] L Herrera, A Di Prisco, J Ospino and J Carot, *Lemaitre-Tolman-Bondi dust spacetimes: Symmetry properties and some extensions to the dissipative case*, Phys. Rev. D **82**, 024021, 2010

[99] W B Bonnor, A K G de Oliveira and N O Santos, *Radiating spherical collapse*, Phys. Rep. **181**, 269 1989

[100] L Herrera, A Di Prisco, J Hernandez-Pastora, J Martin and J Martinez, *Thermal conduction in systems out of hydrostatic equilibrium*, Class. Quantum Grav. **14**, 2239, 1997

[101] L Herrera and N O Santos, *Dynamics of dissipative gravitational collapse*, Phys. Rev. D **70**, 084004, 2004

[102] L Herrera, *The inertia of heat and its role in the dynamics of dissipative collapse*, Int. J. Mod. Phys. D **15**, 2197, 2006

[103] D Jou, J Casas-Vazquez and G Lebon, *Extended irreversible thermodynamics*, Rep. Prog. Phys. **51**, 1105, 1988

[104] L Herrera and D Pavon, *Hyperbolic theories of dissipation: Why and when do we need them?*, Physica A **307**, 121, 2002

[105] A Banerjee, S Chatterjee and N Dadhich, *Spherical collapse with heat flow and without horizon*, Mod. Phys. Lett. A **17**, 2335, 2002

[106] S D Maharaj, G Govender and M Govender, *Radiating stars with generalised Vaidya atmospheres*, Gen. Relativ. Gravit. **44**, 1089, 2012

[107] L Herrera, A Di Prisco and J Ospino, *On the stability of the shear-free condition*, Gen. Relativ. Gravit. **42**, 1585, 2010

[108] P P S Joshi, N Dadhich and R Maartens, *Why do naked singularities form in gravitational collapse?*, Phys. Rev. D **65**, 101501, 2002

[109] W Baretto, L Herrera and N Santos, *A generalization of the concept of adiabatic index for non-adiabatic systems*, Astrophys. Space Sci. **187**, 271, 1992

[110] L. Herrera, *Cracking of self-gravitating compact objects*, Phys. Lett. A **165**, 206, 1992

[111] H Abreu, H Hernández and L A Núñez, *Sound speeds, cracking and the stability of self-gravitating anisotropic compact objects*, Class. Quantum Grav. **24**, 4631, 2007

[112] R Sharma and B S Ratanpal, *Relativistic stellar model admitting a quadratic equation of state*, Int. J. Mod. Phys. D **22**, 1350074, 2013

[113] G Michaud and J-P Zahn, *Turbulent transport in stellar interiors*, Theoret. Comput. Fluid Dynamics **11**, 183, 1998

[114] M Kalam, F Rahaman, S Molla and S M Hossien, *Anisotropic quintessence stars*, Astrophys. Space Sci. **349**, 865, 2014

[115] B V Ivanov. *The importance of anisotropy for relativistic fluids with spherical symmetry*, Int. J. Theor. Phys. **49**, 1236, 2010

[116] P S Florides, *A new interior Schwarzschild solution*, Proc. R. Soc. Lond. A. **337**, 529, 1974